

Aus dem
Comprehensive Pneumology Center (CPC) München
Institut für Experimentelle Pneumologie
komm. Direktorin: Dr. Antje Brand



Development of Novel Nanoparticle-Based Therapeutics for Treatment of Lung Cancer

Dissertation zum Erwerb des Doktorgrades der Naturwissenschaften
an der Medizinischen Fakultät der Ludwig-Maximilians-Universität München

vorgelegt von

Deniz Ali Bölükbaş
aus Zonguldak, Türkei

2017

**Gedruckt mit Genehmigung der Medizinischen Fakultät der
Ludwig-Maximilians-Universität München**

Betreuerin: Prof. Dr. Silke Meiners

Zweitgutachter: PD Dr. Markus Rehberg

Dekan: Prof. Dr. med. dent. Reinhard Hickel

Tag der mündlichen Prüfung: 03.07.2017

"Imagination is more important than knowledge. For knowledge is limited, whereas imagination embraces the entire world, stimulating progress, giving birth to evolution."

-Albert Einstein, What Life Means to Einstein (1929)

Table of contents

Zusammenfassung	1
Summary	4
1. Introduction	6
1.1. Lung cancer	6
1.1.1. Pathogenesis of lung cancer	7
1.1.1.1. Molecular alterations	7
1.1.1.2. Tumor microenvironment and immunotherapy	9
1.1.2. Diagnosis and treatment of lung cancer	10
1.1.2.1. Targeted therapies for lung cancer	12
1.2. Nanoparticle-based drug delivery	13
1.2.1. Passive <i>versus</i> active targeting of nanoparticles	14
1.2.2. Theranostic nanoparticles	15
1.2.3. Cell-specific delivery of nanoparticles	16
1.2.4. Pulmonary application of nanoparticles	16
1.2.4.1. Preclinical studies of nanomedicines for lung cancer treatment	17
1.2.4.2. Clinical studies of nanomedicines for lung cancer treatment.....	19
1.2.5. Challenges of nanomedicines	21
2. Aims of the study	22
3. Materials and methods	23
3.1. Materials	23
3.1.1. Reagents and chemicals.....	23

3.1.2. Buffer formulations	25
3.1.3. Antibodies and applications	27
3.1.4. Laboratory equipment and software	28
3.1.5. Consumables	30
3.1.6. Human tissue	31
3.2. Synthesis of mesoporous silica nanoparticles (MSNs)	31
3.3. Cell culture	32
3.3.1. Cell growth and maintenance	32
3.3.2. Metabolic activity assessment	33
3.3.2.1. MTT reduction	33
3.3.2.2. WST-1 assay.....	33
3.3.3. Live/dead staining by Annexin V/PI	33
3.3.4. Calcein-AM release experiments	34
3.3.5. Flow cytometry.....	34
3.3.6. Genetic engineering for flank tumor models.....	34
3.4. Human and mouse 3D-lung tissue cultures (3D-LTCs).....	35
3.5. Animal experiments	35
3.5.1. Animals and maintenance	36
3.5.1.1. BALB/c WT mice for IT application of MSNs.....	36
3.5.1.2. C57BL/6 double flank tumor mice for IV application of MSNs	36
3.5.1.3. <i>Kras</i> mutant mice with lung tumors for IT application of MSNs	36
3.6. Protein analysis.....	37
3.6.1. Immunofluorescence analysis in cryo-sections (IHF).....	37

3.6.2. Immunohistochemistry (IHC) analysis in paraffin sections	38
3.6.3. Immunocytofluorescence (ICF)	38
3.6.4. Zymography	39
3.6.5. Preparation of cellular protein lysates	39
3.6.6. Western blot analysis.....	39
3.6.7. Protein corona analysis.....	40
3.6.8. Statistical analysis	40
4. Avidin-coated mesoporous silica nanoparticles as drug carriers in the lung	41
4.1. Introduction	41
4.2. Results	43
4.2.1. Deposition of the non-functionalized MSN _{NH₂} in mouse lungs.....	43
4.2.2. Homogeneous uptake of the functionalized MSN _{AVI} in mouse lungs	44
4.2.3. MSN instillation into the lungs does not affect lung histology	44
4.2.4. Comparing the uptake of MSN _{AVI} <i>versus</i> MSN _{NH₂}	45
4.2.5. Epithelial uptake of MSN _{AVI} in mouse lungs.....	46
4.2.6. MSN _{AVI} exert less cytotoxic effects than MSN _{NH₂} <i>in vitro</i>	47
4.3. Discussion	47
5. MMP9-responsive MSN_{AVI} particles for lung cancer therapy	49
5.1. Introduction	49
5.2. Results	50
5.2.1. Successful synthesis of MMP9-responsive MSNs.....	50
5.2.2. Cytotoxicity of MSNs in lung cancer cell lines	51

5.2.3. Induction of apoptosis by MSNs in lung cancer cell lines	52
5.2.4. MMP9-dependent calcein-AM release <i>in vitro</i>	53
5.2.5. MMP9-dependent cell death in lung cancer cell lines	56
5.2.6. Cell-secreted MMP9-induced death of lung cancer cell lines.....	58
5.2.7. Synergistic effect of combination therapy.....	59
5.2.8. Murine 3D-lung tissue cultures for MSN _{AVI} exposure.....	60
5.2.9. MSN _{AVI} -based MMP9-responsive drug release to murine 3D-LTCs	62
5.2.10. Co-localization of MMP9 and cleaved caspase-3 in murine 3D-LTCs	65
5.2.11. Human 3D-LTCs for MSN _{AVI} exposure	66
5.2.12. MMP9-responsive tumor cell death in human 3D-LTCs.....	67
5.3. Discussion	69
6. Combination therapy of lung cancer by EGFR- and CCR2-targeted MSNs	72
6.1. Introduction	72
6.2. Results	73
6.2.1. Complementary overexpression of EGFR and CCR2 in lung cancer	73
6.2.2. Synthesis and characterization of the receptor-targeted MSNs.....	74
6.2.3. Receptor-mediated targeting of MSNs <i>in vitro</i>	76
6.2.4. Systemic delivery of MSN _{GE11} <i>versus</i> MSN _{AVI} in mouse flank tumor models..	80
6.2.5. Local intratracheal delivery of MSN _{GE11} and MSN _{ECL1i} in <i>Kras</i> mutant transgenic mouse model	86
6.2.6. Protein corona formation on MSNs in distinct biological environments.....	92
6.3. Discussion	93

7. Concluding remarks	95
References	98
Abbreviations	119
Acknowledgements	123
Eidesstattliche Versicherung	124

Zusammenfassung

Trotz großer Forschungsanstrengungen ist Lungenkrebs die derzeit tödlichste Krebsform mit einer 5-Jahres-Überlebensrate von nur 15%. Lungentumore werden meist in einem fortgeschrittenen Stadium diagnostiziert, wenn der Tumor chirurgisch nicht mehr zu entfernen ist. Die Patienten werden dann meist nur mit Chemo- und/oder Strahlentherapie behandelt. Eine frühere Diagnose und zielgerichtete Therapie würden eine bessere Überlebenschance für die Patienten bedeuten. Neueste Forschungsergebnisse belegen die Vorteile von Nanopartikel-basierten Ansätzen für die Diagnose und Therapie von Tumoren. Solche Nanopartikel-basierte Therapeutika ermöglichen einen gezielten Wirkstofftransport zur Tumorkläsion, welcher die systemischen Nebenwirkungen im Vergleich zu einer Chemotherapie deutlich reduzieren würde.

In der vorliegenden Dissertation wurde der Frage nachgegangen, ob mesoporöse Silikananopartikel (MSN) für die nanomedizinische Therapie von Lungentumoren verwendet werden können. Dieses Konzept wurde mittels funktionalisierter Nanopartikel *in vitro*, in Tiermodellen *in vivo* sowie in *ex vivo* Lungentumorgewebe von Lungenkrebspatienten untersucht.

In einem ersten Ansatz wurden die Biodistribution sowie die Aufnahme von Avidin-funktionalisierten vs. nicht-funktionalisierten MSN nach intratrachealer Gabe der Nanopartikel in gesunden Wildtyp-Mäusen untersucht. Während die nicht-funktionalisierten MSN nach lokaler Gabe in die Lunge zeitnah von Alveolarmakrophagen phagozytiert wurden, wurden die Avidin-funktionalisierten MSN zunächst von alveolären Epithelzellen aufgenommen und reicherten sich erst nach circa drei Tagen in den Makrophagen der Lunge an. Diese Daten belegen somit das Potential, Avidin-funktionalisierte MSN für den zielgerichteten Transport von Wirkstoffen in das pulmonale Epithel einzusetzen.

In einem weiteren Ansatz untersuchten wir das Konzept der Stimulus-abhängigen Freisetzung von Wirkstoffen aus funktionalisierten MSN. Dazu wurden MSN hergestellt, die sich mittels eines Matrixmetalloproteinase 9 (MMP9)-sensitiven Linkers öffnen lassen, um das in ihnen geladene Chemotherapeutikum freizusetzen. In Tumorzellen konnten wir *in vitro* zeigen, dass die Freisetzung des Medikaments und das Absterben der Tumorzellen nur in Abhängigkeit von MMP9 erfolgte. Interessanterweise führte die gleichzeitige Beladung der MSN von zwei Chemotherapeutika zu einem additiven zytotoxischen Effekt. Die MMP9-abhängige

Wirkstofffreisetzung von MSN wurde in einem weitergehenden Ansatz in *ex vivo* Lungentumorkulturen getestet. Hierfür wurde Tumormaterial von transgenen Mäusen, die eine mutierte Variante des *Kras* Onkogens exprimieren und somit spontan Lungenkrebs entwickeln, sowie Adenokarzinomgewebe von Lungenkrebspatienten verwendet. Unsere Daten belegen einen MMP9-abhängigen Zelltod in diesen Geweben, der hochspezifisch für das Tumorgewebe und nicht in gesundem Gewebe zu beobachten war. Diese Ergebnisse veranschaulichen das vielversprechende Potential einer Stimulus-abhängigen Freisetzung von Wirkstoffen aus Nanopartikeln, welche bei einer gleichzeitigen Verminderung unerwünschter toxischer Nebeneffekte auf gesundes Gewebe tumorspezifisch zytotoxisch wirken.

Ein weiteres Projekt beschäftigte sich mit dem Tumor- und Immunzell-spezifischen Targeting mittels funktionalisierter MSN. MSN wurden dazu mit spezifischen Liganden für den Epidermalen Wachstumsfaktorrezeptor (EGFR) bzw. den C-C-Motiv-Chemokin-Rezeptor 2 (CCR2) funktionalisiert, um zielgerichtet EGFR- bzw. CCR2-überexprimierende Tumorzellen und Tumor-assoziierte Makrophagen zu erreichen. *In vitro* zeigten die funktionalisierten MSN eine EGFR-abhängige Aufnahme in EGFR-überexprimierenden Tumorzelllinien, während EGFR-negative Zelllinien signifikant weniger MSN aufnahmen. Die CCR2-spezifischen Partikel wurden in Abhängigkeit von der CCR2-Expression verstärkt von Makrophagen aufgenommen. In einem *in vivo* Experiment wurden die mit EGFR-Liganden funktionalisierten MSN sodann auf ihre Tumorzellspezifität hin untersucht. Dazu wurden in Mäusen zunächst durch Injektion von Tumorzellen subkutane Flankentumore induziert, die einerseits EGFR überexprimierten bzw. niedrige Expressionslevel von EGFR aufwiesen. Die nachfolgende systemische intravenöse Injektion funktionalisierter und Fluoreszenz-markierter MSN führte jedoch nicht zu einer spezifischen Anreicherung von EGFR-gerichteten MSN in EGFR-positiven Tumorzellen, wie die mikroskopische Untersuchung des Tumorgewebes zeigte. Vielmehr akkumulierten die MSN unabhängig von ihrer Funktionalisierung in Zellen der Leber. In ähnlicher Weise wurden sowohl EGFR- wie auch CCR2-gerichtete MSN nach lokaler Gabe der Partikel in *Kras*-Mäusen mit Lungentumoren unspezifisch von Alveolarmakrophagen aufgenommen und zeigten keinerlei Spezifität für die EGFR- und CCR2-überexprimierenden Tumorerläsionen. Diese Daten belegen einen Verlust der *in vitro* nachgewiesenen Spezifität bei *in vivo* Applikation funktionalisierter Nanopartikel sowohl bei systemischer wie auch lokaler Gabe und machen die Bedeutung einer stringenten *in vivo* Analyse Zelltyp-gerichteter Nanopartikel mit zellulärer Auflösung deutlich.

Zusammenfassend lässt sich sagen, dass die vorliegende Dissertation ein – wenn auch begrenztes – therapeutisches Potential funktionalisierter mesoporöser Silikananopartikel für die Therapie von Lungentumoren aufzeigt. Die funktionalisierten MSN werden nach lokaler Gabe vom pulmonalen Epithel aufgenommen. Eine Zelltyp-gerichtete Therapie mittels MSN erscheint eingeschränkt, da die phagozytierende Kapazität der Alveolarmakrophagen das Zelltyp-spezifische Targeting überwiegt. Hingegen bietet eine Stimulus-abhängige Wirkstofffreisetzung das Potential eines regional gut kontrollierbaren Wirkstofftransports. Diese vielversprechenden Ergebnisse tragen somit zu einer differenzierten Betrachtung des translationalen Potentials nanomedizinischer Ansätze bei und erfordern eine weitere Untersuchung in relevanten *in vivo* Lungentumormodellen.

Summary

Despite recent advancements, lung cancer is the most lethal cancer with a 5-year survival rate of 15%. It is mostly diagnosed at an advanced stage when the malignancy is non-resectable and the patients undergo radiation and/or chemotherapy. Early detection and targeted therapy of lung cancer, however, may offer benefits for patients and their prospective survival. Recent evidence supports the advantages of employing nanoformulations for diagnosis and treatment of cancer. Such nanomedicines have the potential for targeted delivery of drugs to cancer lesions with minimization of systemic side effects. In this thesis, we investigated the potential of mesoporous silica nanoparticles (MSNs) to be applied as nanomedicines for the treatment of lung cancer using *in vitro* and *in vivo* models as well as *ex vivo* lung tumor samples from cancer patients. In particular, we evaluated local lung-specific application of functionalized nanoparticles for lung tumor targeting.

Firstly, biodistribution and uptake of avidin-functionalized *versus* non-functionalized MSNs were analyzed upon intratracheal application into wild type mice lungs. Avidin-functionalized MSNs were rapidly taken up by alveolar epithelial cells, followed by macrophage clearance at later stages. In contrast, non-functionalized MSNs were rapidly cleared by alveolar macrophages in the lung. These data support the concept that avidin-functionalized MSNs can be used for fast delivery of drugs to the pulmonary epithelium.

In the next step, we investigated the concept of stimuli-responsive drug release from MSNs for tumor treatment. For that, we generated matrix metalloproteinase-9 (MMP9) -sensitive drug-loaded MSNs. Our *in vitro* data confirmed MMP9-specific drug release in lung cancer cell lines with no side effects. Encouragingly, a combination load of cisplatin and bortezomib in the same MSN system resulted in significantly enhanced cell death. To certify our *in vitro* findings in a more relevant model, we exposed 3D-lung tissue cultures (3D-LTCs) from human and mouse to drug-loaded MSNs. Our results validated MMP9-responsive drug release by local cell death in tumorous human and mouse 3D-LTCs *ex vivo*.

We further analyzed the potential of MSNs for cell-specific targeting using tumor cell- and immune cell-specific targeting ligands. We thus functionalized the particles with the artificial ligands GE11 and ECL1i to address epidermal growth factor receptor (EGFR) overexpressing lung tumors and C-C chemokine receptor type 2 (CCR2) overexpressing tumor-associated

macrophages, respectively. The functionalized nanoparticles both showed superior uptake in EGFR and CCR2 overexpressing cells *in vitro*, respectively. To prove our *in vitro* findings in *in vivo* setting, we exploited systemic and local delivery of the MSNs in mouse tumor models and monitored cell-specific targeting with cellular resolution. Intravenous application of the nanoparticles was studied in two distinct flank tumor models where subcutaneous tumors were formed within the same mouse at the right and left flanks with two corresponding cell clones that had high or low levels of EGFR, respectively. However, in both models significant deposition of the nanoparticles into the liver was observed irrespective of the functionalization on the particles. Similarly, nanoparticles that were intratracheally applied into the tumorous lungs of V-Ki-ras2 Kirsten rat sarcoma viral oncogene homolog (*Kras*) mutant mice were non-specifically taken up by hyperplastic tumor cells and alveolar macrophages regardless of their functionalization. These data show loss of cell-specific targeting efficiency of functionalized MSNs upon systemic and local delivery of the particles *in vivo* and thus stress the need for detailed analysis of targeting efficiency with cellular resolution.

Taken together, this study evaluates the potential of targeted mesoporous silica nanoparticles with controlled release function for lung cancer treatment. It supports the concept that functionalization of nanoparticles plays a vital role in their biodistribution and toxicity in the lung. Nonetheless, this study also reveals *in vivo* loss of targeting ability of receptor-targeted MSNs due to the high phagocytic capacity of the mononuclear phagocyte system. On the other hand, it proves effective stimuli-responsive release of drugs from these nanoparticles resulting in a well-controlled region-restricted therapeutic effect. All in all, this study not only shows the potential of nanomedicines for lung cancer treatment, but also stresses the impact of underlying mechanisms affecting nanoparticle biodistribution and specificity *in vivo* while highlighting the need for stringent analysis to detect and circumvent these factors for better understanding and clinical translation of future nanomedicines.

1 Introduction

1.1 Lung Cancer

In spite of vast continuous research, cancer remains to be a major cause of morbidity and mortality all around the world. Lung cancer, in particular, is by far the most common cause of cancer-related deaths in the world (Figure 1.1) (Ferlay et al., 2013; Gridelli et al., 2015). The five-year survival rate for lung cancer patients is around 15%. Patients are usually diagnosed at an advanced stage with metastasis due to lack of biomarkers and early diagnostic tools, hence the treatment options for lung cancer are mostly palliative (Bölükbas and Meiners, 2015; Herbst et al., 2008).

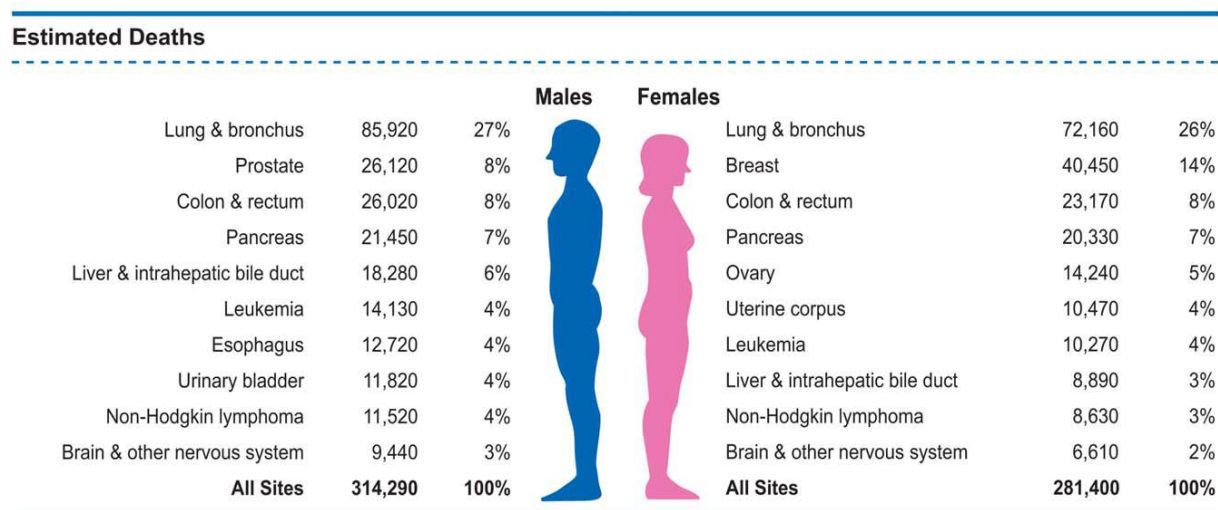


Figure 1.1 The most common cancer types in the USA by gender, 2016 (Siegel et al., 2016)

Lung cancer is classified into several histological subtypes such as small cell lung cancer (SCLC) and non-small cell lung cancer (NSCLC) types of lung adenocarcinoma, squamous cell carcinoma, and large cell carcinoma (Figure 1.2) (Gridelli et al., 2015). While SCLCs and squamous cell carcinomas form around the major bronchi, adenocarcinomas and large cell carcinomas mostly arise at the peripheral regions of the lung (Wistuba and Gazdar, 2006).

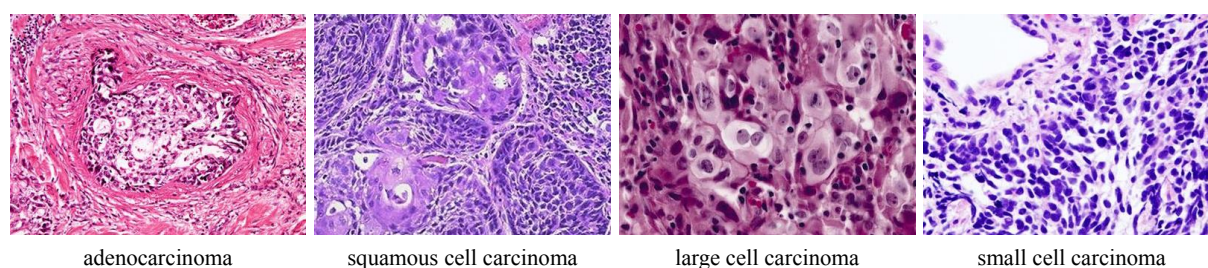


Figure 1.2 Major histopathological types of lung cancer (edited from cancergrace.org)

Smoking is a risk factor for all types of lung cancer, most particularly for SCLC and squamous cell carcinoma, whereas adenocarcinoma is mostly seen in non-smokers (Huang et al., 2015). In fact, 25% of all lung cancer cases are observed in non-smokers globally, *i.e.*, 15% of cases in men, 53% in women (Subramanian and Govindan, 2007). Strong molecular differences between these two groups have been identified, giving evidence that tobacco-induced and not-induced subtypes are indeed two different entities (Sun et al., 2007).

Second-most common risk factor for lung cancer is second-hand smoke exposure depending on the duration time and intensity of the exposure (Collins et al., 2007). The leading occupational risk factor for lung cancer however is asbestos. Several other lung cancer inducing factors are radon, arsenic, chromium, nickel, vinyl chloride, and ionizing radiation (Field and Withers, 2012; Ruano-Ravina et al., 2014). Moreover, preexisting lung diseases such as chronic obstructive pulmonary disease (COPD), idiopathic pulmonary fibrosis (IPF), or tuberculosis are identified as risk factors for lung cancer too (Collins et al., 2007).

1.1.1 Pathogenesis of lung cancer

1.1.1.1 Molecular alterations

Although the origins of the distinct lung cancer types are not fully understood, it is believed that lung cancer arises upon pathological changes known as preneoplastic or premalignant lesions (Westra, 2000; Wistuba et al., 2002). Despite the fact that many genetic and epigenetic changes have been detected in lung cancer biopsies (Minna et al., 2002; Zöchbauer-Müller and Minna, 2000), the underlying mechanisms which lead to these changes are poorly known. Majority of those studies have been performed for the most common types of lung cancer. Several growth factor receptors and regulatory peptides have been found to be overexpressed by cancer cells next to the healthy epithelium, and contribute to further proliferation of the cancer. Indeed, the approach of chemotherapy shifted from applying the same drug to one type of cancer to formulating new strategies to target the drivers of the disease in each tumor (Ene and Fine, 2011). However due to intratumor heterogeneity, multiple drivers may play a role in tumor formation, and might be addressed with several specific agents applied in parallel (Duffy, 2013). Common oncogenes triggering lung oncogenesis involve v-myc avian myelocytomatosis viral oncogene homolog (*CMYC*), mutant Kirsten rat sarcoma viral oncogene homolog (*KRAS*), translocations of the anaplastic lymphoma kinase (*ALK*) gene (Shaw and Engelman, 2013), overexpressed *Cyclin D1*, B-cell lymphoma 2 (*BCL2*), and mutant ERBB family genes such as epidermal growth factor

receptor (*EGFR*) (Paez et al., 2004; Shigematsu et al., 2005) and receptor tyrosine-protein kinase erbB-2 (*HER2*) (predominantly in the Asian population and in non-smokers) (Table 1.1) (Network, 2012, 2014; Project and NGM, 2013; Stephens et al., 2004). In addition, abnormalities in several tumor suppressor genes such as tumor protein 53 (*TP53*) or retinoblastoma protein (*RB*) are also evident in lung cancer (Cerami et al., 2012; Wistuba and Gazdar, 2006).

Table 1.1 Major lung-specific genetic abnormalities in lung cancer (Herbst et al., 2008)

Abnormality	NSCLC		SCLC
	Adenocarcinoma	Squamous cell carcinoma	
Precursor			
Lesion	atypical adenomatous hyperplasia (probable)	dysplasia	neuroendocrine field (probable)
Genetic change	KRAS mutation, EGFR mutation	p53 mutation	c-MET overexpression
Cancer			
KRAS mutation	10-30%	very rare	very rare
BRAF mutation	2%	3%	very rare
EGFR			
Kinase domain mutation	10-40%	very rare	very rare
Amplification	15%	30%	very rare
Variant III mutation	very rare	5%	very rare
HER2			
Kinase domain mutation	4%	very rare	very rare
Amplification	6%	2%	not known
ALK fusion	7%	very rare	not known

c-MET: hepatocyte growth factor receptor, *BRAF*: v-Raf murine sarcoma viral oncogene homolog B, *HER2*: receptor tyrosine-protein kinase erbB-2

1.1.1.2 Tumor microenvironment and immunotherapy

Lesions are not only composed of cancer cells. Genetic alterations alone were reported to be insufficient for complete tumor growth and metastasis without the contribution of local non-malignant parenchymal cells (Coussens and Werb, 2002; Hanahan and Weinberg, 2000). There are indeed numerous non-malignant cell types which are associated with the tumor microenvironment (TME) (Balkwill et al., 2012), forming a complex platform rich of vital chemokines, cytokines, growth factors for tumor survival and progression (Hanahan and Coussens, 2012). For instance, various reports support the idea that proteinases such as matrix metalloproteinases (MMPs) drive extracellular matrix (ECM) remodeling at tumor sites and set the ground for cancer cell migration. As MMPs control several physiological events and cellular signaling, they are crucial for the communication between tumor and stroma (Kessenbrock et al., 2010). In particular, matrix metalloproteinase-9 (MMP9), degrading a variety of ECM components such as collagens, elastin, and fibrin (Roeb et al., 2002), has been shown to be commonly overexpressed in lung cancer patients (El-Badrawy et al., 2014) and correlates with poor prognosis of the disease (Cox et al., 2000; Shou et al., 2001).

One of the most encouraging recent strategies for lung cancer treatment is immunotherapy (Gridelli et al., 2015). Several studies have investigated therapeutic efficiency of targeting programmed cell death protein 1 (PD1) or cytotoxic T-lymphocyte-associated protein 4 (CTLA4) checkpoint pathways of T cells (Brahmer et al., 2012; Topalian et al., 2012). Normally, when CTLA4 binds to its ligands, cluster of differentiation 80 (CD80) and cluster of differentiation 86 (CD86), on the antigen-presenting cells, proliferation of T cells is inhibited. Likewise, when PD1 binds to its ligands, (programmed death-ligand 1) PDL1 or (programmed death-ligand 2) PDL2, T cell proliferation is inhibited, but in addition it interferes with cytokine production and results in T cell exhaustion (Fife and Bluestone, 2008). A human monoclonal CTLA4-specific antibody, Ipilimumab, which is already FDA-approved for melanoma treatment, has shown heartening results in patients with advanced-stage squamous NSCLC when combined with carboplatin and paclitaxel (Gridelli et al., 2015; Lynch et al., 2012). PD1-targeting monoclonal antibodies nivolumab and pembrolizumab have also shown promising results and are in clinical development. Further successful examples of immunotherapy in lung cancer involve monoclonal antibodies BMS-936559, MPDL3280A, and MEDI4736, targeting PDL1 (Casaluce et al., 2014; Herbst et al., 2014).

Among the most commonly reported immune cell types in lung cancer TME are tumor-associated macrophages (TAMs). There is indeed a valid correlation between poor prognosis and macrophage density in various cancer types including lung cancer (Qian and Pollard, 2010). Based on their phenotype, macrophages at tumor lesions can have tumor preventive or tumor promoting effects (Mosser and Edwards, 2008). Nonetheless, as tumors grow larger, TME strongly influences TAMs. Numerous growth factors and chemokines play a role in macrophage differentiation and chemotaxis (Pollard, 2009). TAMs possess common features with the regulatory type of macrophages (Murray and Wynn, 2011; Pollard, 2008). For instance, recent studies showed that cancer cells can secrete C-C chemokine ligand 2 (CCL2) and attract macrophages to the tumor site (Qian et al., 2011; Zhang et al., 2010). CCL2 overexpression was confirmed in a variety of cancer types (Mantovani and Sica, 2010) and this corresponds to poor prognosis of the disease (Qian and Pollard, 2010), whereas its absence was demonstrated to have tumor preventive effects in patients with cervical cancer (Zijlmans et al., 2006). Indeed in lung cancer, a recent study revealed the presence of a cross-talk between TAMs and tumor cells via CC chemokine receptor type 2 (CCR2), and its inhibition resulted in less tumor formation in lung cancer mouse models *in vivo* (Schmall et al., 2015).

1.1.2 Diagnosis and treatment of lung cancer

90% of all lung cancer patients present symptomatic at the stage of diagnosis (Collins et al., 2007). Only 10% are diagnosed asymptomatic with chest radiographs. Most of the patients present with systemic symptoms of fatigue, anorexia, and weight loss. Chest discomfort, cough, dyspnea, and hemoptysis are the most common signs of primary tumors.

Treatment of lung cancer depends heavily on the type of lung cancer, the stage of the disease at diagnosis (Table 1.2), and functional analysis of the patients. Surgery is the optimal treatment option for early stage lung cancer, which is mostly followed by chemotherapy (Collins et al., 2007). However majority of the NSCLC tumors are unresectable and require treatments with chemotherapy and radiation therapy. Likewise, SCLCs are mostly treated with chemotherapy.

Table 1.2 Staging of lung cancer (Spira and Ettinger, 2004)

Stage	Description	Survival rate	
		1 yr	5 yr
NSCLC			
Local			
IA	tumor \leq 3 cm, surrounded by lung or pleura, no invasion of main bronchus	94	67
IB	tumor $>$ 3 cm, invasion of pleura, main bronchus	87	57
IIA	tumor \leq 3 cm, invasion of ipsilateral peribronchial or hilar nodes and intrapulmonary nodes	89	55
Locally advanced			
IIB	tumor $>$ 3 cm, invasion of chest wall, diaphragm, pericardium	73	39
IIIA	invasion of ipsilateral mediastinal or subcarinal nodes	64	23
IIIB	invasion of contralateral lung nodes or any supraclavicular node	32	3
Advanced			
IIIB	invasion of mediastinum, heart, great vessels, trachea, esophagus, vertebral body, carina, separate tumor nodules, malignant pleural effusion	37	7
IV	distant metastasis	20	1
SCLC			
Limited disease	confined to the ipsilateral hemithorax		
Extensive disease	metastasis beyond the ipsilateral hemithorax		

Being the ideal treatment for early stage NSCLC (Chuang et al., 2017), lung cancer surgery may include pneumonectomy, lobectomy, or lymph node dissection if the tumor has spread to mediastinal nodes (Cariboni and Stella, 2015; Collins et al., 2007). Adjuvant therapy is the term used for radiation or chemotherapy once the tumor has already been resected surgically. Adjuvant radiotherapy is used for elimination of small lesions left after surgery at the region of resection. Even at early stage lung cancers, there might still be remaining cancer cells left after surgical resection at the microscopic level. Thus, adjuvant chemotherapy must be applied in order to eliminate micrometastases. Platinum-based agents are the most commonly used chemotherapeutics, as these are the most effective ones against NSCLC (Spira and Ettinger, 2004). Neoadjuvant therapy stands for the use of radiation or chemotherapy for cancer treatment as the primary option, where surgery is not preferred (Chuang et al., 2017). Neoadjuvant radiotherapy aims for shrinkage in tumor size, making a surgical resection possible afterwards. Neoadjuvant chemotherapy instead, can result in tumor shrinkage in addition to elimination of micrometastases (Spira and Ettinger, 2004).

Stage III lung tumors as well as tumors which are localized at vital regions are categorized as nonresectable. At this stage, concurrent radiation and cisplatin-based chemotherapy have been the gold standard. At advanced stages like IIIB or IV, the treatment heavily depends on chemotherapy, however with poor prognosis (Spira and Ettinger, 2004).

1.1.2.1 Targeted therapies for lung cancer

Discoveries of somatic driver mutations in lung tumors have paved the way for development of novel agents which are directed against these mutations. Treating lung cancer with conventional platinum-based chemotherapy has started to be shifted to a more personalized manner since 2005 by such targeted therapies (Jett and Carr, 2013). The first agents were designed to target the first discovered driver mutation in lung cancer, *i.e.* EGFR mutation at its tyrosine kinase (TK) domain (Paez et al., 2004). Driver mutations result in disrupted signaling for proteins vital for controlled cellular proliferation and tumorigenesis. In NSCLC patients with EGFR mutations, *i.e.* exon 19 deletion or exon 21 mutation (L858R), EGFR-TK inhibitor (EGFR-TKI) gefitinib had resulted in dramatic responses (Vecchione et al., 2011). This was followed by identification of another mutation which was confirmed for the transforming echinoderm microtubule-associated protein like 4 (EML4) -(ALK) gene fusion (Soda et al., 2007) in NSCLC tumors. By continuous research many more mutations have been identified such as BRAF, KIT proto-oncogene receptor tyrosine kinase (KIT), and HER2 (Haber et al., 2011). Similar to gefitinib, novel small-molecule inhibitors directed against these mutations resulted in significant initial regression in tumors, however most of which were followed by acquired-resistance of the tumors (Chong and Jänne, 2013). Such resistance forms as a result of a secondary mutation against the activity of the inhibitors in resistance-acquired variants. Consequently, targeted therapies may result in an encouraging regression of the tumors initially, however most of the times this effect is not steady due to acquired-resistance and aggressive re-growth of the tumors. Alternative approaches to enhance therapeutic efficiency of targeted therapies involve simultaneous use of conventional chemotherapy or immunotherapy for a more persistent outcome (Sawyers, 2004; Vanneman and Dranoff, 2012).

1.2 Nanoparticle-based drug delivery

Over the last decades, there have been various studies supporting the use of nanotechnology in diagnosis and treatment of human diseases, most particularly in cancer research. Materials at the nanoscale engineered for biomedical purposes, termed as nanomedicines, can vary in sizes, compositions, shapes in accordance with the disease to be applied (Figure 1.4). In addition to their use as early diagnostic agents, nanomedicines offer various therapeutic advantages such as prolonged circulation of the active drug, enhanced local concentrations at the disease site, reduced systemic toxicity, and cell-specific targeting (Doane and Burda, 2012; Duncan and Gaspar, 2011; Peer et al., 2007; Schütz et al., 2013; Wagner et al., 2006; Wang et al., 2012).

So far, there have been various kinds of nanoparticles generated such as dendrimers, micelles, liposomes, polymeric nanoparticles, carbon nanotubes, mesoporous silica nanoparticles, metallic nanoparticles, protein nanoassemblies, and much more (Figure 1.4). The features the nanoparticles possess depend heavily on the type of the particle and its surface characterizations (Torchilin, 2014; van Rijt et al., 2014).

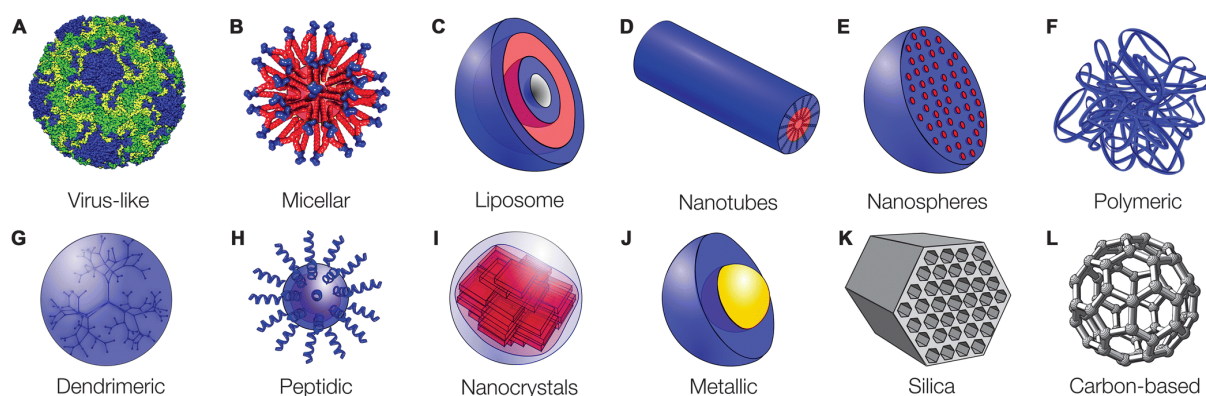


Figure 1.4 Several types of nanoparticles used for biomedical applications (Ageitos et al., 2016)

1.2.1 Passive *versus* active targeting of nanoparticles

Deposition of nanomedicines in diseased regions depends on two distinct targeting approaches: passive *versus* active targeting. Passive targeting is based on so-called enhanced permeability and retention (EPR) effect (Figure 1.5) (Matsumura and Maeda, 1986). This principle works as nanomedicines travel through the bloodstream, they cannot escape through the blood vessels of healthy regions, whereas in tumorous regions they penetrate through the leaky pathological blood vessels and accumulate at the tumor site also due to the impaired lymphatic drainage present at the tumor site (Figure 1.5).

Active targeting of nanomedicines, on the other hand, is achieved by surface functionalizations of nanoparticles with monoclonal antibodies or ligands that specifically target tumor-related antigens or receptors (Peer et al., 2007) (Figure 1.5, top right frame). For this, nanoparticles are constructed to specifically bind to targets that are overexpressed only on cancer cells (Gu et al., 2007). Thus, active targeting may be more effective than passive targeting strategies as it gives the possibility of targeting and killing of not only primary tumors but also circulating metastatic cancer cells.

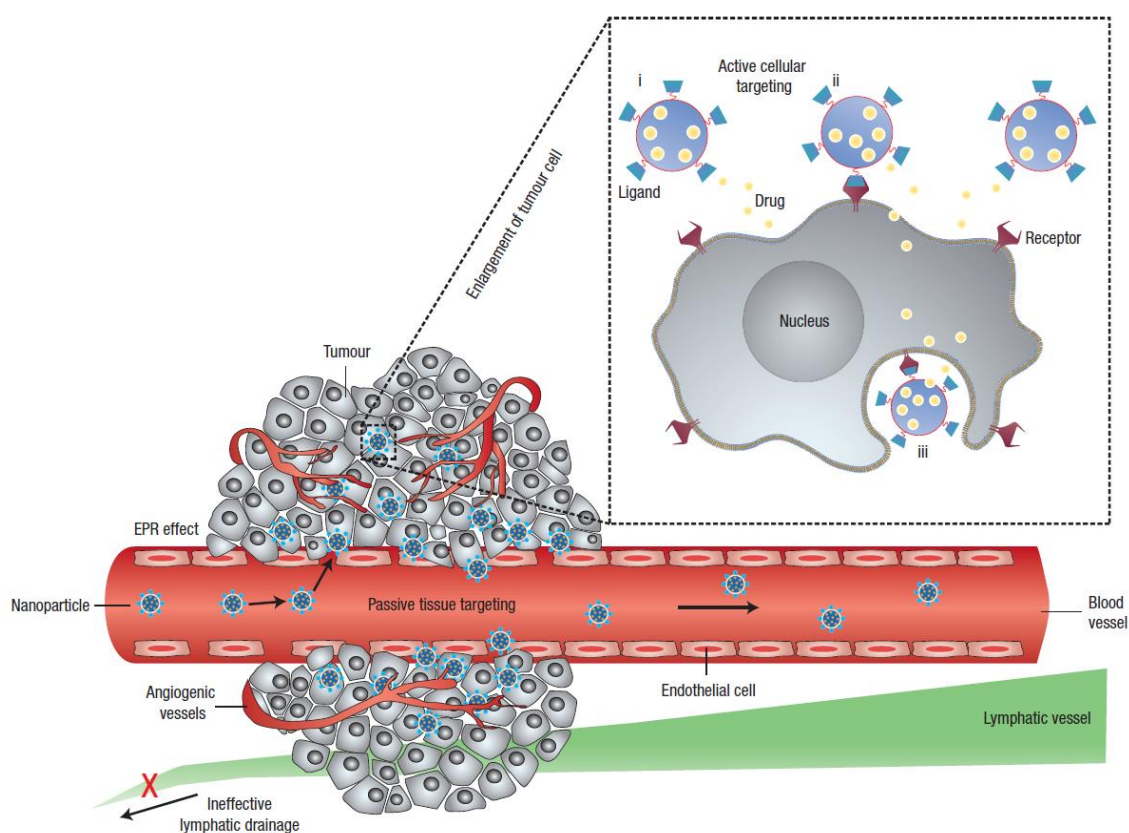


Figure 1.5 Nanoparticle accumulation at tumor site via passive *versus* active targeting (Peer et al., 2007)

1.2.2 Theranostic nanoparticles

Another emerging concept of nanomedicines is nanotheranostics. The term defines nano-platforms that are designed both for imaging and therapy simultaneously. Thus, these particles allow for disease monitoring and treatment in parallel (Janib et al., 2010; Lim et al., 2015). Ideal features for theranostic nanoparticles are, specific and rapid localization at the region of interest, stating molecular and morphological information about the tissue, successfully unloading the drug with no adverse effects in off-target or healthy tissue, leaving the body in short time or biodegrading into safe products (Chow and Ho, 2013; Jokerst and Gambhir, 2011). Just as any nanomedicine, theranostic particles may contain targeting moieties and additional functionalization such as shielding molecules to induce biocompatibility. But in addition, theranostic particles contain therapeutics and contrast agents within their formulation (Figure 1.6). These contrast agents allow for non-invasive detection of the nanoparticles in a variety of modalities such as optical imaging, magnetic resonance imaging (MRI), computer tomography (CT), or positron emission tomography (PET) (Lim et al., 2015).

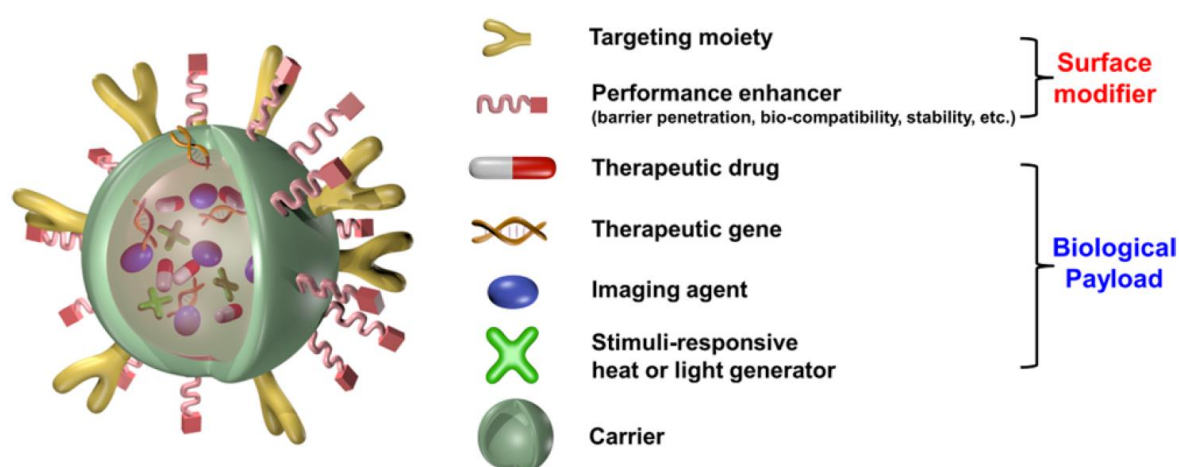


Figure 1.6 Schematic representation of theranostic nanoparticles (Lim et al., 2015)

Up to date, there have been several examples for efficient theranostic applications of nanomedicines for passive targeting but not so much for active targeting (Chen et al., 2014). Some examples to these nanocarriers involve several MRI contrast agents by superparamagnetic nanoparticles (Lee et al., 2011; Mertens et al., 2014), carbon nanotube-based optoacoustic imaging agents (De La Zerda et al., 2008), and photothermal polymeric nanoparticles (Yang et al., 2011).

1.2.3 Cell-specific delivery of nanoparticles

Potency of cell-specific targeting with nanoparticles opens many doors for targeting not only the tumor cells but also non-malignant cells (Irvine et al., 2015). For instance, nanoparticles targeted to immune cells for drug delivery offer several advantages for a more specific immunotherapy with less off-target effects (Moyer et al., 2016). Additionally, solid tumors may potentiate structural hurdles in delivery of nanoparticles due to rigid tumor stroma (Jain and Stylianopoulos, 2010), however immune cells which are also present in the circulation and in immune organs can be targeted more efficiently (Glass et al., 2016).

Among the immune cells, in particular macrophages offer several benefits, *e.g.*, high endocytosis activity, and represent as potential targets for drug delivery via nanoparticles (Jain et al., 2013; Weissleder et al., 2014). Indeed, several studies have shown successful delivery of nanoparticles to macrophages for treatment of several diseases (Chono et al., 2007, 2008; Muraoka et al., 2014; Pei and Yeo, 2016; Schmitt et al., 2010; Wijagkanalan et al., 2011).

1.2.4 Pulmonary application of nanoparticles

The lung is indeed a well-fit organ for local or systemic administration of nanoparticles by inhalation, as it offers a large surface area with thin epithelial barrier, rapid absorption, high bioavailability, limited proteolytic activity, and the lack of first-pass metabolism (Sung et al., 2007). Additionally, the charge and size of the nanoparticles play a role for their deposition inside the lung: particles smaller than 200 nm are mostly delivered to the respiratory airways (Figure 1.6) (Choi et al., 2010; van Rijt et al., 2014), whereas larger particles are removed via mucociliary clearance. On top of that, pulmonary application of nanomedicines is further attractive since it is noninvasive and patients have the possibility for self-administration.

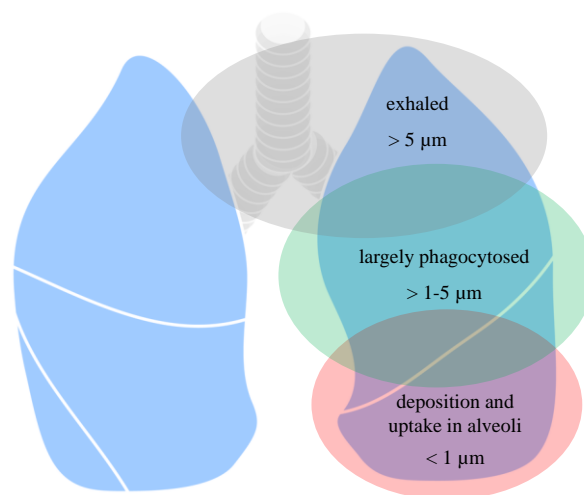


Figure 1.6 Size-dependent deposition of particles in the lung (van Rijt et al., 2014)

In fact, there have been numerous preclinical studies showing improved therapeutic efficacy of nanomedicines for lung diseases (Howell et al., 2013; Lu et al., 2014; Ozeki and Tagami, 2014; Ruge et al., 2013; Thorley and Tetley, 2013; van Rijt et al., 2014), most particularly for lung cancer (Babu et al., 2013; Badrzadeh et al., 2014; Bandyopadhyay et al., 2015; Bölükbas and Meiners, 2015; Fujita et al., 2015; Key et al., 2014; Kim et al., 2015; Sukumar et al., 2013).

1.2.4.1 Preclinical studies of nanomedicines for lung cancer treatment

Numerous nanomedicines with several functions have been developed and tested experimentally in preclinical models as potential treatment strategies for lung cancer. Literature research shows that the span of particle design, targeting strategy, administration route, and experimental models used is vast. Table 1.4 summarizes recent studies with nanomedicines which have been designed for active targeting of lung cancer in experimental models. In some studies, tumor-specific activators such as overexpressed tumor-associated proteases were used to activate the particles for contrast enhancing in imaging or for controlled drug release at the tumor site (Crisp et al., 2014; van Rijt et al., 2015). In the study by Crisp *et al.* for instance, MMP2-stimulated activation of alpha-v beta-3 ($\alpha_v\beta_3$)-targeted particles was used for detection of lung metastases that are smaller than 0.5 mm by use of fluorescence imaging as a result of the high local MMP2 concentrations (Crisp et al., 2014).

Table 1.4 Recent preclinical studies on active targeting of lung cancer (Bölükbas and Meiners, 2015)

Target	Trigger	Model	Type	Reference
EGFR	-	s.c. human lung cancer cells	conjugated	(Peng et al., 2011)
			liposomal	(Cheng et al., 2014)
			mesoporous silica-based	(Sundarraj et al., 2014)
		i.v. human lung cancer cells	polymeric	(Karra et al., 2013)
	magnetic field	i.v. human lung cancer cells	SPIONs	(Sadhukha et al., 2013)
$\alpha_v\beta_3$	MMP2	i.v. murine mammary tumor cells	peptide-based	(Crisp et al., 2014)
	-	i.v. murine melanoma cells	liposomal	(Yonenaga et al., 2012)
		s.c. human lung cancer cells	peptide-based	(Liu et al., 2014)
		i.t. murine lung cancer cells	Au-based	(Conde et al., 2013)
sigma receptor	pH	s.c. human lung cancer cells	lipid/calcium /phosphate	(Li et al., 2010; Li et al., 2012; Yang et al., 2012a; Zhang et al., 2013a)
		i.v. murine melanoma cells	lipid/calcium /phosphate	(Yang et al., 2012b)
		s.c., sur. human lung cancer cells	lipid/calcium /phosphate	(Zhang et al., 2013b)
CD44	-	s.c. human lung cancer cells	conjugated	(Ganesh et al., 2013b)
		s.c. human lung cancer cells, i.v. murine melanoma cells	conjugated	(Ganesh et al., 2013a)
DR 4/5	-	s.c. human lung cancer cells	conjugated	(Guo et al., 2012)
		i.v. human lung cancer cells	polymeric	(Kim et al., 2013)
			protein-based	(Choi et al., 2015)
LHRHR	-	i.t. human lung cancer cells	lipid-based	(Taratula et al., 2013)
			mesoporous silica-based	(Taratula et al., 2011b)
		s.c. human lung cancer cells	SPIONs/ dendrimeric	(Taratula et al., 2011a)
$\alpha_v\beta_6$	-	s.c. human lung cancer cells	liposomal	(Gray et al., 2013)
$\alpha_v\beta_3$, neuropilin-1	-	s.c. human lung cancer cells	peptide-based	(Shen et al., 2013)
DR 4/5, ES ligand	-	i.v. human colon cancer cells	liposomal	(Mitchell et al., 2014)
transferrin receptor	-	s.c. human lung cancer cells	lipid-based	(Guo et al., 2015; Han et al., 2014)
EphA2	-	i.v., sur. human lung cancer cells	lipid-based	(Patel et al., 2014a)

LDLR	irradiation	i.v. murine breast cancer cells, transgenic (<i>EML4-ALK</i>)	B/Gd-based	(Alberti et al., 2015)
folate receptor	-	s.c. human lung cancer cells	liposomal	(Morton et al., 2014)
laminin receptor	-	s.r. murine melanoma cells	polymeric	(Sarfati et al., 2011)
phosphatidylserine	pH	s.c. human lung cancer cells, i.v. murine lung cancer cells	protein /lipid-based	(Zhao et al., 2015)
PSMA	-	s.c. human lung cancer cells	polymeric	(Hrkach et al., 2012)
HER2	irradiation	s.c. human lung cancer cells	Au/Ag-based	(Shi et al., 2014)
IGF-1R	magnetic field	s.c. human lung cancer cells	magnetic lipoplexes	(Wang et al., 2011)
GC4	-	i.v. murine melanoma cells	liposomal/ protein-based	(Chen et al., 2010)
CD47	-	i.v. murine melanoma cells	liposomal/ protein-based	(Wang et al., 2013)
NSCLC	-	s.c. human lung cancer cells	peptide-based/ dendrimeric	(Liu et al., 2011)
clotted plasma proteins	-	i.v., i.t. human lung cancer cells	lipid-based	(Patel et al., 2014b)
neoplasms	irradiation	i.v. murine colon carcinoma cells	protein-based	(Yang et al., 2010)

CD44: cluster of differentiation 44, *DR 4/5*: death receptor 4/5, *LHRHR*: luteinizing hormone releasing hormone receptor, $\alpha_v\beta_6$: alpha-v beta-6 integrin, *ES*: E-selectin, *EphA2*: ephrin type-A receptor 2, *LDLR*: low density lipoprotein receptor, *PSMA*: prostate-specific membrane antigen, *IGF-1R*: Insulin-like growth factor 1 receptor, *CD47*: cluster of differentiation 47, *s.c.*: subcutaneous, *i.v.*: intravenous, *i.t.*: intratracheal, *s.r.*: subretinal, *sur.*: surgical, *SPIONs*: superparamagnetic iron oxide nanoparticles

1.2.4.2 Clinical studies of nanomedicines for lung cancer treatment

Nanomedicines ultimately aim for targeted delivery of the agents and eliminate adverse side effects by avoiding off-route targets. The very first FDA-approved nanoparticle-based drug is called Doxil and it has been in use to treat several malignancies such as refractory metastatic ovarian cancer and AIDS-related Kaposi's Sarcoma for over 20 years (Barenholz, 2012). Doxil is a PEGylated liposomal formulation of doxorubicin and its therapeutic efficacy is based on the EPR effect. Patients treated with Doxil present with less side-effects and prolonged survival rates. Doxil was also evaluated for treatment of lung tumors of NSCLC, SCLC, or mesothelioma either as a monotherapeutic agent or in combination with other agents in phase I to III clinical trials and resulted in promising efficacies (clinicaltrials.gov) (Koukourakis et al., 2002; Numico et al., 2002; Patlakas et al., 2005; Samantas et al., 2000; Skubitz, 2002; Tsoutsou et al., 2008). Yet, the first FDA-approved nano-based drug for lung cancer treatment is a nanoformulation of albumin-bound paclitaxel called nab-Paclitaxel,

Abraxane (Bölükbas and Meiners, 2015). Abraxane is applied as a combination therapy in patients with advanced or metastatic NSCLC. Approval of the first nano-based lung cancer drug has led to several studies investigating its application further on NSCLC and SCLC (Grilley-Olson et al., 2015; Lammers et al., 2015; Langer et al., 2014). Likewise, a liposomal formulation of cisplatin, called Lipoplatin, was also developed and evaluated for NSCLC and mesothelioma treatment in several studies (Fantini et al., 2010; Stathopoulos et al., 2011). These studies resulted in at least a comparable therapeutic efficacy but with significantly less toxicity in comparison to cisplatin (Stathopoulos and Boulikas, 2011).

More examples of nanomedicines in the clinics are given in Table 1.5. Genexol-PM which is a polymeric micellar formulation of paclitaxel, has been the second agent to be clinically approved for lung cancer therapy (in East Asia). Genexol-PM has shown significant therapeutic efficacy in advanced NSCLC patients when combined with cisplatin in Phase II trials (Kim et al., 2007), yet there have been some studies reporting some adverse effects of Genexol-PM treatment as well (Ahn et al., 2014; Kim et al., 2011).

Table 1.5 Clinical nanomedicines for lung cancer treatment (Bölükbas and Meiners, 2015)

Product	Formulation	Company	Indication	Phase
Abraxane	albumin-bound paclitaxel	Celgene Co.	NSCLC	FDA-approved
Genexol-PM	paclitaxel-loaded micelle	Samyang Co.	NSCLC	approved
Paclitaxel poliglumex	polyglutamate paclitaxel	CTI BioPharma	NSCLC	III
MPDL3280A	anti-PDL1 antibody	Genentech	NSCLC	III
Tecemotide	liposomal vaccine	Oncothyreon	NSCLC	III
Doxil	liposomal doxorubicin	Johnson & Johnson	SCLC	II
BIND-014	targeted docetaxel	Bind Therapeutics	NSCLC	II
CRLX101	polycyclodextrin camptothecin	Cerulean Pharma	SCLC	II
NKTR 102	PEGylated irinotecan	Nektar Therapeutics	lung metastases	II
Kadcyla	Ab-emtansine conjugate	Genentech	NSCLC	II
IMMU-132	Ab-SN-38 conjugate	Immunomedics inc	NSCLC	I/II
IMGN901	Ab-mertansine conjugate	ImmunoGen	SCLC	I/II

NC-6004	micellar cisplatin	NanoCarrier Co.	NSCLC	I/II
MM-398	liposomal irinotecan	Merrimack Pharmaceuticals	NSCLC	I
DNIB0600A	Ab-MMAE conjugate	Genentech	NSCLC	I
AuroShell	Gold-silica nanoshells	Nanospectra Biosciences	lung cancer	I

1.2.5 Challenges of nanomedicines

In spite of the tremendous amount of publications within the last decades on lung cancer nanomedicines, pulmonary application of these agents is undoubtedly restricted by their potential toxic and inflammatory side-effects (Ferreira et al., 2013). Yet, there are additional challenges to achieve the complete translation of nanomedicines for lung disease therapy (Bölükbas and Meiners, 2015). Generation of novel clinical nanotherapies heavily depends on new technologies in nanoparticle formulations, discoveries of novel cell-specific receptors, findings about tumor-heterogeneity and microenvironment, and use of realistic animal models. Moreover, biomarkers of different types of lung tumors must be identified in detail for a more personalized application (Network, 2012; Rizvi et al., 2015; Schulze et al., 2015; Suzuki et al., 2015). At this step, having limited information on different cell-specific receptors of lung tumors is the first drawback active targeted nanotherapies face. Furthermore, in a large number of studies, validation analyses involving nanoparticle penetration in targeted tissue/organ and accumulation of particles in targeted cells in appropriate animal models in cellular resolution are often ignored.

Another inevitable challenge the nanomedicine society faces is the mass production and characterization of the nanoparticles as well as to meet the demands of FDA or EMA for clinical approval. Moreover, sophisticated nanoformulations suffer from reproducibility and stability. Collectively, numerous factors burden the clinical translation of nanomedicines with high costs and risks. An alternative approach to tackle these problems could start with a close interaction between all partners including academia, pharmaceutical industry, and physicians.

2 Aims of the study

Despite recent advancements, lung cancer remains to be the most common cause of deaths among all malignancies. The majority of the patients are treated with conventional chemotherapy which is however limited due to its serious side effects and acquired resistance. Recent studies encourage the use of stimuli-responsive nanocarriers for a more targeted treatment of diseases with lower systemic toxicity. Nanomedicines also have the potential for combinatorial targeting of lesions as well as delivery of a combination of drugs within the same system. In this regard, novel mesoporous silica nanoparticles (MSNs) offer numerous advantages for controlled drug delivery; nevertheless, their stringent *in vitro* and *in vivo* characterization requires further investigation before reaching the bedside.

Therefore, the overall goal of this study was to explore whether MSNs are suitable nanocarriers for lung cancer therapy. Our analyses were designed to supply information on how different functionalizations on the nanoparticles would affect their biodistribution and biocompatibility in different biological models and routes of delivery.

To achieve these goals, local biodistribution, preferential uptake as well as the effects of protein-functionalization on the nanoparticles in the lung were initially compared. Then, biocompatibility and tumor site-associated enzyme-responsive controlled release of chemotherapeutic agents encapsulated in the particles were validated in various *in vitro* and *ex vivo* models. Next, lung cancer cell- and tumor-associated macrophage-specific targeting of these nanoparticles for combination therapy was demonstrated *in vitro*. Finally, the MSNs were examined for receptor-specific targeting in mouse cancer models for both intravenous and intratracheal administration.

Taken together, this study should provide detailed information on the advantages and the feasibility of distinctly functionalized stimuli-responsive targeted mesoporous silica nanoparticles for use in lung cancer therapy.

3 Materials and methods

3.1 Materials

3.1.1 Reagents and chemicals

The following reagents and chemicals were used during the study:

Table 3.1 Reagents and chemicals

Reagent	Solvent	Stock concentration	Manufacturer
2,5-diphenyltetrazolium bromide (MTT)	-	-	Sigma-Aldrich (St. Louis, MO)
2-mercaptoethanol	-	-	AppliChem (Damstadt, Germany)
4-(2-hydroxyethyl)-1-piperazineethanesulfonic acid (HEPES)	-	-	AppliChem
4',6-diamidin-2-phenylindol (DAPI)	PBS	300 nM	Sigma-Aldrich
Acetic acid	-	absolute	AppliChem
Acrylamide/bisacrylamide solution	H ₂ O	30%	Carl Roth (Karlsruhe, Germany)
Agarose (low gelling temperature)	-	-	Sigma-Aldrich
Amphotericin B	H ₂ O	250 µg/mL	Sigma-Aldrich
Annexin V-FITC	-	-	BD Biosciences (San Jose, CA)
ATTO-488 mal	-	-	ATTO-TEC (Siegen, Germany)
ATTO-633 mal	-	-	ATTO-TEC
Avidin from egg white	-	-	Merck Millipore (Billerica, MA)
Bortezomib	-	-	Millennium (Cambridge, MA)
Bromophenol blue	-	-	AppliChem
Calcein acetoxymethyl ester (calcein-AM)	-	-	Sigma-Aldrich
cis-Diamineplatinum(II) dichloride (cisplatin)	-	-	Sigma-Aldrich
Citric acid monohydrate	-	-	AppliChem
cOmplete® protease inhibitor	-	-	Roche (Basel, Switzerland)
DAKO fluorescent mounting medium	-	-	Dako (Hamburg, Germany)
Dimethyl sulfoxide (DMSO)	-	-	Carl Roth
ECL Plus detection reagent	-	-	GE Healthcare (Chalfont St Giles, UK)
ECLi peptide: CKLFTGL (ECLi)	-	-	GenScript (Nanjing, China)
Entellan	-	-	Merck Millipore

Eosin	-	-	Carl Roth
Ethanol	-	absolute	AppliChem
Ethylenediaminetetraacetate (EDTA)	-	-	AppliChem
Fetal bovine serum (FBS)	-	-	PAA Laboratories (Pasching, Austria)
GE11 peptide: YHWYGYTPQNV I(GE11)	-	-	GenScript
Gelatin (from porcine skin)	-	-	Sigma-Aldrich
Glycerol	H ₂ O	87%	AppliChem
Hank's Balanced Salt Solution (HBSS)	-	-	Life Technologies (Carlsbad, CA)
Hematoxylin	-	-	Carl Roth
Hoechst 33342	-	-	Enzo Life Sciences (Farmingdale, NY)
Hydrochloric acid	H ₂ O	37%	AppliChem
Hydrogen peroxide	H ₂ O	30%	Sigma-Aldrich
IGEPAL CA-630	-	-	Sigma-Aldrich
Isopropanol	-	absolute	Fisher Scientific (Hampton, NH)
Ketamin	-	-	Bela Pharm (Vechta, Germany)
MACH 2 rabbit AP-polymer	-	-	Biocare (Concord, CA)
Magnesium chloride	-	-	AppliChem
Mannitol	-	-	Sigma-Aldrich
Methanol		absolute	AppliChem
MMP9-cleavable heptapeptide: PLGMWSR	-	-	GenScript
MMP9-noncleavable heptapeptide: PLLMWSR	-	-	GenScript
Paraformaldehyde (PFA)	PBS	4%	AppliChem
Penicillin/streptomycin	-	-	Life Technologies
Phalloidin	-	-	Life Technologies
Pierce BCA protein assay kit	-	-	Thermo Fisher Scientific (Waltham, MA)
Pierce silver stain kit	-	-	Thermo Fisher Scientific
Potassium chloride	-	-	AppliChem
Propidium iodide staining solution	-	-	BD Biosciences
Protein marker VI (10 - 245) prestained	-	-	AppliChem
Proteinase K	-	-	AppliChem

Puromycin dihydrochloride (puromycin)	HEPES	10 mg/mL	Life Technologies
Recombinant EGF protein	-	-	PeproTech (Rocky Hill, NJ)
Recombinant MMP9 protein	-	-	Enzo Life Sciences
Rodent block M	-	-	Biocare
Roti®-Block	H ₂ O	10x	Carl Roth
Roti®-Immunoblock	H ₂ O	10x	Carl Roth
SatisFection transfection reagent	-	-	Agilent Technologies (Santa Clara, CA)
Sodium chloride	-	-	AppliChem
Sodium deoxycholate	-	-	Carl Roth
Sodium pyruvate	-	-	AppliChem
Sodiumdodecylsulfate (SDS)	-	-	AppliChem
Tetramethylethylenediamine (TEMED)	-	-	AppliChem
Tissue-Tek® O.C.T. compound	-	-	Sakura (Leiden, the Netherlands)
Tris(hydroxymethyl)-aminomethane (Tris)	-	-	AppliChem
Triton™ X-100	-	-	Life Technologies
Tween-20	-	-	AppliChem
Vulcan Fast Red	-	-	Biocare
WST-1 assay	-	-	Roche
Xylazine hydrochloride	-	-	Bela Pharm
Xylene	-	absolute	AppliChem

3.1.2 Buffer formulations

The following buffers were used in the study. All buffers were prepared with Milli-Q™ water if not stated otherwise.

Table 3.2 Buffer formulations

Buffer	Compounds	Concentration
Annexin V binding buffer pH 7.4	HEPES	10 mM
	NaCl	140 mM
	CaCl ₂	2.5 mM

Citrate buffer pH 6	Citric acid monohydrate	1.8 mM
	Sodium citrate tribasic	8.2 mM
FACS buffer (in PBS)	FBS	2%
	EDTA	20 μ M
Phosphate buffered saline (PBS) pH 7.4	NaCl	137 mM
	KCl	2.7 mM
	Na ₂ HPO ₄	10 mM
	KH ₂ PO ₄	2 mM
RIPA buffer pH 7.5	Tris	50 mM
	NaCl	150 mM
	IGEPAL CA-630	1%
	Sodium deoxycholate	0.50%
	SDS	0.10%
SDS PAGE running buffer	Tris	25 mM
	Glycin	192 mM
	SDS	0.10%
Tris buffered saline and Tween (TBST) pH 7.6	Tris	20 mM
	NaCl	135 mM
	Tween-20	0.02%
Western blot transfer buffer	Tris	25 mM
	Glycine	192 mM
	Methanol	10%
6x Laemmli buffer	Tris	300 mM
	Glycerol	50%
	SDS	6%
	Bromophenol blue	0.01%
	DTT	600 mM

3.1.3 Antibodies and applications

Antibodies used for production of the presented data were:

Table 3.3 Primary antibodies used for analyses

Antibody	Host	Manufacturer	Product No	Dilution
Anti-T1 α	Gt	R&D Systems (Minneapolis, MN)	AF3244	IHF 1:100
Anti-pro-SPC	Rb	Merck Millipore (Billerica, MA)	AB3786	IHF 1:1000
Anti-Kras	Ms	Santa Cruz (Dallas, TX)	SC30	IHF 1:100
Anti-MMP9	Rb	Merck Millipore	AB19016	IHC 1:100
				IHF 1:100
Anti-E-cadherin	Ms	BD Biosciences (San Jose, CA)	610181	IHF 1:200
Anti-cleaved caspase-3	Rb	Cell Signaling (Cambridge, UK)	9661	WB 1:1000
				ICF 1:100
Anti-EGFR	Rb	Abcam (Cambridge, UK)	Ab52894	WB 1:100000*
				ICF 1:200
				IHC 1:100
				IHF 1:100
Anti-CCR2	Rb	Novus Biologicals (Littleton, CO)	NB110-55674	WB 1:1000
				ICF 1:500
				IHC 1:1000
				IHF 1:100
Anti-CD68	Ms	Novus Biologicals	NBP1-55674	IHF 1:50
Anti- α -tubulin	Ms	GeneTex (Irvine, CA)	GTX628802	WB 1:1000
Anti- β -Actin (HRP conjugated)	Ms	Sigma-Aldrich (St. Louis, MO)	A5228	WB 1:40000

*Gt: goat, Rb: rabbit, Ms: mouse, * for WB analysis of murine B16F10 clones, the dilution factor for the EGFR antibody was 1:10000.*

Table 3.4 Secondary antibodies used for analyses

Antibody	Host	Manufacturer	Product No	Dilution
Anti-rabbit IgG (Alexa Fluor 488 conjugated)	Gt	Invitrogen (Carlsbad, CA)	A11008	IHF/ICF 1:750
Anti-mouse IgG (Alexa Fluor 488 conjugated)	Gt	Invitrogen	A11001	IHF/ICF 1:750
Anti-rabbit IgG (Alexa Fluor 568 conjugated)	Gt	Invitrogen	A11011	IHF/ICF 1:750
Anti-mouse IgG (Alexa Fluor 568 conjugated)	Gt	Invitrogen	A11004	IHF/ICF 1:750
Anti-mouse IgG (HRP conjugated)	Gt	Cell Signaling	7076	WB 1:40000
Anti-rabbit IgG (HRP conjugated)	Gt	Cell Signaling	7074	WB 1:40000

Gt: goat

3.1.4 Laboratory equipment and software

The following laboratory equipment and software were used in the study.

Table 3.5 Laboratory equipment used for the study

Product	Manufacturer
-20°C freezer MediLine LGex 410	Liebherr, Biberach, Germany
-80°C freezer U570 HEF	New Brunswick, Hamburg, Germany
Analytical scale XS20S dual range	Mettler-Toledo, Gießen, Germany
Autoclave DX-45	Systec, Wettenberg, Germany
Autoclave VX-120	Systec, Wettenberg, Germany
Axiovert 40 C light microscope	Zeiss, Jena, Germany
BD LSR II flow cytometer	BD Biosciences, Franklin Lakes, NJ
Cell culture bench Herasafe KS180	Thermo Fisher Scientific, Waltham, MA
Centrifuge MiniSpun plus	Eppendorf, Hamburg, Germany
Centrifuge Rotina 420R	Hettich, Tuttlingen, Germany
Centrifuge with cooling, Micro200R	Hettich, Tuttlingen, Germany
CO ₂ cell incubator BBD6620	Thermo Fisher Scientific, Waltham, MA
Confocal microscope LSM 710	Zeiss, Jena, Germany
Decloaking chamber	Biocare Medical, Concord, CA
Dismembrator S	Sartorius, Göttingen, Germany

Dry ice container Forma 8600 Series	Thermo Fisher Scientific, Waltham, MA
Electronic pipette filler	Eppendorf, Hamburg, Germany
Electrophoretic transfer cell	Bio-Rad, Hercules, CA
Film developer Curix 60	Agfa, Morsel, Belgium
Fume cupboard	Vinitex, Sint-Oedenrode, the Netherlands
Gasprofi 1 SCS micro gas burner	WLC-TEC, Göttingen, Germany
Gel Doc EZ imager	Bio-Rad, Hercules, CA
Gel imaging system ChemiDOC XRS+	Bio-Rad, Hercules, CA
Hyrax C 50 cryotome	Zeiss, Jena, Germany
Hyrax M 55 microtome	Zeiss, Jena, Germany
Hyrax V 50 vibratome	Zeiss, Jena, Germany
Ice machine ZBE 110-35	Ziegra, Hannover, Germany
Intelli-mixer RM-2	Omnilab, Munich, Germany
Liquid nitrogen cell tank BioSafe 420SC	Cryotherm, Kirchen/Sieg, Germany
Liquid nitrogen tank Apollo 200	Cryotherm, Kirchen/Sieg, Germany
Magnetic stirrer KMO 2 basic	IKA, Staufen, Germany
Mastercycler gradient	Eppendorf, Hamburg, Germany
Mastercycler Nexus	Eppendorf, Hamburg, Germany
Microm HMS 740 robot stainer	Thermo Fisher Scientific, Waltham, MA
Microm STP 420D tissue processor	Thermo Fisher Scientific, Waltham, MA
Milli-Q™ advantage A10 ultrapure water purification system	Merck Millipore, Darmstadt, Germany
Minicentrifuge MCF-2360	Omnilab, Munich, Germany
Mirax scanner	Zeiss, Jena, Germany
Multipipette stream	Eppendorf, Hamburg, Germany
Nalgene freezing container	Omnilab, Munich, Germany
pH meter InoLab pH 720	WTW, Weilheim, Germany
Pipettes research plus	Eppendorf, Hamburg, Germany
Plate centrifuge 5430	Eppendorf, Hamburg, Germany
Plate reader Sunrise	Tecan, Crailsheim, Germany
Plate reader TriStar LB941	Berthold Tech., Bad Wildbach, Germany
PowerPac HC power supply	Bio-Rad, Hercules, CA

Roll mixer	VWR International, Darmstadt, Germany
Scale XS400 2S	Mettler-Toledo, Gießen, Germany
Shaker Duomax 1030	Heidolph, Schwabach, Germany
Thermomixer compact	Eppendorf, Hamburg, Germany
Vacuum pump N 022 AN.18	KNF, Freiburg, Germany
Vortex mixer	IKA, Staufen, Germany
Water bath, Aqua Line AL 12	Lauda, Lauda-Königshofen, Germany

Table 3.6 Software used for the study

Product	Manufacturer
FlowJo 7.6.5	FlowJo LLC, Ashland, OR
GraphPad Prism 5	GraphPad Software, La Jolla, CA
Image Lab version 4.0	Bio-Rad, Hercules, CA
ImageJ 1.46r	NIH, Bethesda, MD
Imaris 7.6.4	Bitplane, Zurich, Switzerland
Magellan software	Tecan, Crailsheim, Germany
Microsoft Office professional plus 2010	Microsoft, Redmond, USA
Pannoramic Viewer 1.15.1	3DHISTECH, Budapest, Hungary
Tristar MicroWin 2000	Berthold Technologies, Bad Wildbach, Germany

3.1.5 Consumables

The consumables used for this study are as follows.

Table 3.7 Consumables used for the study

Product	Manufacturer
6-24-96 well plates	TPP, Trasadingen, Switzerland
Cell culture dishes	Nunc, Wiesbaden, Germany
Cell culture flasks	Nunc
Cryovials	Greiner Bio-One, Frickenhausen, Germany
Falcon tubes	BD Biosciences, Franklin Lakes, NJ
Film X-Omat LS (Kodak)	Carestream Health, Rochester, NY

Filtered pipette tips	Biozym Scientific, Hessisch Oldendorf, Germany
Glass pasteur pipettes	VWR International, Darmstadt, Germany
Nalgene cryogenic tubes	Thermo Fisher Scientific, Waltham, MA
Pipette tips	Eppendorf, Hamburg, Germany
Polyvinylidene fluoride (PVDF) membrane	Bio-Rad, Hercules, CA
QuadriPERM dishes	Nunc
Reaction tubes	Eppendorf
Sterican cannulas	BD Biosciences
Superfrost™ ultra plus adhesion slides	Thermo Fisher Scientific
Syringes	Neolab, Heidelberg, Germany
Whatman blotting paper (3 mm)	GE Healthcare, Freiburg, Germany

3.1.6 Human tissue

All experiments with human material were approved by the Ethics Committee of the Ludwig-Maximilians-University Munich, Germany (LMU, project no. 455-12). The tissues were provided by the Asklepios Biobank for Lung Diseases, Gauting, Germany (project no. 333-10). Written informed consent was received from all subjects. Tumorous or tumor-free tissues from patients who were surgically treated for lung cancer were used.

3.2 Synthesis of mesoporous silica nanoparticles (MSNs)

The core-shell functionalized MSNs have been synthesized by a delayed co-condensation approach resulting in functionalization of the internal pore system with thiol groups and the external particle surface with amino groups as described before (Cauda et al., 2009) in collaboration with the research group of Thomas Bein at the Physical Chemistry Department of the Ludwig-Maximilians-University Munich. The additional core functionalization offers a site for covalent attachment of fluorescent dyes for particle tracking in *in vitro* and *in vivo* studies. The external amino functionalization was used to attach a linker system with avidin as the bulky gatekeeper. Subsequently, different targeting ligands were covalently attached on the outer periphery of the particles and the synthesized particle system was used for *in vitro* and *in vivo* uptake studies.

3.3 Cell culture

3.3.1 Cell growth and maintenance

Cells were grown at 37°C in a humidified atmosphere containing 5% CO₂. Growth medium of the cells (Table 3.8) was changed every two to three days. All cell lines were grown until 100% confluency before passaging into a new cell culture flask. The following growth media were used. All growth media were obtained from Life Technologies.

Table 3.8 Cell culture media

Cell line	ATCC no	Medium	Product no	Supplementation
human NSCLC cell line A549	CCL-185™	DMEM	21885-025	10% FBS
				1% Penicillin/streptomycin
human NSCLC cell line H1299	CRL-5803™	DMEM	21885-025	10% FBS
				1% Penicillin/streptomycin
human NSCLC cell line H520	HTB-182™	RPMI 1640	21875-034	10% FBS
				1% Penicillin/streptomycin
mouse melanoma clones B16F10	CRL-6475™	DMEM	21885-025	10% FBS
				1% Penicillin/streptomycin
				2 ng/μL Puromycin
mouse lung epithelial cell line MLE-12	CRL-2110™	RPMI 1640	21875-034	10% FBS
				1% Penicillin/streptomycin
mouse alveolar macrophage cell line MH-S	CRL-2019™	RPMI 1640	21875-034	10% FBS
				1% Penicillin/streptomycin
				10 mM HEPES
				1 mM Sodium pyruvate
				0.05 mM 2-mercaptoethanol

3.3.2 Metabolic activity assessment

3.3.2.1 MTT reduction

The MTT assay was performed to assess cell viability after exposure to the MSNs *in vitro*. MLE-12, MH-S, A549, and H1299 cells were seeded in 96-well plates. In the case of transiently transfected A549 and H1299 cells, 24 h after seeding, the cells were transfected with 0.15 μg MMP9 cDNA (DNASU) or empty vector cDNA per well using SatisFection transfection reagent (Agilent Technologies), according to manufacturer's instructions. 24 h after seeding (for MLE-12 and MH-S cells) and 24 h after transfecting (for A549 and H1299 cells), the cells were exposed to the corresponding concentrations of nanoparticle suspensions for the presented time-points. After the exposure, 10 μL of fresh 5 mg/mL thiazolyl blue tetrazolium bromide (MTT, Sigma-Aldrich) was added to each well and the cells were incubated at 37°C for 1 h. Later, the supernatant was removed and the violet crystals were dissolved in isopropanol with 0.1% Triton X-100 solution. Absorbance was measured at 570 nm with a Tristar LB 941 plate-reader (Berthold Technologies).

3.3.2.2 WST-1 assay

Metabolic activity of MLE-12 and MH-S cells upon empty MMP9-cleavable MSNs (cMSNs) exposure was assessed by the WST-1 assay (Roche). MLE-12 and MH-S cells were seeded in 96-well plates. 24 h after seeding, the cells were exposed to either cMSNs or MMP9-noncleavable MSNs (ncMSNs) for 4 or 24 h. After treatment, 10 μL of WST-1 reagent was added to each well, and the cells were incubated at 37°C for 30 min. Absorbance was measured at 450 nm with a Tristar LB 941 plate-reader (Berthold Technologies).

3.3.3 Live/dead assay with Annexin V/PI

Induction of apoptosis or necrosis was investigated in A549 and H1299 cells using Annexin V-FITC and propidium iodide (PI) double staining (BD Biosciences). Cells were seeded in 6-well plates and incubated for 24 h. Then the cells were treated with either MSN_{AVI} or MSN_{NH_2} for 4 or 24 h. The medium containing particles was then aspirated and the cells were washed, trypsinized, and stained with Annexin V-FITC and propidium iodide in binding buffer for 15 min at 37°C. Samples were then measured by flow cytometry using Becton Dickinson LSR II and analyzed with FlowJo software (version 7.6.5).

3.3.4 Calcein-AM release experiments

The release of calcein acetoxymethyl ester (calcein-AM, Sigma-Aldrich) from the particles, hence the staining of the cells was assessed by confocal microscopy analysis. Freshly prepared calcein-AM containing cMSN or ncMSN particles were incubated with 0, 1, or 2 $\mu\text{g}/\text{mL}$ recombinant MMP9 for 2 h at 37°C in a thermoblock shaking at 700 rpm. After the incubation time, the particles were removed by centrifugation, and the cells were incubated with the supernatants for 30 min, so that the released calcein-AM could be taken up by the living cells. Afterwards, the nuclei of the cells were counterstained with Hoechst 33342. Live cell imaging was performed using the confocal microscope LSM 710 (Zeiss).

3.3.5 Flow cytometry

A549, H520, and MH-S cells were plated on 6-well plates and incubated overnight. The next day, the cells were treated with ATTO 488 or ATTO 633-labeled nanoparticles for 1 h. Afterwards, the cells were washed three times with PBS, once with NaCl (0.15 M, pH 3.0), and then three times with PBS again to create a final cell suspension. Samples were then analyzed by flow cytometry (BD LSR II). MSN uptake in different cell types was quantified by the median fluorescence signal collected in the Alexa Fluor 488 or 647 channels with FlowJo software (version 7.6.5).

3.3.6 Genetic engineering for flank tumor models

C57BL/6 mouse Lewis lung carcinoma (LLC) and B16F10 skin melanoma cells were obtained from the NCI Tumor Repository. For RNA interference, the following proprietary lentiviral shRNA pools were obtained from Santa Cruz Biotechnology: random control shRNA (shC, sc-108080), GFP control (sc-108084), anti-EGFR-shRNA (sc-29302-V). Stable transfections of the LLC and B16F10 cells were generated by the Stathopoulos Laboratory for Molecular Respiratory Carcinogenesis at the University of Patras in Greece.

3.4 Human and mouse 3D lung tissue cultures (3D-LTCs)

The whole 3D-lung tissue culturing procedure was conducted under sterile conditions and performed as described before (Uhl et al., 2015). WT FVB as well as *Kras* mutant mice with lung tumor burden were anaesthetized with a mixture of ketamine and xylazin hydrochloride. *Kras* mice of approximately three months of age that had several tumor lesions in each lung tissue slice were used. After intubation and diaphragm dissection, lungs were perfused via the right ventricle with sodium chloride solution. Using a syringe pump, airways were filled with warm 2% (w/v) low gelling temperature agarose solution prepared in DMEM/F12 (Life Technologies) supplemented with 1x penicillin/streptomycin and amphotericin B. Later, tracheae were knotted with a thread to keep the liquid agarose inside the airways. Afterwards, the lungs were excised and transferred into tubes loaded with cultivation medium, left to cool on ice to allow for the solidification of the agarose. Finally, lobes were separated and cut with the Hyrax V55 vibratome to a thickness of 200 μm . The 3D-LTCs were cultivated for up to 3 days in 24-well plates. The amount of sections per mouse varied between 30 and 50 slices. Directly after cutting, mouse 3D-LTCs were exposed to 0.2 or 1 mM cisplatin, combination therapy (0.2 mM cisplatin and 0.2 μM bortezomib, CB), or 50 $\mu\text{g}/\text{mL}$ ATTO 633-labeled MSN particles containing cisplatin or CB, administered directly into the medium. For human 3D-LTCs, tumorous and tumor-free regions excised from lung cancer surgeries were used. Airways at tumor-free segments were filled with 3% (w/v) agarose dissolved in DMEM/F12 as described above, via the respective bronchi. Both the tumorous and tumor-free segments were then cut to a thickness of 300 μm with the vibratome. Directly after cutting, mouse and human 3D-LTCs were exposed to 50 $\mu\text{g}/\text{mL}$ of MSN particles containing cisplatin and/or bortezomib, administered directly into the medium for 24-72 h.

3.5 Animal experiments

Animal experiments were conducted in collaboration with the research groups of Tobias Stöger at the Comprehensive Pneumology Center Munich and Georgios Stathopoulos at the University of Patras. MSN instillations to WT BALB/c mice for the pulmonary uptake and biodistribution study were conducted by David Kutschke at the research group of Tobias Stöger. Subcutaneous (s.c.) flank tumor formation, intravenous delivery of targeted-MSNs, and dissections of the treated mice were conducted at the University of Patras by Malamati Vreka from the research group of Georgios Stathopoulos. In all other cases, maintenance,

characterization, nanoparticle application, tissue extraction, and subsequent analysis were performed by Deniz A. Bölükbas in collaboration with Charlotte Meyer-Schwickerath.

3.5.1 Animals and maintenance

Animal experiments were carried out according to the German law of protection of animal life and were approved by an external review committee for laboratory animal care.

3.5.1.1 BALB/c WT mice for IT application of MSNs

8–12 week-old female BALB/cAnNCrl mice (Charles River Laboratories) were intratracheally instilled, as previously described (Stoeger et al., 2006). 1, 3, or 7 d post-instillation, mice were sacrificed with an overdose of ketamine (188.3 mg per kg body weight) and xylazine hydrochloride solution (4.1 mg per kg body weight) (bela-pharm, Germany).

3.5.1.2 C57BL/6 double flank tumor mice for IV application of MSNs

C57BL/6 mice were obtained from Jackson Laboratories (Bar Harbor) and were bred at the Center for Animal Models of Disease of the University of Patras. Experiments were approved a priori by the Veterinary Administration of the Prefecture of Western Greece, and were conducted according to Directive 2010/63/EU. Experimental mice were sex-, weight-, and age-matched. For induction of solid tumors, mice were anesthetized using isoflurane inhalation and received s.c. injections of 100 μ L PBS containing 0.5×10^6 LLC or B16F10 clones. Two weeks after s.c. inoculation of EGFR-abundant and EGFR-scarce LLC and B16F10 tumor clones, 1 mg ATTO 633-labeled MSN_{AVI} or MSN_{GE11} particles suspended in 200 μ L Hank's Balanced Salt Solution (HBSS) was applied to each mouse retro-orbitally. The mice were sacrificed with an overdose of isoflurane three days after the administration.

3.5.1.3 *Kras* mutant mice with lung tumors for IT application of MSNs

129S/Sv-*Kras*^{tm3Tyj/J} (*Kras*^{LA2}) mutant mice were obtained from the Jackson Laboratory, USA, and cross-bred with FVB-NCrl WT females obtained from Charles River Laboratories, Germany, for over seven generations. Animals were kept in rooms maintained at constant temperature and humidity with a 12/12 h light/dark cycle and were allowed food and water *ad libitum*. Animal experiments were carried out according to the German Law of Protection of Animal Life and were approved by an external review committee for laboratory animal

care. 12 week-old *Kras*^{LA2} mutant mice were intratracheally instilled with ATTO 633-labeled targeted or non-targeted MSNs, as described previously (Stoeger et al., 2006). Three days post-instillation, the mice were sacrificed with an overdose of ketamine (188.3 mg/kg) and xylazine hydrochloride (4.1 mg/kg) (bela-pharm). Lung lobes from each group (n = 5 mice per group) were excised and prepared for cryoslicing.

3.6 Protein analysis

3.6.1 Immunofluorescence analysis in cryo-sections (IHF)

For local IT delivery studies, animals were sacrificed and the lungs were perfused via the right ventricle with sodium chloride solution. Airways were then filled with approximately 1 mL Tissue-Tek (Sakura). Later, the lung lobes were separated, transferred into cryomolds, and covered with Tissue-Tek. For the systemic IV delivery experiment, internal organs as well as flank tumors were dissected and placed initially in 4% PFA overnight after which the suspension medium was exchanged to PBS. Representative parts of the organs were frozen in Tissue-Tek and kept at -80°C. Samples were left to freeze on dry ice and then stored at -80°C. For both experiments, 5 µm thick cryo-sections were sliced with the cryostat (Zeiss Hyrax C 50) and placed on Superfrost™ plus adhesion slides (Thermo Fisher Scientific).

Immediately before staining, all cryo-sections were fixed with 4% (w/v) PFA for 10 min, then washed with PBS, and permeabilized with 0.5% Triton-X. The sections were incubated with Roti®-Immunoblock (Carl Roth) for 1 h at room temperature (RT), and then incubated with the corresponding primary antibodies at 4°C overnight. Afterwards, the sections were washed with PBS and incubated with Alexa Fluor 488 secondary antibody for 1 h at RT. After another PBS wash, the sections were finally stained with DAPI. In case phalloidin staining was used, the sections were first incubated with phalloidin (Life Technologies) for 45 min and then with DAPI for 10 min at RT directly after the fixation and washing step. The sections were mounted using fluorescence mounting medium (DAKO) and analyzed using confocal microscopy (LSM710, Carl Zeiss). Quantification of the cellular uptake of the MSNs in the tissues was conducted using the IMARISx64 software (version 7.6.4, Bitplane).

3.6.2 Immunohistochemistry (IHC) analysis in paraffin sections

For paraffin embedding, fresh human and mouse tissues were fixed in 4% PFA solution overnight at 4°C. Of note, the mouse lungs were treated by intratracheal instillation of 4% PFA in PBS before extraction. Specimens were then processed for paraffin embedding. 3 µm thick paraffin sections were sliced with the microtome (Zeiss Hyrax M 55) and placed on superfrost plus adhesion slides. Deparaffinized sections were subjected to quenching of endogenous peroxidase activity using a mixture of methanol/H₂O₂ (3 mL 30% H₂O₂, 7 mL distilled water, 40 mL methanol) for 20 min, followed by antigen retrieval in a decloaking chamber (30 sec at 125°C followed by 10 sec at 90°C). From this step on, the slides were washed with TBST (20 mM Tris, 135 mM NaCl, 0.02% Tween-20) after each incubation with the reagents throughout the procedure. The sections were incubated first with Rodent Block M for 30 min and then with the corresponding primary antibodies or IgG control for 1 h. The cuts were then incubated with Rabbit-on-Rodent AP-Polymer for 30 min, which was followed by Vulcan Fast Red AP substrate solution incubation for 10-15 min. Sections were counterstained with hematoxylin and dehydrated, respectively in consecutively grading ethanol and xylene (both AppliChem) incubations. Dried slides were mounted in Entellan (Merck Millipore).

3.6.3 Immunocytofluorescence (ICF)

A549, H520, and MH-S cells which were grown on coverslips were treated with ATTO 633-labeled nanoparticles for 1 h. Afterwards, the cells were washed three times with PBS, then once with NaCl (0.15 M, pH 3.0), and then three times with PBS. Cells were fixed with 70% ethanol and permeabilized with 0.1% Triton-X for 5 min. After another PBS wash, cells were incubated with Roti®-Immunoblock (Carl Roth) for 1 h at RT. Afterwards, A549 and H520 cells were stained with EGFR antibody (Abcam), whereas MH-S cells were stained with CCR2 antibody (Novus Biologicals) overnight at 4°C. The following day, the cells were incubated with the Alexa Fluor secondary antibodies for 1 h at RT, washed with PBS, incubated with DAPI for 10 min for nuclear staining, and then mounted with fluorescent mounting medium (Dako).

3.6.4 Zymography

To assess catalytically active MMP-9 expression and transfection efficiency in A549 and H1299 cells, gelatin zymography was performed. In short, collected cell culture supernatants were centrifuged to discard cellular debris and then electrophoresed on 10% SDS-gels containing 1% gelatin substrate in non-reducing conditions (*i.e.*, no 2-mercaptoethanol) at 90-110 V at RT, so that the proteins could renature afterwards. After electrophoresis, the enzymes were renatured by incubation with 2.5% Triton-X-100 in developing buffer (50 mM Tris, 200 mM NaCl, 5 mM CaCl₂, pH 7.5) for 1 h at RT, to ensure that the proteins were catalytically active. Afterwards, the gels were incubated in developing buffer at 37°C for 24 h, to allow the enzyme reaction take place. Thereafter, the gels were stained using PAGE-Blue™ (Fermentas) protein staining, according to the manufacturer's instructions. Gels were analyzed using the ChemiDoc™ XRS+ software (Bio-Rad).

3.6.5 Preparation of cellular protein lysates

Prior to protein extraction, cells were trypsinized, washed with PBS and cell pellets were stored at -20°C until further processing. For preparation of denatured protein lysates, cell pellets were lysed by incubation in RIPA buffer supplemented with cComplete® protease inhibitor cocktail (Roche) for 20-30 minutes at 4°C. Cell debris was removed from the protein lysate by centrifugation at 14,000 rpm at 4°C for 20 min. The supernatant containing the protein lysate was stored at -20°C until use. Protein content was assessed using the Pierce BCA protein assay kit (Thermo Fisher Scientific).

3.6.6 Western blot analysis

For Western blot analysis, 10-20 µg of protein lysates were mixed with 6x Laemmli buffer and incubated at 95°C for 5 min. After the incubation, samples were subjected to electrophoresis on 10% SDS-PAGE gels and blotted onto polyvinylidenedifluoride (PVDF, Bio-Rad) membranes. Electrophoretic separation in SDS gels was performed at 90-110 V at RT and transfer to PVDF membranes (Bio-Rad) was performed at 250 mA for 90 min at 4°C. Membranes were blocked using Roti®-Block (Carl Roth) and treated with antibodies using standard Western blot techniques. The ECL Plus Detection Reagent (GE Healthcare) and Super Signal West Femto (Thermo Fisher Scientific) were used for chemiluminescent detection and membranes were analyzed using X-Omat LS films (Carestream) in a Curix 60 developer (Agfa).

3.6.7 Protein corona analysis

100 μg MSN_{AVI} and MSN_{GE11} were shaken overnight (16 h) either in cell culture medium in the presence of 10% FCS, human serum, or murine lung lining fluid (diluted in 1 mL PBS containing cOmplete® protease inhibitor cocktail, Roche) at RT. The suspension was centrifuged and the nanoparticles were resuspended in PBS three times (15,000 rpm, for 30 min, at 4°C). The proteins adsorbed on the pelleted nanoparticles were eluted by incubating them at 95°C for 5 min in Laemmli buffer. The suspension was centrifuged again and the supernatant was subjected to electrophoresis on 10% SDS-PAGE gels. Silver staining was conducted as described in the instructions manual of the Pierce Silver Stain Kit (Thermo Fisher Scientific). The gels were scanned with the ChemiDoc XRS+ (Bio-Rad).

3.7 Statistical analysis

All MTT experiments were done in triplicates and the data are shown as means with standard deviation. For comparison of two groups, one-way ANOVA was performed. Therapeutic efficiency of the drug loaded particles on 3D-LTCs was assessed by immunofluorescent stainings with the apoptosis marker (cleaved caspase-3) for 15 different *Kras* mutant animals that were prepared and exposed to the MSNs or free drugs in three independent experiments. Similarly sized tumors were chosen for imaging from a minimum of three different mice per individual staining. Furthermore, each staining was performed a minimum of three times per mouse. For the experiments where cellular uptake of the targeted *versus* non-targeted nanoparticles were compared, Two-Way ANOVA analysis with Bonferroni post-tests was performed. In the flank tumor models, three representative images of five different mice were chosen for quantification which was blinded by using the IMARISx64 software (version 7.6.4, Bitplane, Switzerland). For controls, four WT mice were treated with HBSS, stained and quantified with the same principle. For the IT delivery experiment, six adult *Kras* mutant mice with lung tumors were used. As controls, six mice were treated with non-targeted nanoparticles. All statistical analysis was performed using GraphPad Prism software (version 5.00). Significance was illustrated in the figures as *: $p < 0.05$, **: $p < 0.01$ or ***: $p < 0.001$.

4 Avidin-coated mesoporous silica nanoparticles as drug carriers in the lung

Parts of this chapter have previously been published as:

van Rijt S.H., Bölükbas D.A., Argyo C., Wipplinger K., Naureen M., Datz S., Eickelberg O., Meiners S., Bein T., Schmid O., and Stoeger T. (2016). *Applicability of avidin protein coated mesoporous silica nanoparticles as drug carriers in the lungs*. *Nanoscale*, 8, 8058-8069.

4.1 Introduction

Over the last decades, the use of nanoparticles for drug delivery has gained notable attention. Various formulations of nanomedicines have been clinically approved by the U.S. Food and Drug Administration (FDA) or European Medicines Agency (EMA) (Dawidczyk et al., 2014). These nanomedicines allow for enhanced bio-availability of the loaded agent, cell-specific delivery, and reduction in adverse side-effects of the agents (Schütz et al., 2013; van Rijt et al., 2014). Mesoporous silica nanoparticles (MSNs), in particular, are versatile nanocarriers with features like high volume and surface area, inertness for many agents, and tunable size (Argyo et al., 2013). Moreover, MSNs have a wide range of specific functionalization possibilities, allowing for *e.g.* covalent binding of fluorescent molecules for tracking of the nanoparticles (Cauda et al., 2009). Additionally, the surface of the MSNs can be selectively functionalized for controlled release of the agents (Argyo et al., 2013). There have been indeed several studies showing *in vivo* efficacy of mesoporous silica nanoparticles functionalized with *e.g.* PEG linkers (Na et al., 2012), folic acid (Lu et al., 2012), or transferrin (Liu et al., 2012).

Although MSNs are promising candidates for future nanomedicines (Chen et al., 2013), their *in vivo* validation in terms of biocompatibility has not been fully exploited. Several studies revealed that their biocompatibility heavily depends on their size (He et al., 2011), shape (Huang et al., 2011), porosity (Lin and Haynes, 2010), and surface functionalization (He et al., 2011; Zhao et al., 2011). Furthermore, the route of application was shown to play a striking role in their biodistribution and biocompatibility (Taratula et al., 2011). It is indeed heartening that numerous studies have proven MSNs to be nontoxic as nanomedicines

(Hudson et al., 2008; Kupferschmidt et al., 2013; Lu et al., 2010; Vallhov et al., 2012; Yu et al., 2012); however there have not been many studies investigating their application directly into the lung. Pulmonary application of the mesoporous silica nanoparticles directly into the lung could offer several advantages for lung diseases such as chronic obstructive pulmonary disease (COPD), idiopathic pulmonary fibrosis (IPF), asthma, or lung cancer. With this manner, the drugs could target the lungs at first place, which would result in increased local concentration of the drugs in the lung, and lower systemic concentrations limiting the adverse effects. Additionally, when compared to oral application, drugs applied via the pulmonary route would stay more stable as they would not encounter the digestive system, and act much faster because of the large blood supply in the lung. Beyond these, inhalation of drugs is non-invasive and has the possibility of self-administration (Labiris and Dolovich, 2003; Rau, 2005). Despite the fact of being considered as safe for systemic application, polymeric nanomedicines have shown adverse effects when applied directly into the lung (Beyerle et al., 2011). Particularly, inflammatory potential of nanomedicines must be critically investigated before their direct application into the lung, as it could worsen the inflammation which is already present in lung diseases such as COPD and asthma.

In this study, we examined the biodistribution and bioresponse of intratracheally applied functionalized mesoporous silica nanoparticles within one week time. For this, we applied 20 or 100 $\mu\text{g}/\text{mouse}$ of avidin-functionalized (MSN_{AVI}) *versus* non-functionalized (MSN_{NH_2}) mesoporous silica nanoparticles intratracheally into adult BALB/c mice. Later, we investigated the biodistribution of the nanoparticles and the bioresponse after 1, 3, and 7 days. The particles were covalently labeled with the fluorescent ATTO 633 dye in the core to allow for tracking in lung cryo-sections. With several additional complementary validations, avidin-functionalized MSNs (MSN_{AVI}) were found to be significantly more biocompatible in comparison to their non-functionalized controls (MSN_{NH_2}). These data reveal that the intratracheally instilled avidin-functionalized mesoporous silica nanoparticles reach the alveolar space in mouse lungs evenly and are taken up by alveolar epithelial cells initially. Later, the nanoparticles are rather collected by alveolar macrophages within 3-7 days. Additionally, avidin-functionalized nanoparticles were found to be superior to non-functionalized particles with no significant toxic effects, suggesting their use as potential nanomedicines for direct pulmonary application into the lung.

4.2 Results

To investigate the biodistribution and cellular uptake of the avidin-functionalized MNS_{AVI} versus non-functionalized MSN_{NH_2} , the nanoparticles were given intratracheally to adult BALB/c mice for 1, 3, or 7 days. The distribution of the MSNs in the lungs was assessed by preparing cryo-sections of (non-lavaged) lungs, which were analyzed by immunofluorescence imaging. ATTO 633-labeled MSNs could easily be detected by confocal microscopy on 14 μm thick lung cryo-sections (Figures 4.1-2 and Figures 4.4-5).

4.2.1 Deposition of the non-functionalized MSN_{NH_2} in mouse lungs

Intratracheally instilled non-functionalized MSN_{NH_2} nanoparticles successfully reached the alveolar space, and were taken up by the cells of the lung after 1 day (Figure 4.1).

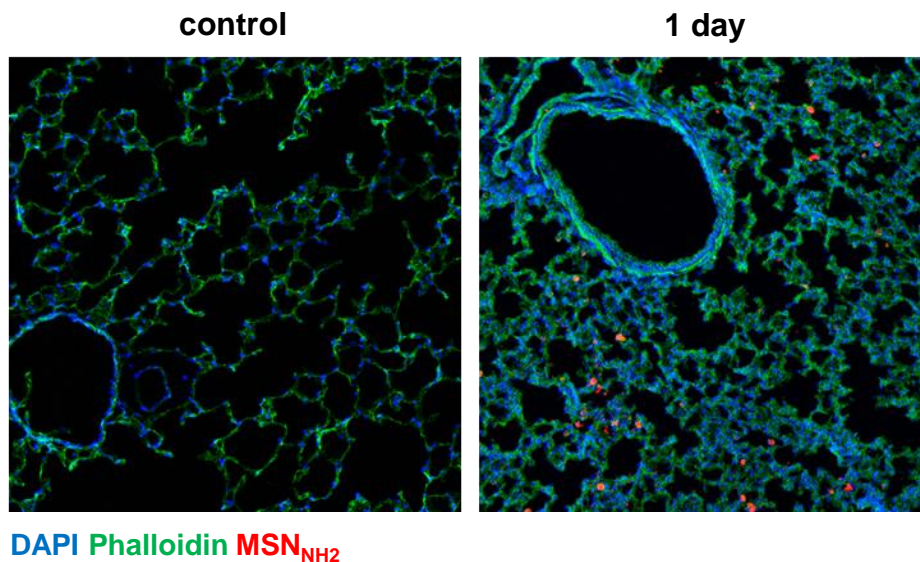


Figure 4.1 Nanoparticle distribution in lung cryo-slices of BALB/c mice exposed to PBS control or 100 μg MSN_{NH_2} after 1 day. Cell nuclei are shown in blue (DAPI), ATTO 633 labeled MSN_{NH_2} are shown in red, cell actin staining (phalloidin) is shown in green. Images are representative for $n = 4$ animals. Scale bar is 20 μm .

4.2.2 Homogeneous uptake of the functionalized MSN_{AVI} in mouse lungs

The instilled functionalized MSN_{AVI} particles were distributed evenly over the alveolar regions of the lungs. Furthermore, the nanoparticles showed widespread and significant accumulation in the lungs for at least 7 days (Figure 4.2). Intriguingly, MSN_{AVI} particles showed an even distribution in the lung parenchyma 1 day after the application (Figure 4.2, left panel). However after 3 to 7 days, fewer but bigger MSN_{AVI} agglomerates were observed in the alveolar space, which is a sign for macrophage clearance of the particles (Figure 4.2).

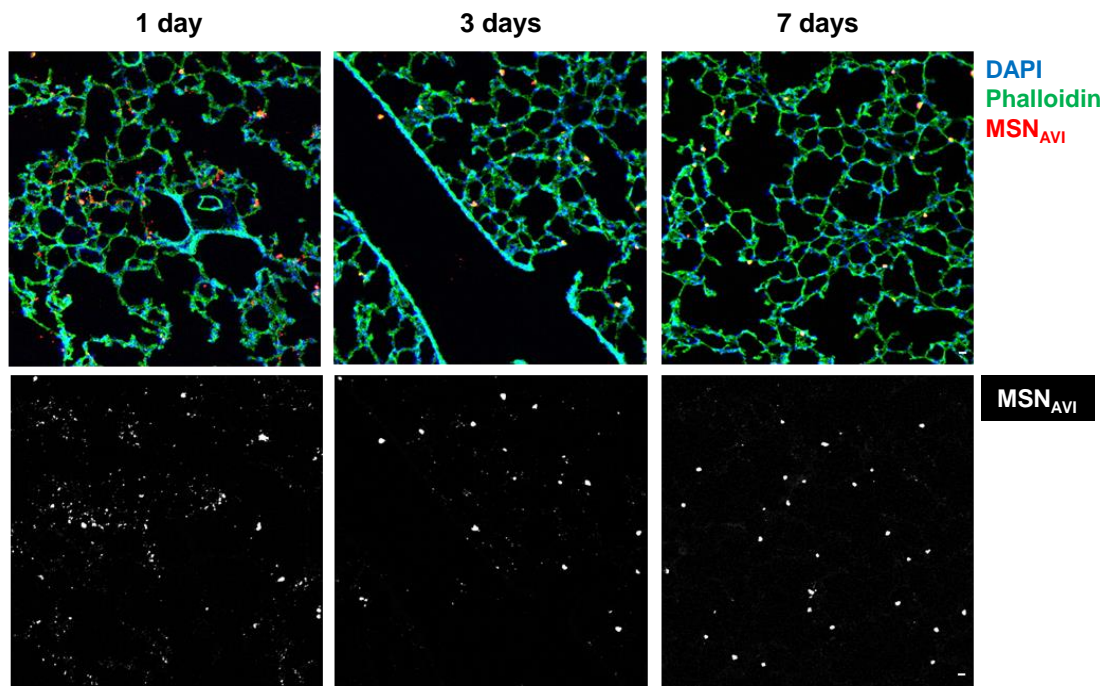


Figure 4.2 Biodistribution of MSN_{AVI} in mouse lungs 1-7 days post-instillation. Lung cryo-slices of BALB/c mice exposed to 100 μg MSN_{AVI} for 1, 3, or 7 days with phalloidin co-staining shown in green. Cell nuclei are shown in blue (DAPI), ATTO 633 labeled MSN_{AVI} are shown in red and at lower panel, MSN_{AVI} alone shown in white for ease of view. Images are representative images for $n = 4$ animals. Scale bar is 20 μm .

4.2.3 MSN instillation into the lungs does not affect lung histology

To investigate the morphological changes in the alveolar space upon MSN administration, we stained the lungs of the MSN_{AVI} and MSN_{NH_2} treated mice with hematoxylin & eosin staining. Our stainings revealed that there have been no changes in the alveolar structure upon MSN administration in 1-7 days (Figure 4.3).

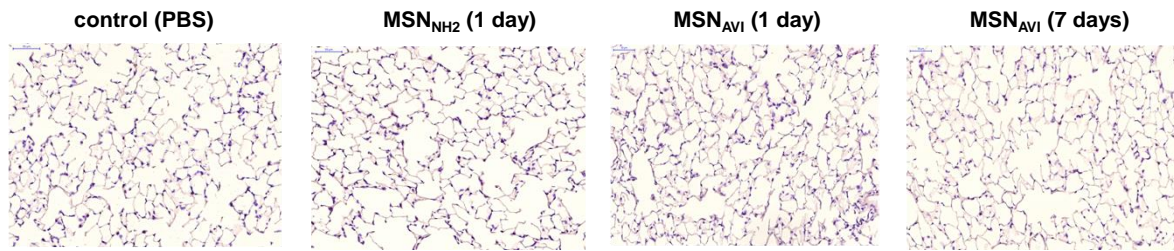


Figure 4.3 Lungs of BALB/c mice treated with 100 μg MSN_{AVI} or MSN_{NH_2} for 1 or 7 days stained with hematoxylin & eosin. Cell nuclei are shown in blue (hematoxylin), and the rest cellular fragments in violet (eosin). Scale bar is 50 μm .

4.2.4 Comparing the uptake of MSN_{AVI} versus MSN_{NH_2}

Having validated alveolar deposition of the nanoparticles, we compared the uptake of the functionalized (MSN_{AVI}) versus non-functionalized (MSN_{NH_2}) particles with cellular resolution. After examining the cryo-sections at higher zoom, we observed, after 1 day, the majority of the MSN_{NH_2} particle uptake was done by macrophages, whereas only a small fraction of the particles were taken up by epithelial cells (Figure 4.4A). Besides, z-stack analyses revealed that the non-taken up MSN_{NH_2} particles seem to associate with the extracellular matrix rather than being internalized into the cells (Figure 4.4A, right panel). Contrary to that, high resolution images of the MSN_{AVI} particle-treated lungs revealed a high uptake of the particles after 1 day by alveolar epithelial cells (Figure 4.4B, left panel), and that a small fraction of these particles remained in the epithelium for 7 days (Figure 4.4B, right panel).

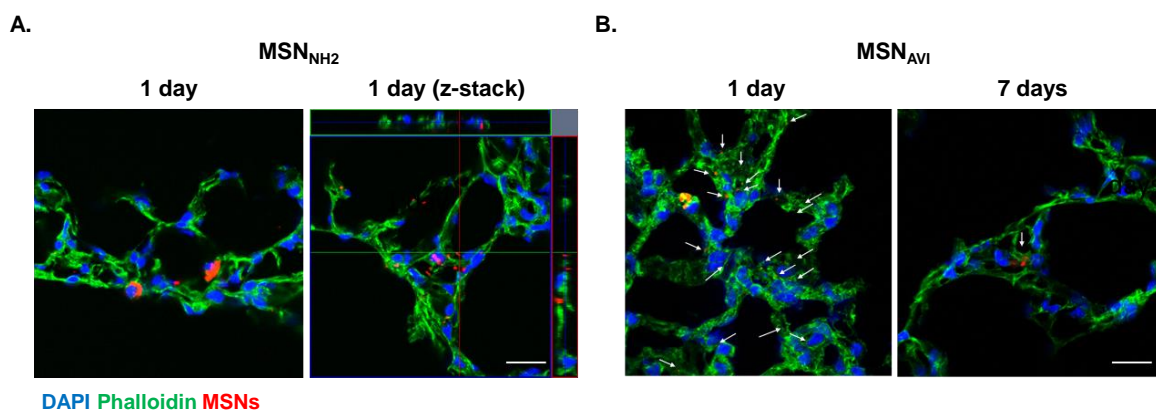


Figure 4.4 Lung cryo-slices of BALB/c mice exposed to (A) 100 μg MSN_{NH_2} for 1 day and (B) 100 μg MSN_{AVI} for 1 day (left) and 7 days (right) (arrowheads point locations of MSN_{AVI}). Cell nuclei are

shown in blue (DAPI), cell actin in green (phalloidin), and ATTO 633 labeled MSNs are shown in red. Images are representative images for $n = 4$ animals. Scale bar is 20 μm .

4.2.5 Epithelial uptake of MSN_{AVI} in mouse lungs

Next, we were interested in preferential cell-specific uptake of the instilled MSNs. Counterstaining the sections with epithelial type I and II cell markers, podoplanin ($\text{T1}\alpha$) and pro-surfactant associated protein C (Pro-SPC), respectively, revealed that MSN_{AVI} particles were internalized by epithelial lung cells (Figures 4.5A-C) as confirmed by confocal z-stack imaging (Figure 4.5C).

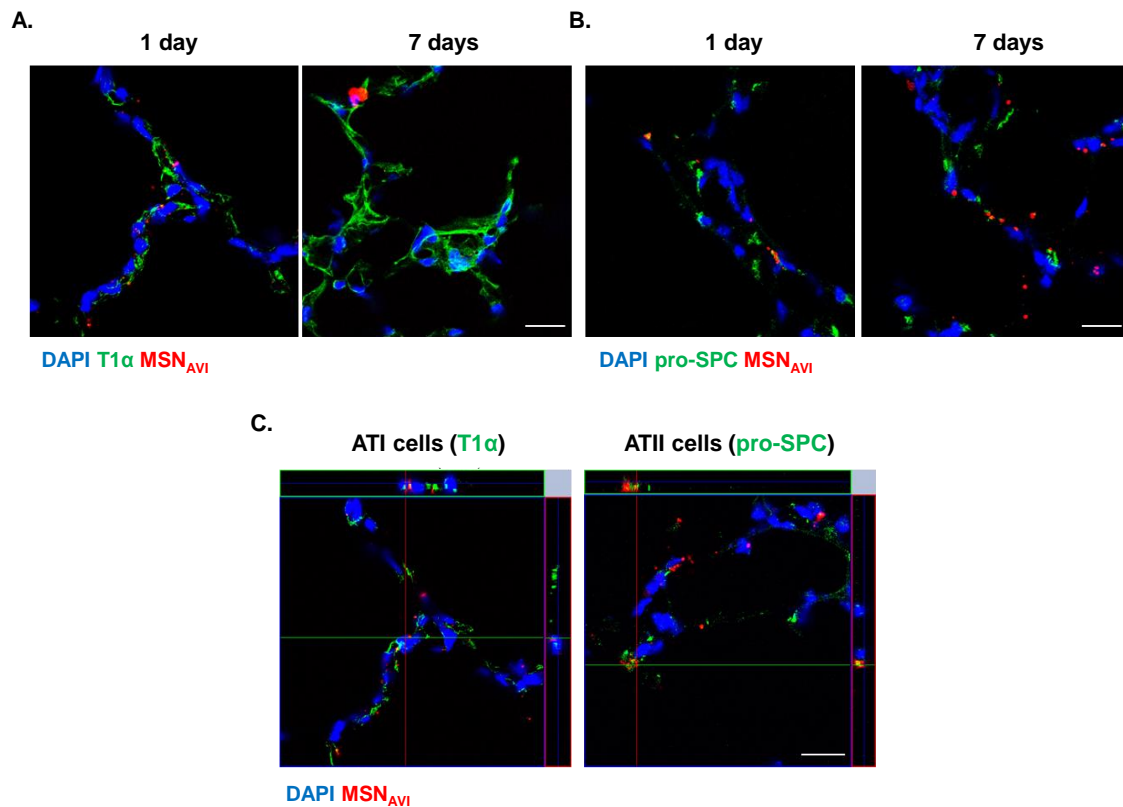


Figure 4.5 Immunofluorescence staining of mouse lungs that were exposed to 100 μg MSN_{AVI} with (A) epithelial cell type 1 co-staining ($\text{T1}\alpha$, green), and (B) epithelial cell type 2 co-staining (pro-SPC, green) for 1 day (left) and 7 days (right). (C) Z-stack images (63x objective) from sections of BALB/c mice exposed to MSN_{AVI} for 1 day after instillation, co-stained with alveolar epithelial cell type 1 (ATI) marker ($\text{T1}\alpha$, left image) and alveolar epithelial cell type 2 (ATII) marker (pro-SPC, right image) in green. Cell nuclei are shown in blue (DAPI), ATTO 633 labeled MSNs are shown in red. Images are representative images for $n = 4$ animals. Scale bar is 20 μm .

4.2.6 MSN_{AVI} exert less cytotoxic effects than MSN_{NH₂} *in vitro*

To validate whether the avidin-functionalization on the particles would have effects on cytotoxic behavior of the MSNs, we analyzed the metabolic activity of MH-S and MLE-12 cells that were exposed to increasing concentrations (0 - 500 $\mu\text{g/mL}$) of MSN_{NH₂} and MSN_{AVI} by MTT cytotoxicity assay. Interestingly, our data revealed that the non-functionalized MSN_{NH₂} particles had significantly more cytotoxic effects on MH-S alveolar macrophage cells in high doses particularly ($> 250 \mu\text{g/mL}$) (Figure 4.6A), but not in MLE-12 epithelial cells of the lung (Figure 4.6B).

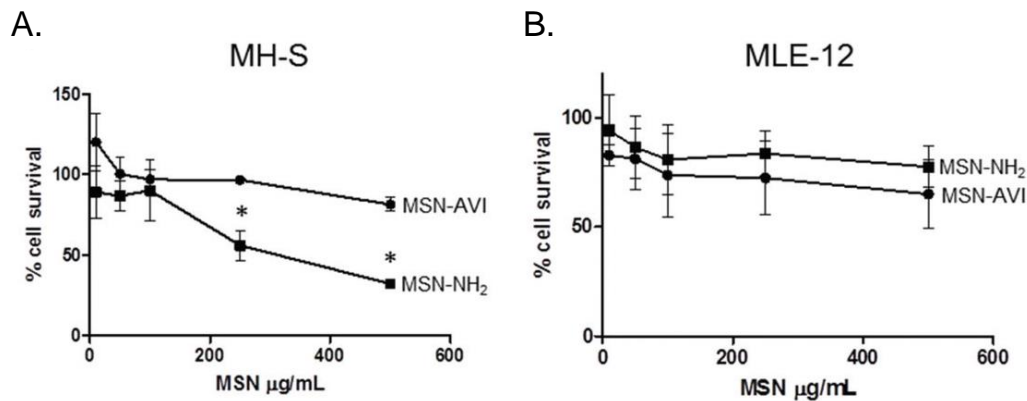


Figure 4.6 Percent cellular survival of the MH-S and MLE-12 murine cell lines of the lung exposed to increasing concentrations (0 - 500 $\mu\text{g/mL}$) of MSN_{NH₂} and MSN_{AVI} for 16 h assessed by MTT assay.

4.3 Discussion

We hereby tested the applicability of avidin-functionalized MSNs (MSN_{AVI}) as novel nanocarriers for lung diseases therapy by investigating their biodistribution, clearance, cell-specific uptake after direct (intratracheal) instillation in the lungs of mice. Due to the fact that MSNs allow for various functionalizations, which were shown to be paramount for their biocompatibility, we also tested only amino-functionalized; MSN_{NH₂} (so called ‘non-functionalized’ in this study) particles in this study. Our data revealed that avidin-functionalization on the surface of the MSNs had an impact not only on cytotoxicity, but also on the preferential cell-specific uptake and biodistribution in the lungs (van Rijt et al., 2016). Especially, non-functionalized particles (MSN_{NH₂}) were seldom taken up by epithelial cells. On the other hand, MSN_{AVI} particles were internalized by alveolar epithelial type I and type II cells in the lung. Our data encourages the use of avidin-functionalized

MSNs for epithelial cell-associated chronic lung diseases such as COPD, IPF, or lung cancer by the limited and cell-specific cytotoxicity, initial even biodistribution in the lung parenchyma followed by macrophage clearance of the particles in the lung. Hence, avidin-functionalized MSN_{AVI} particles are promising candidates to be used for inhalative therapies in chronic lung diseases. Additionally, our data strongly show the importance of surface modifications for cytotoxic effects and biodistribution of the nanoparticles and suggest stringent validation of these functionalizations for future nanoparticles for therapeutic use.

As a conclusion, immunofluorescence analyses for different cell types showed that non-functionalized MSN_{NH_2} particles were specially taken up by macrophages *in vivo* and that this had a cytotoxic effect on the macrophages (van Rijt et al., 2016). Contrary to that, avidin-functionalized MSN_{AVI} particles were first efficiently internalized by the epithelial type I and type II cells of the lung, and later cleared by the alveolar macrophages. Thus, potential drug-loaded MSN_{AVI} particles would have enough time to deliver the incorporated agents into the epithelial cells of the lung before their clearance. There have been studies showing that the cellular uptake of MSNs heavily depends on the surface charge and surface modifications of the nanoparticles, and is cell type-specific (Chung et al., 2007; Tao et al., 2009). Moreover, numerous *in vitro* studies revealed that the cellular uptake of MSNs is cell-, dose-, and time-dependent (Tang et al., 2012; Vivero-Escoto et al., 2010). Remarkably, there were studies showing that the amination of MSN particles thwarts particle uptake in T-lymphocyte cells (Jurkat) and in a human neuroblast cell line (Kreyling et al., 2013; Tao et al., 2009). These findings emphasize the significance of outer surface functionalizations and their impact on nanoparticle interactions with different cell types; and avidin-functionalization stands as a good strategy to minimize issues associated with macrophage uptake and particle toxicity.

Experiments for the presented data were conducted in collaboration with Sabine van Rijt.

5 MMP9-responsive MSN_{AVI} particles for lung cancer therapy

Parts of this chapter have previously been published as:

van Rijt S.H., Bölükbas D.A., Argyo C., Datz S., Lindner M., Eickelberg O., Königshoff M., Bein T., and Meiners S. (2015). *Protease-mediated release of chemotherapeutics from mesoporous silica nanoparticles to ex vivo human and mouse lung tumors*. ACS Nano, 9(3):2377-2389.

5.1 Introduction

Release principles of many nanoparticle-mediated drug delivery agents are based on free degradation of the nanoparticle in biological environments (*e.g.*, hydrolysis) but do not involve controlled release of the drug. Controlled release can be accomplished for instance by taking advantage of the pathological features of malignant microenvironments such as reducing conditions, alterations in pH (*e.g.*, acidic conditions in endosomes), or elevated levels of disease-associated enzymes (Torchilin, 2014). To give an example, several enzymes such as matrix metalloproteinases 2 and 9 (MMP2 and MMP9) are overexpressed in lung cancer, however negligibly expressed in healthy tissue (Egeblad and Werb, 2002). Furthermore, increased levels of MMP2/9 in the tumor microenvironment promote the metastasis potential of cancer cells and contribute to tumor growth, angiogenesis, or metastasis (Gialeli et al., 2011). Especially, elevated levels of MMP9 have been associated with poor prognosis of lung cancer (Iniesta et al., 2007; Martins et al., 2009). Specific peptide linkers can be used as enzyme-responsive linkers (Turk et al., 2001) to allow for controlled release of drugs from nanocarriers, as previously presented by other groups where they made use of MMP2/9-sensitive linkers for controlled drug release (Chien et al., 2013a; Chien et al., 2013b; Chiou et al., 2012; Gu et al., 2013; Hatakeyama et al., 2011; Li et al., 2013; Yamada et al., 2010; Zhu et al., 2013). Therefore, developing nanoparticles with MMP2/9-responsive drug release represents a promising approach for treatment of lung cancer.

Multifunctional mesoporous silica nanoparticles (MSNs) are versatile agents for drug delivery (Argyo et al., 2013). MSNs have exclusive features such as tunable pore sizes and

volumes for high drug payload and effective encapsulation for a rich diversity of cargos (Li et al., 2012). Moreover, these nanocarriers can be efficiently functionalized at different sites within the nanoparticle (Cauda et al., 2009). For instance, an outer-shell modification allows for attachment of external molecules selectively on the outer surface of the particle, having no impact on the porous part. This feature can be used to generate stimuli-responsive pore sealing for controlled drug release (Aznar et al., 2011; Giri et al., 2005; Popat et al., 2012; Sauer et al., 2010; Zhao et al., 2010). As an example, the sealing of the pores could be attained by exploiting strong biotin-avidin interactions, that would clot the openings of the pores in a responsive manner (Schlossbauer et al., 2009).

In this study, we demonstrate avidin-functionalized MSNs modified with MMP2/9-responsive peptide linkers, resulting in controlled release of FDA-approved drugs in MMP9-rich lung tumor regions. We show efficient enzyme-specific release of the encapsulated chemotherapeutic cisplatin (CP), as well as the proteasome inhibitor bortezomib in two lung cancer cell lines. To validate the efficiency of the particles in malignant tissue, we developed a novel experimental setup exploiting 3D lung tissue cultures (3D-LTCs). This method grants spatio-temporal information and validation of nanoparticle-mediated drug delivery in the original 3D environment of malignant mouse and human tissue. We here present MMP9-mediated lung tumor site-selective drug release and tumor cell death in mouse and human lung tumors illuminating the feasibility of MMP9-controlled drug delivery with MSNs for treatment of lung cancer.

5.2 Results

5.2.1 Successful synthesis of MMP9-responsive MSNs

MSNs were successfully synthesized by a sol-gel procedure, as in previous studies (Cauda et al., 2009; Mackowiak et al., 2013). To generate MMP9-responsive MSNs, MMP9-specific cleavable heptapeptide linker (**RSWMGLP**, cleavage site in bold) was attached to the core-shell functionalized MSN_{NH₂} particles (Figure 5.1i). As a control system, the cleavage site was disturbed by a change in the specific heptapeptide sequence (**RSWMLLP**, change in bold) (Figure 5.1i). Later, the particles were labeled with ATTO 633 dye and/or loaded with drugs, and finally capped with the avidin-biotin complex for further experiments (Figure 5.1ii).

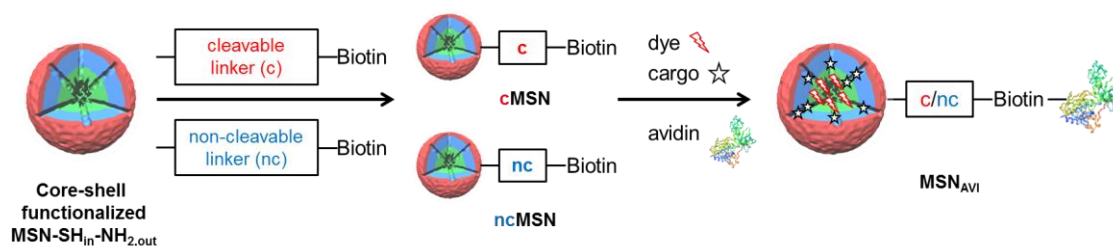


Figure 5.1 Synthesis of MMP9-cleavable cMSN_{AVI} *versus* MMP9-non-cleavable ncMSN_{AVI} particles

5.2.2 Cytotoxicity of MSNs in lung cancer cell lines

Before we validated MMP9-responsive cell death induced by our nanoparticles, we investigated whether the avidin-functionalized *versus* non-functionalized MSN_{AVI} particles exert cytotoxic effects on lung cancer cells. Thus, we exposed A549 and H1299 cell lines to MSN_{NH2} and MSN_{AVI} particles in doses between 0 - 500 $\mu\text{g}/\text{mL}$ for 4 and 24 h at normal cell growth conditions, and afterwards we measured the metabolic activity by WST-1 assay as a read-out for cellular survival. No toxic effects were observed after 4 h (Figures 5.2A&C). However, after 24 h (Figures 5.2B&D), MSN_{NH2} particles induced cytotoxic effects at high doses ($> 250 \mu\text{g}/\text{mL}$).

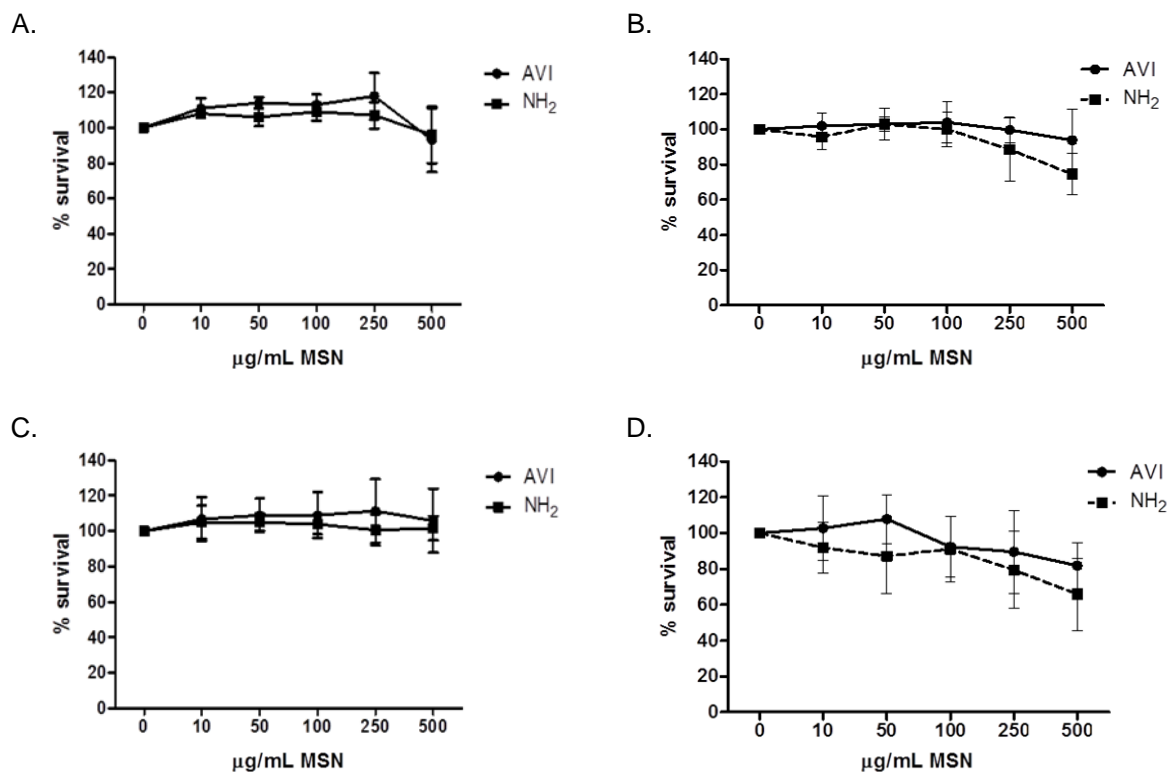


Figure 5.2 Percent survival of human lung cancer cell lines (A&B) A549 and (C&D) H1299 exposed to increasing concentrations (0 – 500 µg/mL) of MSN_{NH2} and MSN_{AVI} for (A&C) 4 and (B&D) 24 h as a read-out from metabolic activity assessed by WST-1 cytotoxicity assay.

5.2.3 Induction of apoptosis by MSNs in lung cancer cell lines

Next, we dissected the apoptotic and necrotic effects of the avidin-functionalized *versus* non-functionalized MSN_{AVI} particles on lung cancer cell lines by Annexin V/propidium iodide staining followed by flow cytometry analysis. Hence, we exposed A549 and H1299 cell lines to 250 µg/mL MSN_{NH2} and MSN_{AVI} particles for 24 h at normal cell growth conditions, then stained the treated cells for Annexin V and propidium iodide staining, and afterwards measured the apoptosis and necrosis induced by the nanoparticles. As a positive control, H₂O₂ was used as a cytotoxic agent at the experiment. Our data revealed that, both in (Figure 5.3A) A549 and (Figure 5.3B) H1299 cells, MSN_{NH2} particles (left panels) caused more apoptosis in comparison to MSN_{AVI} particles (middle panels), when assessed by flow cytometry analysis of Annexin V-FITC/propidium iodide (PI) staining (Figure 5.3).

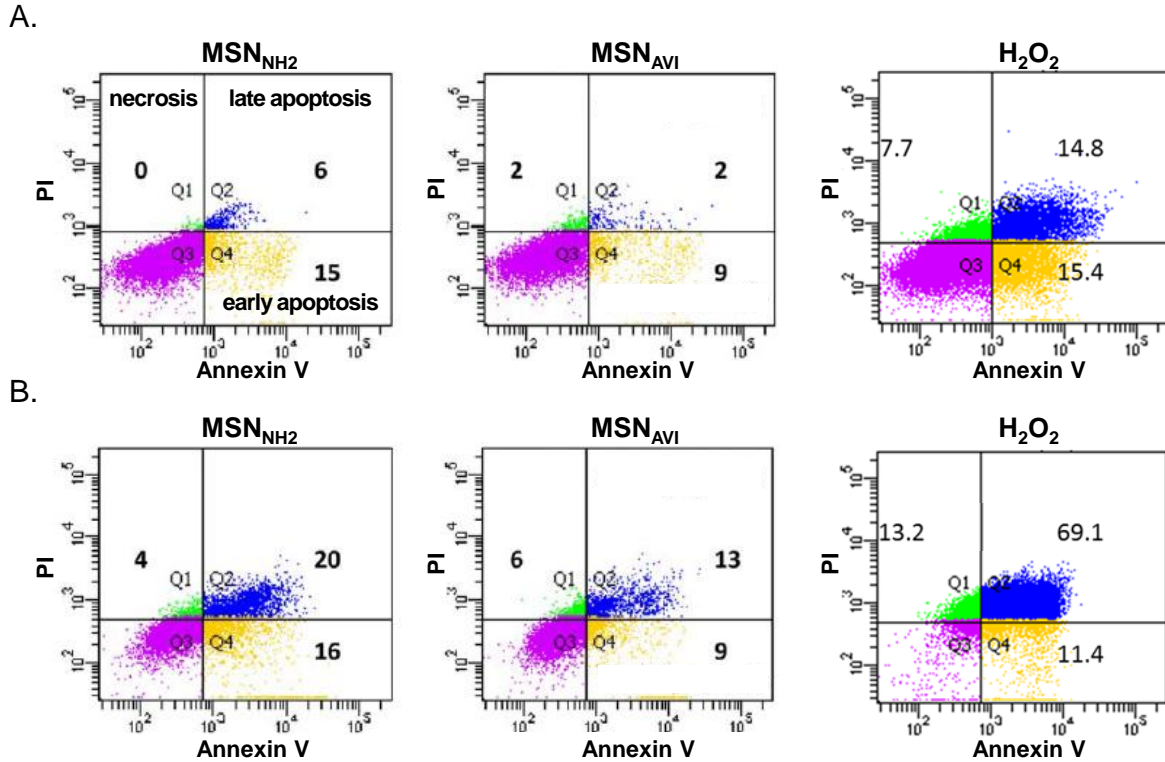


Figure 5.3 Apoptotic *versus* necrotic effects of the non-functionalized MSN_{NH₂} *versus* avidin-functionalized MSN_{AVI} nanoparticles on (A) A549 and (B) H1299 cell lines compared to H₂O₂-treated cells after 24 h, measured by Annexin V/propidium iodide staining analysis by flow cytometry.

5.2.4 MMP9-dependent calcein-AM release *in vitro*

We next validated MMP9-responsive cargo release from the cleavable *versus* non-cleavable nanoparticles by confocal microscopy. Calcein-AM is a non-fluorescent cell membrane permeable compound, that is hydrolyzed by intracellular esterases into the cell impermeable green fluorescent calcein. More specifically, calcein-AM is taken up by the cells via endocytosis, and can be detected in the cytoplasm even at low doses (Figures 5.4A&C). Here, we used calcein-AM as a model drug which is, after being released from the nanoparticles into the extracellular matrix, subsequently taken up actively by the cancer cells. In the cells, it is metabolized, and becomes active, as evidenced by fluorescence emission. Thus, MSN_{AVI} particles containing either MMP9-cleavable or non-cleavable linkers (cMSN_{AVI} and ncMSN_{AVI}), encapsulating solutions of calcein-AM with different concentrations, were incubated with increasing amounts of recombinant MMP9. After 2 h of incubation with recombinant MMP9, effective calcein release and delivery to the cytosol was observed in

both cell lines (Figures 5.4B&D, right panels). Notably, in both cell lines, the amount of calcein staining was dependent on not only the MMP9 concentration, but also the amount of calcein-AM encapsulated in the particles. The MSNs containing non-cleavable linkers (ncMSN_{AVI}) displayed only limited release of calcein-AM (Figures 5.4B&D, left panels). Calcein staining was more effective on H1299 cells, compared to the A549 cells, where significant fluorescence was observed when 20 μ M solution of calcein-AM encapsulated MSNs were exposed to 1 μ g/mL MMP9. This coincides with the observation that H1299 cells were more sensitive towards calcein staining, as seen in the calcein-AM titration curves (Figure 5.4C) which may relate to an increased endosomal uptake capacity of these cells. Interestingly, we did not observe any dose-dependent staining for non-cleavable linker-bearing ncMSN_{AVI} particles in both cell lines (Figures 5.4B&D right panels), showing that the calcein-release from our functionalized MSNs was MMP9-specific and the avidin capping was tight enough to prevent leakage from the pores of the MSNs. Conclusively, cMSN_{AVI} particles that were pre-activated with MMP9 showed efficient and stimuli-responsive release of the calcein-AM.

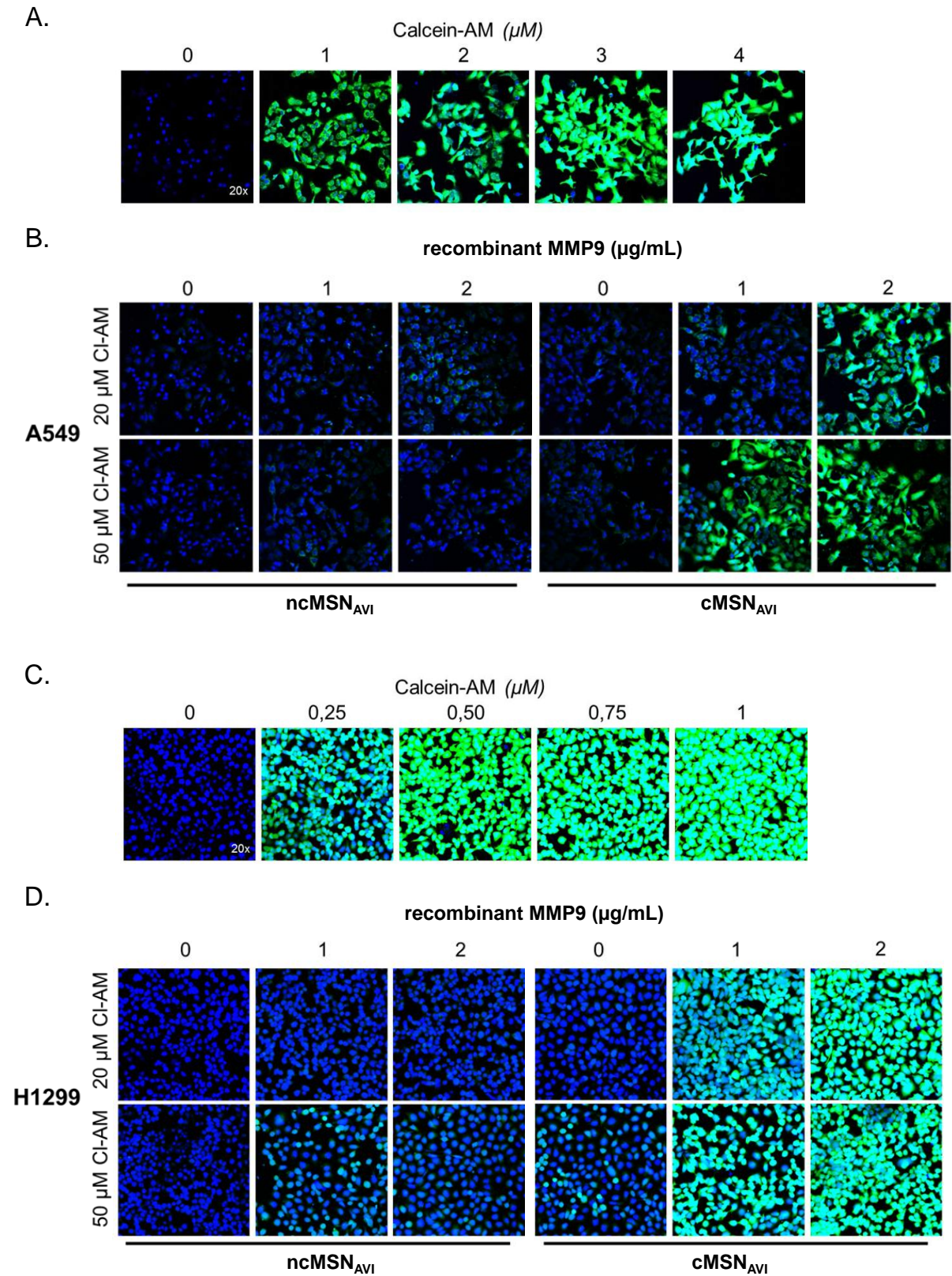


Figure 5.4 Confocal microscopy images of calcein-AM titration on (A) A549 and (C) H1299 cells, and calcein staining as a result of MMP9-responsive release from 20 μM and 50 μM calcein-AM (CI-AM, green) loaded MSNs bearing MMP9 cleavable or non-cleavable linkers (cMSN_{AVI} and

ncMSN_{AVI}), after 2 h of incubation with either 0, 1, or 2 $\mu\text{g}/\text{mL}$ recombinant MMP9 administration in (B) A549 and (D) H1299 human lung cancer cells. Hoechst (blue) was used for nuclei staining. Pictures show representative micrographs from three independent experiments. Image sizes are 450 x 450 μm .

5.2.5 MMP9-dependent cell death in lung cancer cell lines

Cisplatin is a commonly used chemotherapeutic agent for treatment of several solid cancers, including lung cancer (Adelstein and Rodriguez, 2008). Drawbacks of cisplatin therapy include nephrotoxicity, nausea, hair loss, and acquired resistance of tumors towards the treatment. A more targeted and local delivery of cisplatin may result in lower administered therapeutic doses, and consequently reduced systemic toxicity. For these reasons, we decided to use cisplatin as one of the chemotherapeutic loads in our MSNs. Accordingly, cisplatin release from the particles was measured as a function of cell viability. In both cell lines, cells exposed to particles (cMSN_{AVI}) loaded with cisplatin in the absence of MMP9 showed only minor loss of cell viability, compared to untreated control cells (white bars in Figures 5.6A&B). These results clearly demonstrate the tight sealing of the cisplatin loaded MSNs by the avidin capping. Strikingly, in both cell lines the cytotoxic effects of cisplatin were dependent on both the release from the particles by MMP9 and the cisplatin encapsulated dose (Figures 5.6A&B). Significant cell death was already observed for cells exposed to particles loaded with a 10 μM solution of cisplatin when 1 $\mu\text{g}/\text{mL}$ MMP9 was administered into the medium, and to a similar extent in cells exposed to particles loaded with a 20 μM solution of cisplatin in the presence of 0.5 $\mu\text{g}/\text{ml}$ MMP9. H1299 cells were more sensitive towards the cisplatin loaded MSNs, in analogy to the calcein-AM release experiments. As a control, we exposed A549 and H1299 cells to the non-cleavable linker bearing ncMSN_{AVI} particles loaded with cisplatin. Our data showed that even in the presence of 1 $\mu\text{g}/\text{mL}$ recombinant MMP9, no significant cell death was observed in A549 and H1299 cell lines, proving that the cleavable linker was indeed MMP9-specific, and this specificity was lost in the non-cleavable linker bearing ncMSN_{AVI} system (Figure 5.6C).

It is important to remark that the MSNs were pre-loaded by diffusing a defined dilution of cisplatin into the particles, which were afterwards sealed and washed to remove non-incorporated cisplatin. In our figures, these loading concentrations are referred to as loaded cisplatin concentrations. Nonetheless, the total cisplatin released from the MSNs,

i.e., the bioactive cisplatin dose the cells or tissues were exposed to, was much less, since the encapsulated amount is lower than the actual amount in the stock solution. However, ICP-OES measurements showed an efficient cisplatin loading of $440 \pm 0.02 \mu\text{g}/\text{mg}$ MSN when 10 mM cisplatin stock solution was diffused into the particles at the synthesis (Table 5.1). Yet when we treated the nanoparticles in the presence of MMP9, we observed $7 \pm 0.8 \mu\text{g}$ cisplatin release per mg MSN. In contrast, the cisplatin release was below detection limit in the absence of MMP9 (Table 5.1). We also analyzed a dose-response viability curve using direct cisplatin application in A549 and H1299 cells and thereby calculated the amount of bioactive cisplatin released from the MSNs as around 10-fold less than the loading stock solution (Figure 5.5). This 10-fold dilution of cargo in MSNs accords very well with our results obtained with calcein-AM experiments when comparing the calcein titration curve to the release of calcein-AM loaded particles (Figure 5.4).

Table 5.1 Quantification of the uptake and release of cisplatin in cMSN_{AVI} particles measured by ICP-OES. Release was achieved by MMP9 administration. Values given are average of three independent experiments \pm SD.

cisplatin amount (at stock solution)	10 mM
uptake of cisplatin	$440 \pm 0.02 \mu\text{g}/\text{mg}$ cMSN _{AVI}
release of cisplatin (+ MMP9)	$7 \pm 0.8 \mu\text{g}/\text{mg}$ cMSN _{AVI}
release of cisplatin (- MMP9)	<i>below detection limit</i>

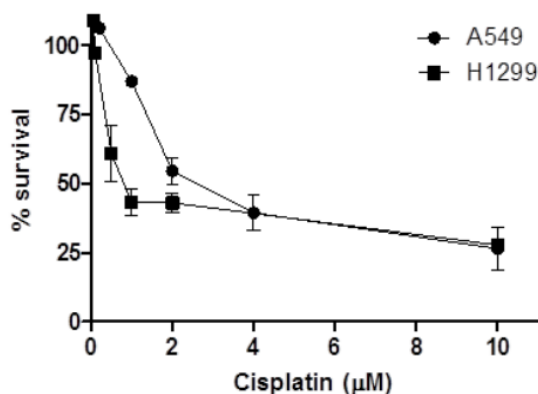


Figure 5.5 Dose-response survival curve of free cisplatin in A549 and H1299 cells after 24 h exposure

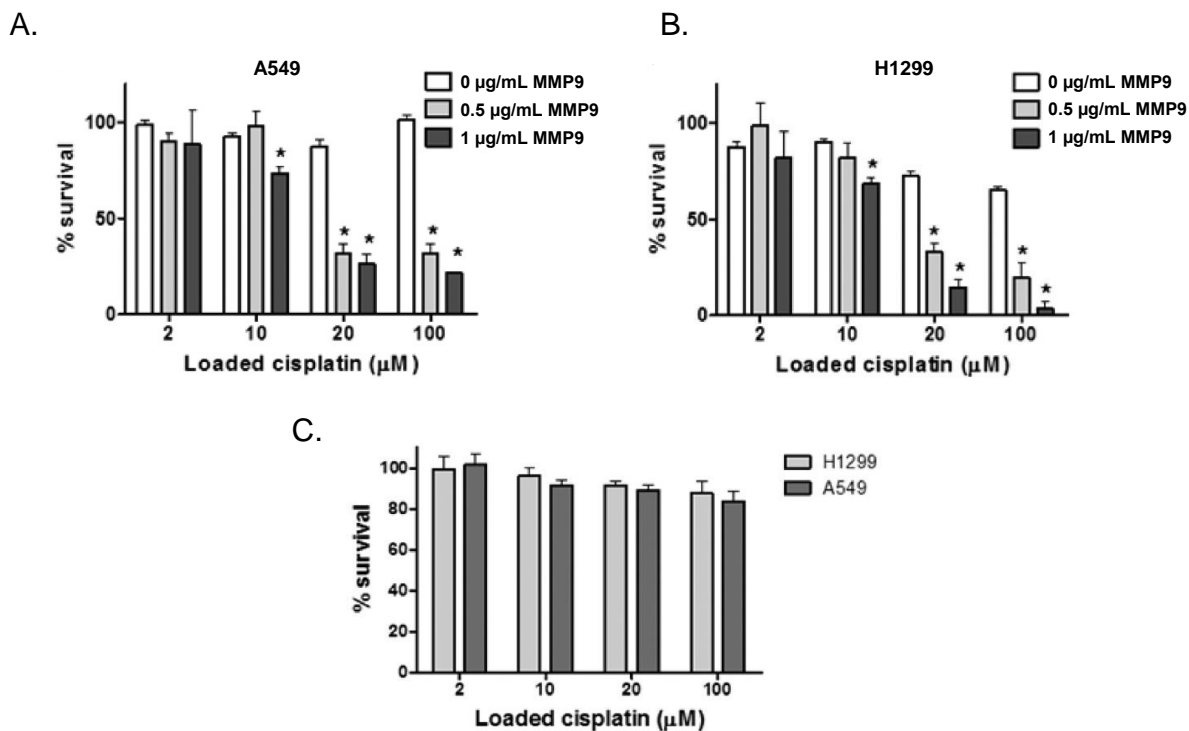


Figure 5.6 Controlled release of cisplatin from cMSN_{AVI} particles as measured by percent cell survival after 24 h exposure, incubated with 0 (white bars), 0.5 (light gray bars), or 1 μg/mL (dark gray bars) MMP9 in (A) A549 and (B) H1299 cells. (C) Percent cellular survival of H1299 (light gray bars) and A549 (dark gray bars) cells exposed to ncMSN_{AVI} particles loaded with cisplatin, in the presence of 1 μg/mL recombinant MMP9, for 24 h. Untreated cells were set to 100% survival; * means a significant decrease in percent cell survival compared to control ($p < 0.05$). Values given are an average of three independent experiments \pm SD.

5.2.6 Cell-secreted MMP9-induced death of lung cancer cell lines

Next, we investigated whether MMP9 that is secreted from tumor cells induces cleavage of the linkers and results in controlled release of the drugs from the MSNs. For that, we cloned MMP9 cDNA into an eukaryotic expression vector and transiently transfected the A549 and H1299 cells overnight. We first validated the MMP9 overexpression of transiently transfected cells in comparison to recombinant MMP9 concentrations by gelatin zymography (Figure 5.7A). Then we exposed these transfected cells to MSNs for 24 h. Remarkably, our survival data showed that cell-secreted MMP9 was sufficient to cleave the MMP9-specific linker and result in dose-dependent cell death (Figure 5.7B, gray bars). In contrast, no signs of toxic effects were observed in empty vector transfected cells (Figure 5.7B, white bars).

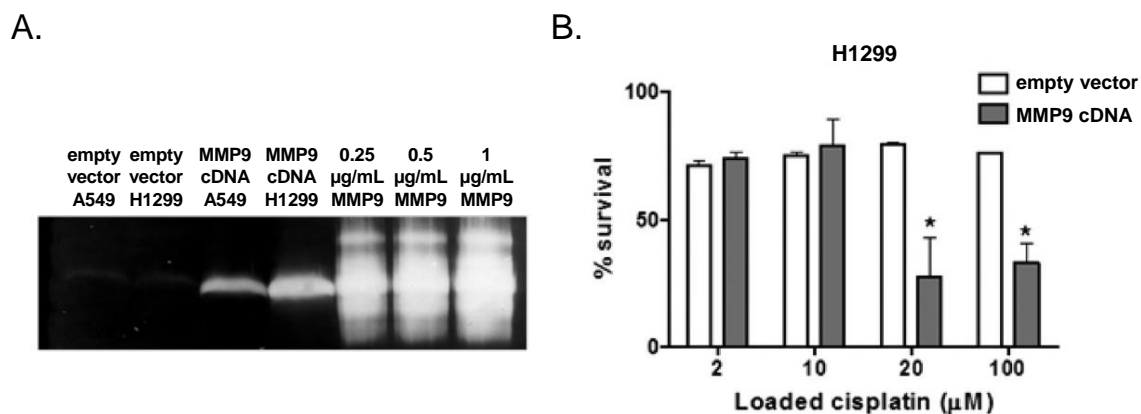


Figure 5.7 (A) Gelatin zymography comparing MMP9 secretion of transiently MMP9 cDNA or empty vector transfected A549 and H1299 cells with recombinant MMP9 concentrations of 0.25, 0.5, and 1 µg/mL. (B) Controlled release of cisplatin from cMSN_{AVI} as measured by percent survival after 24 h exposure, incubated with MMP9 cDNA (gray bars) or empty vector transfected (white bars) H1299 cells. Untreated cells were set to 100% survival. * means a significant decrease in percent cell survival compared to control ($p < 0.05$). Values given are an average of three independent experiments \pm SD.

5.2.7 Synergistic effect of combination therapy

Cisplatin is often given in combination treatments with other chemotherapeutics, in order to overcome the problem of acquired resistance (Dubey and Powell, 2008). Proteasome inhibitors are promising combinatorial drugs as suggested by multiple clinical trials, since they effectively inhibit proliferation of tumor cells, sensitize them to apoptosis, and overcome drug resistance (Davies et al., 2007b). The proteasome inhibitor bortezomib is FDA-approved for treatment of multiple myeloma, and currently tested in phase II clinical trials for lung cancer (clinicaltrials.gov). Accordingly, local and targeted drug delivery of proteasome inhibitors in combination with cisplatin into the lung may sensitize the cancer cells to treatment, reduce systemic side effects as well as overcome acquired resistance towards cisplatin, thus representing a novel therapeutic approach for combating lung cancer. Because MSNs can encapsulate multiple drugs in their mesoporous system efficiently (Chen and Liu, 2016), these carrier systems offer an excellent opportunity for controlled local delivery of two drugs at the same time. This is anticipated to result in lower administered doses of chemotherapeutics necessary to achieve a similar therapeutic effect. To investigate whether we could reduce the amount of cisplatin to obtain a similar therapeutic effect in the presence of bortezomib, we exposed A549 cells to MSNs loaded with a solution containing 2, 10, or

20 μM cisplatin together with 1 μM of bortezomib. When using toxic doses of cisplatin, the concomitant release of bortezomib had no additional effect on cell death. However, non-toxic doses of cisplatin (*i.e.*, particles loaded with 2 and 10 μM solutions), induced significant cell death for particles that contained both drugs (Figure 5.8). Notably, this difference was largest for the lowest cisplatin dose (2 μM), with an increased cell death of over 35 % in the presence of bortezomib. This is a remarkable 5 to 10 folds increase in cytotoxic potency, when bortezomib is added as a combinatorial drug. For 10 μM cisplatin loaded particles, this difference was 17 %. cMSN_{AVI} particles loaded with only 1 μM bortezomib (and no cisplatin) were included as controls, and did not show any effect on cell viability after 24 h of exposure (Figure 5.8, striped bar). Cells exposed to MSNs loaded with 2, 10, or 20 μM cisplatin and 1 μM bortezomib in the absence of MMP9 also showed no significant loss in cell viability (Figure 5.8, white bars).

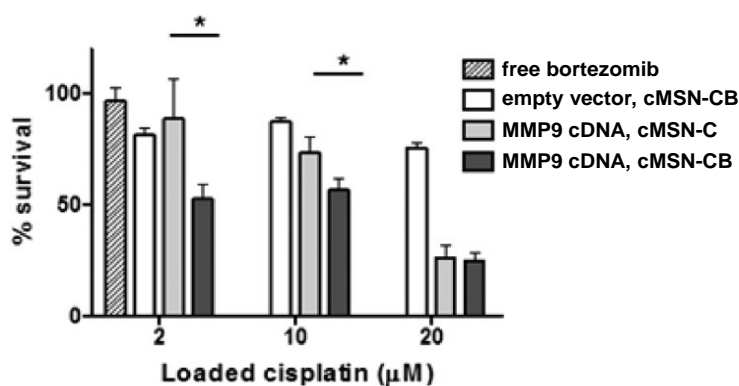


Figure 5.8 Percent cellular survival of A549 cells exposed to cMSN_{AVI} particles loaded with cisplatin alone (cMSN_{AVI}-C, light gray bars) and in combination with 1 μM bortezomib (cMSN_{AVI}-CB, dark gray bars) in MMP9 cDNA transfected A549 cells, in comparison to empty vector transfected A549 cells (white bars) and free 1 μM bortezomib treated cells (striped bar) after 24 h. Untreated cells were set to 100% survival; * means a significant decrease in percent cell survival compared to control ($p < 0.05$). Values given are an average of three independent experiments \pm SD.

5.2.8 Murine 3D-lung tissue cultures for MSN_{AVI} exposure

Having proven successful controlled release from our nanoparticles *in vitro*, we decided to exploit the 3D-lung tissue cultures (3D-LTCs) system as a versatile platform to assess *ex vivo* MMP9-mediated controlled release of chemotherapeutics from MSN_{AVI} particles in tumorous mouse tissue. In sequential 200 μm thick cut 3D lung slices from *Kras* mutant mice with lung

cancer, tumorous regions could be observed readily by bright-field microscopy as dense dark regions (Figure 5.9A right panel) in comparison to tumor-free healthy alveolar structures (Figure 5.9A). The same was validated for fluorescently stained slices measured by confocal microscopy (Figure 5.9B). Additionally, immunofluorescence staining for Kras and MMP9 was positive in tumorous *Kras* mutant lung slices as observed by confocal microscopy (Figures 5.9C&D) and was also validated by immunohistochemistry for the latter (Figure 5.9E).

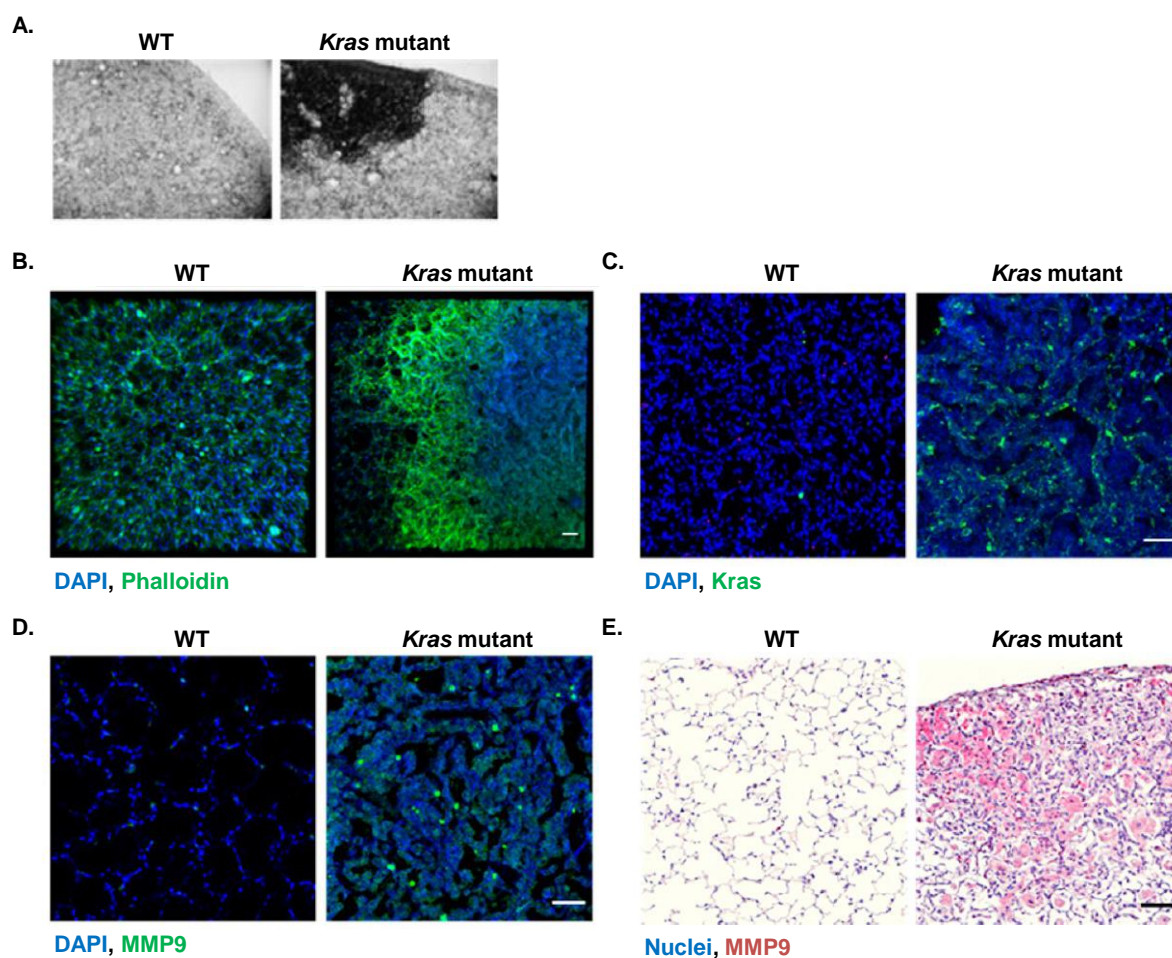


Figure 5.9 3D-lung tissue cultures (3D-LTCs) from tumorous mouse tissue. (A) 5x magnified bright-field microscopy images of tumorous *versus* tumor-free 3D-LTCs from WT and *Kras* mutant mice with lung tumors. Confocal microscopy images of WT and *Kras* mutant mouse 3D-LTCs with (B) phalloidin, (C) Kras, and (D) MMP9 staining. (E) Immunohistochemistry staining for MMP9 in WT and *Kras* mutant mouse lungs. The scale bar is 50 μ m.

5.2.9 MSN_{AVI}-based MMP9-responsive drug release to murine 3D-LTCs

Once we had established the 3D-LTCs of *Kras* mutant mouse lung tumor tissue as a tool for MMP9-mediated drug delivery via nanoparticles, we evaluated controlled drug release from our functionalized nanoparticles (cMSN_{AVI}). For that, lung tissue slices of *Kras* mutant mice were exposed to particles containing various concentrations of cisplatin (cMSN-C_{low} and cMSN-CB_{high}) or a combination of low doses of cisplatin with bortezomib (cMSN-CB) for 24 or 48 h.

Table 5.2 MSN_{AVI} loading concentrations for 3D-LTC exposure experiments

label	loaded drug concentration
cMSN _{AVI} -C _{low}	2 mM cisplatin
cMSN _{AVI} -C _{high}	10 mM cisplatin
cMSN _{AVI} -CB	2 mM cisplatin + 1 μ M bortezomib
ncMSN _{AVI} -C _{low}	2 mM cisplatin
ncMSN _{AVI} -C _{high}	10 mM cisplatin
ncMSN _{AVI} -CB	2 mM cisplatin + 1 μ M bortezomib
C _{low}	0.2 mM cisplatin
C _{high}	1 mM cisplatin
CB	0.2 mM cisplatin + 0.2 μ M bortezomib

First, we proved that the non-loaded MSNs did not induce any cytotoxic effects on WT mouse 3D-LTCs in 72 h. For that, we stained the treated 3D-LTCs with cleaved caspase-3 and analyzed for apoptosis by confocal microscopy (Figure 5.10A). Then, we established the cytotoxic dose for cisplatin by exposing the lung tissue slices to various concentrations of the drug. At the reported cisplatin concentrations of 0.2 and 1 mM (Table 5.2), we observed a significant amount of apoptosis of approximately 12% of the cells after 24 h and 20% after 48 h (Figures 5.10E&G), as indicated by a significant amount of cleaved caspase-3 positive staining (Figure 5.10B, right panel). Due to our *in vitro* findings of about 10-fold less encapsulation efficiency of cisplatin into the MSNs, we loaded 10-fold higher doses of cisplatin inside the pores of the MSNs to possibly achieve a comparable cytotoxic effect and applied these particles to the lung slices. Notably, a similar amount of tumor cell death was observed for both the encapsulated drugs and the free drugs for all tested doses and time

points, indicating that the doses were effective and equipotent (Figures 5.10D&G). Remarkably, all the MSNs containing chemotherapeutics resulted in cell death only in tumorous parts of the *Kras* mutant mice lungs, while not affecting tumor-free regions in the same *Kras* mutant lung tissues (Figure 5.10B). Additionally, a dose-dependent therapeutic effect on apoptotic cell death was observed, having the strongest effect with the combination therapy (cMSN_{AVI}-CB) (Figure 5.10B). However, *Kras* mutant mouse 3D-LTCs exposed to comparable doses of free drug/s (C or CB) had apoptotic effects which were not discriminating between tumorous and tumor-free tissue (Figure 5.10B). Interestingly, MSNs with non-cleavable linkers loaded with both drugs (ncMSN_{AVI}-CB) resulted in no significant apoptotic cell death in *Kras* mice tumors or in healthy tissues of *Kras* mutant lungs (Figure 5.10C, upper panel). Added to that, healthy lungs of WT mice 3D-LTCs exposed to drug-encapsulated cleavable nanoparticles (cMSN_{AVI}-CB) did not show obvious signs of apoptosis, while treatment with the comparable doses of free drugs resulted in apoptotic cell death which distributed homogeneously in the healthy tissue (Figure 5.10C), further validating the specific cytotoxic effect of our MSNs. The dose- and time- dependent therapeutic efficacy of the MSNs was quantified by analyzing the number of apoptotic cells *versus* the total number of cells in lung tissue slices containing tumors of similar size by Imaris software. Importantly, cell death in tumorous regions was 10- to 25-fold stronger when compared to the tumor-free area upon nanoparticle-mediated drug delivery. This effect was even more distinct after 48 h (Figure 5.10F) and was most prominent using the combination therapy with a 25-fold increase in apoptotic tumor cell death. On the other hand, *Kras* mutant mice lungs treated with similar doses of free cisplatin and/or bortezomib for 24 and 48 h showed a similar degree of apoptotic cell death in the tumor and tumor-free areas (Figures 5.10E&G), except for the highest doses (C_{high} and CB) where a small but significant increase in tumor cell death was detected. This can be attributed to the increased vulnerability of fast-dividing tumor cells against cisplatin (Dasari and Tchounwou, 2014).

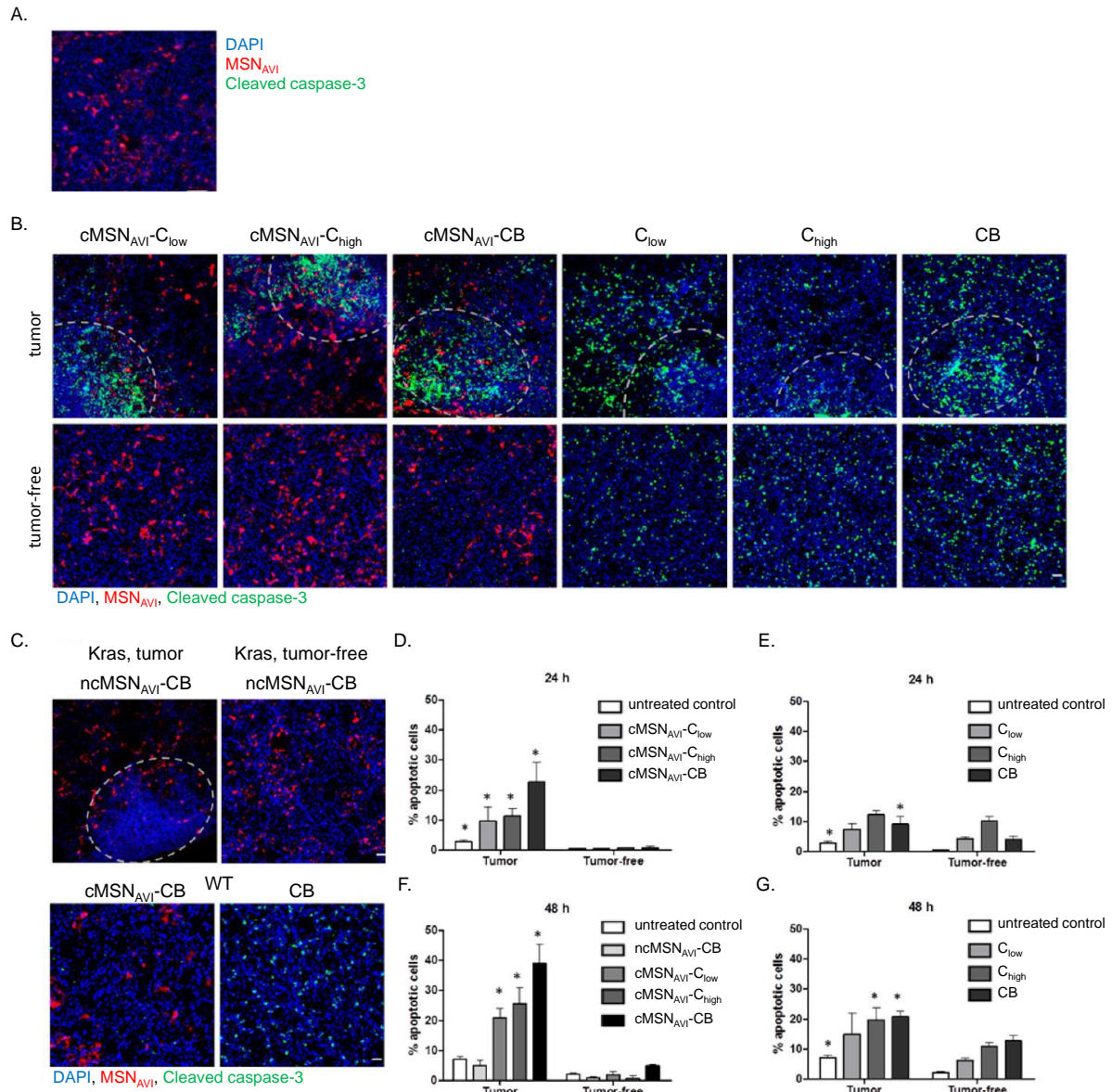


Figure 5.10 Therapeutic efficacy of MMP9-responsive MSNs in *Kras* mutant mouse lungs. (A) No cytotoxic effects of non-loaded MSN_{AVI} particles after 72 h exposure on WT healthy mouse 3D-LTCs stained for cleaved caspase-3 (green) measured by confocal microscopy. (B) *Kras* mutant mouse 3D-LTCs exposed to MSN_{AVI} particles loaded with a low dose of cisplatin (cMSN_{AVI}-C_{low}), high dose of cisplatin (cMSN_{AVI}-C_{high}), low dose of cisplatin in combination with bortezomib (cMSN_{AVI}-CB), or comparable doses of the free drugs cisplatin (C_{low}, C_{high}) or combination therapy (CB) for 48 h. (C) *Kras* mouse 3D-LTCs exposed to MSN_{AVI} particles with non-cleavable linkers loaded with the combination treatment (ncMSN_{AVI}-CB) for 48 h (upper panel) and WT mouse 3D-LTCs exposed to MSN_{AVI} particles with MMP9-cleavable linkers loaded with the combination treatment (cMSN_{AVI}-CB) or free drugs (CB) for 48 h (lower panel). The scale bar is 50 μ m. Comparable sized tumors were chosen for microscopy (indicated by dotted line); tumor-free refers to images that were made in a non-tumor area of a *Kras* mutant 3D-LTC. Nuclear staining (DAPI) is shown in blue,

apoptotic marker (cleaved caspase-3 positive) in green, and ATTO 633-labeled MSNs in red. Images shown are representative for three independent experiments. Quantification of apoptotic cells (cleaved caspase-3) per number of counted nuclei (DAPI) in tumor and tumor-free areas in *Kras* mutant 3D-LTCs after (D, E) 24 h of exposure and (F, G) 48 h of exposure to MSNs loaded with drugs (cMSN-C/CB) or free drugs (C/CB), respectively by Imaris software. Untreated control slices (white bars) and control MSNs (*i.e.*, ncMSN_{AVI}-CB) (light gray bar, 48 h exposure) were also included in the study. * means a significant increase in apoptosis compared to a tumor-free control area ($p < 0.05$). Values given are average of three independent experiments \pm SD.

5.2.10 Co-localization of MMP9 and cleaved caspase-3 in murine 3D-LTCs

Having observed tumor-site localized drug release from the cMSN_{AVI} particles, we focused whether the nanoparticle-based cell death was MMP9-associated using the 3D-LTC model. Detailed confocal microscopy analysis revealed a strong co-localization of cleaved caspase-3 staining with MMP9 staining at the 3D-LTCs, indicating prominent cell death by controlled release of the drugs at tumorous sites with high local MMP9 concentrations (Figure 5.11A). In fact, nanoparticle-based cell death took place throughout the tissue while the MSNs remained mainly on top of the slices where they first associated with the 3D-LTCs (Figure 5.11B). This observation suggests that the particles were initially immobilized on the tissue surface and later cleaved by overexpressed MMP9 nearby, yet the released drugs efficiently diffused into the depths of the tissue. A comparable apoptosis distribution in the tumor tissue was detected for 3D-LTCs exposed to the free drugs (Figure 5.11B). This reveals that deep penetration of the MSNs into the 3D-LTCs is not required, since the released drugs effectively diffuse through the tissue. Additionally, we showed that the apoptosis was mainly limited to epithelial cells in the tumor by co-staining the slices with cleaved caspase-3 and the epithelial cell type marker E-cadherin (Figure 5.11C). Hence, our data clearly demonstrate tumor-site specific controlled drug release by our nanoparticles.

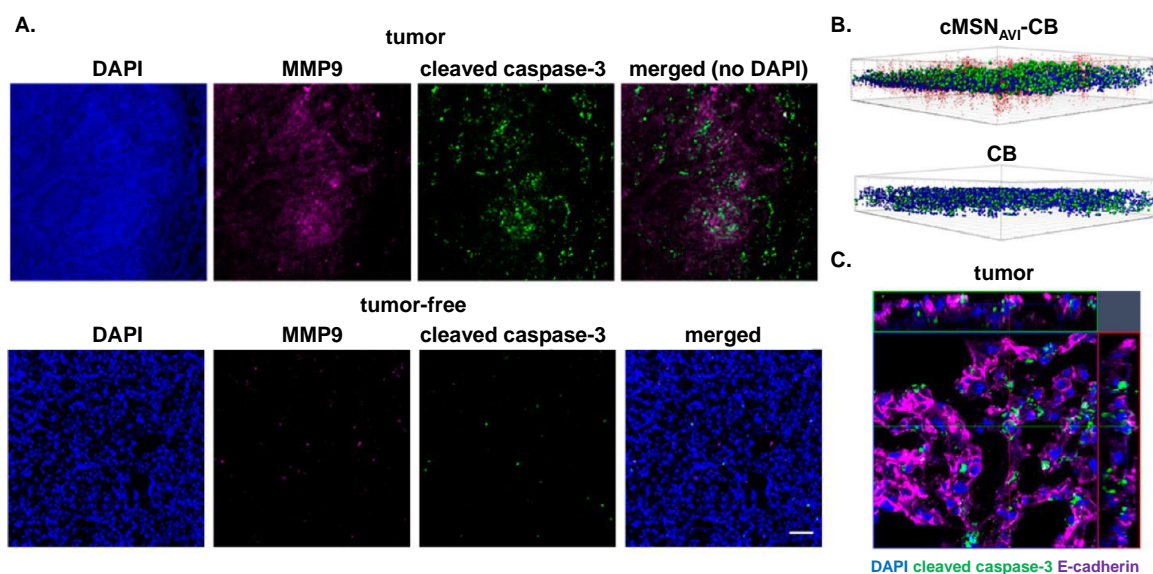


Figure 5.11 (A) *Kras* mutant mice 3D-LTCs exposed to cMSN-CB for 48 h with MMP9 antibody co-staining (magenta, maximum intensity projections of the different channels, white dots in merged image show direct overlay) in tumor (top) and tumor-free (bottom) areas. (B) Nanoparticle-exposed *Kras* mutant 3D-LTCs showing only the calculated number of particles, nuclei, and apoptotic cells per 3D-LTC tissue slice from the side where tumor tissue is located. Red spots represent the calculated particles, blue spots represent the nuclei, and green spots represent the apoptotic cells in cMSN_{AVI}-CB-exposed 3D-LTCs (top panel) and CB-exposed 3D-LTCs (bottom panel). Original stainings were omitted for ease of view. (C) *Kras* mutant 3D-LTCs exposed to cMSN_{AVI}-CB for 48 h with E-cadherin antibody co-staining (magenta, orthographic representation using a 63x objective). The nuclear staining (DAPI) is shown in blue, apoptotic marker (cleaved caspase-3) in green. The fluorescence signal originating from ATTO 633-labeled MSN particles was omitted from the images for ease of view (for A and C). Scale bar is 50 μ m.

5.2.11 Human 3D-LTCs for MSN_{AVI} exposure

The model system of 3D-LTC offers the unique possibility to use human tissue and to test novel therapeutic approach in human diseased tissue (Uhl et al., 2015). We thus optimized our 3D-LTCs system to assess MMP9-responsive drug delivery from functionalized MSNs in human lung tumors. For that purpose, we used 300 μ m thick 3D-LTCs from freshly excised human lung cancer tissue obtained from different donors. Distorted alveolar structure of the tumorous human lungs (Figure 5.12A, right panel) in comparison to healthy lungs was readily observed in fluorescently stained slices by confocal microscopy (Figure 5.12A). We

also validated the tumorous *versus* healthy human tissue used for 3D-LTCs for MMP9 overexpression by immunohistochemistry staining (Figure 5.12B).

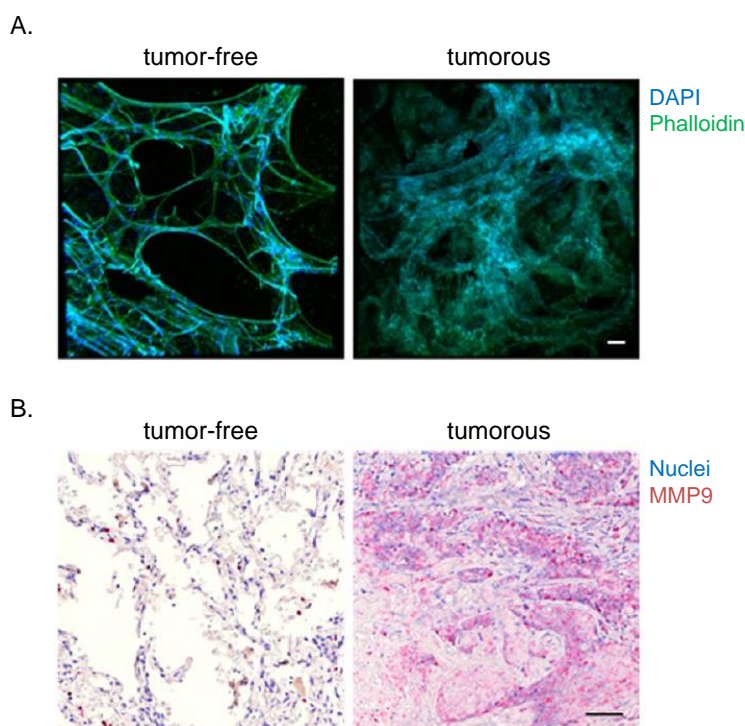


Figure 5.12 3D-lung tissue cultures (3D-LTCs) from human lung cancer tissue. (A) Confocal microscopy images of tumor-free and tumorous human 3D-LTCs stained with phalloidin (green) and DAPI (blue). (B) Immunohistochemistry staining for MMP9 in tumor-free and tumorous human lungs. The scale bar is 50 μm .

5.2.12 MMP9-responsive tumor cell death in human 3D-LTCs

As the final step, we exposed human 3D-LTCs to cisplatin-loaded nanoparticles (cMSN_{AVI}-C_{low}). Our data demonstrated that the cisplatin-loaded MSN_{AVI} nanoparticles effectively induced apoptotic cell death in human tumor tissue after 72 h of exposure. This accorded well with the particle density on the tissue (Figure 5.13A). Moreover, therapeutic efficacy of the cMSN_{AVI}-C_{low} was not tumor type-dependent, as apoptotic cell death was observed in both metastatic and primary lung tumors (Figure 5.13A). Untreated control tissue resulted in only a limited amount of apoptosis, which could be associated with the tissue processing procedure (Figure 5.13A). Strikingly, human 3D-LTCs exposed to non-cleavable cisplatin-loaded MSNs (ncMSN_{AVI}-C_{low}) did not result in obvious cell death when compared to control tissues (Figure 5.13A, middle panel), proving MMP9 sequence-specific controlled

drug release. Remarkably, cMSN_{AVI}-C_{low} particle exposure did not result in any apoptosis in healthy human tissue (Figure 5.13B). Additionally, therapeutic efficiency of the MSNs on 3D-LTCs was also confirmed by quantification of cleaved caspase-3 levels by Western blot analysis (Figure 5.13C).

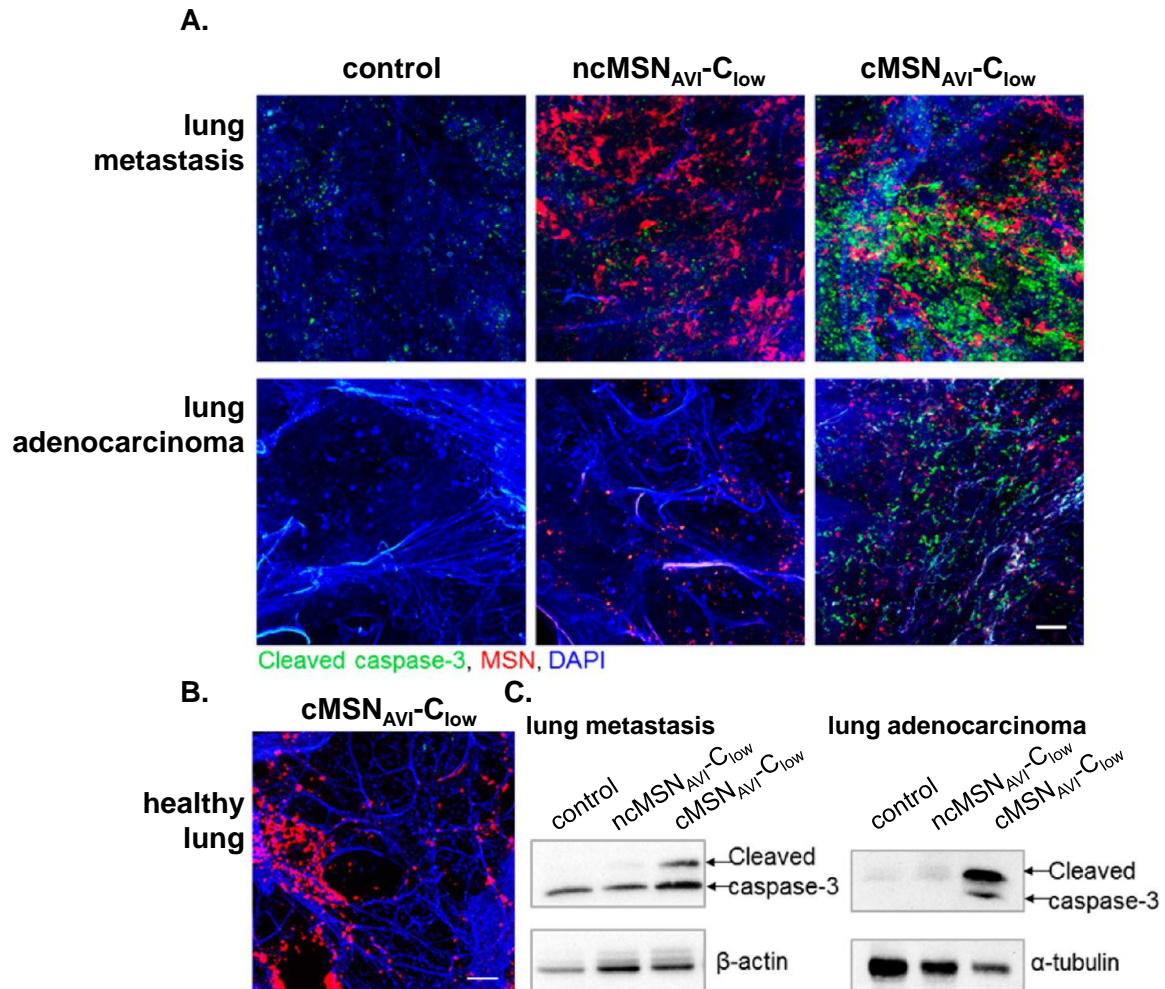


Figure 5.13 Therapeutic efficacy of MMP9-responsive MSN_{AVI} particles in human 3D-LTCs. (A) Human lung adenocarcinoma and (B) human healthy lung 3D-LTCs exposed to cMSN_{AVI}-C_{low} or ncMSN_{AVI}-C_{low} for 72 h. Untreated slices were included in the experiment as controls. Nuclei staining is shown in blue (DAPI), cleaved caspase-3 in green, and MSNs in red. The scale bar is 50 μ m. Images shown are representative for three different sections within the tumor. (C) Western blot analysis of human 3D-LTCs exposed to cMSN_{AVI}-C_{low} and ncMSN_{AVI}-C_{low} for 72 h.

5.3 Discussion

Nanomedicines as smart drug carriers have gained a lot of attention in the last years, and various formulations have been approved by the FDA and EMA for treatment of cancer (Rink et al., 2013). These formulations allow for enhanced pharmacodynamics when compared to free drugs by expanding their bioavailability and tumor delivery efficacy. Moreover, nanoparticles such as mesoporous silica nanoparticles have the possibility to be designed for inhalation therapy (Taratula et al., 2011), which would be beneficial for the treatment of lung cancer particularly, since the agents are directly applied to the target organ, eliminating the digestive system and the liver, and problems of stability in the bloodstream. Indeed, our results have shown that the avidin functionalized MSNs are evenly distributed in the lungs and result in only limited lung toxicity (discussed in Chapter 4 of the thesis). To further increase tumor specificity and thus therapeutic efficacy, the nanoparticles can be functionalized with the ability to release high concentrations of drugs only in the extracellular matrix in close proximity to the tumor site, unlike uncontrolled release from nanoparticles such as liposomes and micelles. Tumor-associated enzymes that are overexpressed at tumor site can be exploited to achieve this goal. For instance, MMP9 overexpressed in lung cancer increases the metastatic potential of malignant cells and therefore associates with poor prognosis of the disease (Egeblad and Werb, 2002; Gialeli et al., 2011; Iniesta et al., 2007; Martins et al., 2009). In fact, MMP2/9-responsive drug delivery has been shown before in *in vivo* mouse xenograft models of the pancreas (Kulkarni et al., 2014), fibrosarcoma (Chien et al., 2013b), glioblastoma (Gu et al., 2013), and hepatoma (Liu et al., 2012), revealing the potency of this approach for treatment of cancers. However, there has not been such a study on lung cancer treatment so far.

Hereby with this study, we demonstrate synthesis of novel mesoporous silica nanoparticles bearing an MMP9-responsive avidin capping system. MMP-responsive MSNs were studied only in three reports before (Singh et al., 2011; Xu et al., 2013; Zhang et al., 2013). Nevertheless, in these studies an MMP9 sequence-specific gating mechanism for controlled release was not employed. In the study by Zhang *et al.*, the particles were functionalized with a polyanion coating to avoid particle uptake by healthy cells, which could be disturbed by MMP cleavage in MMP2-expressing colon and squamous cancer cell lines. In their study, doxorubicin release was achieved by a redox-driven mechanism upon tumor cell uptake of the particles. In the study by Singh *et al.*, the MSNs were coated with a polymer shell

generated with MMP substrate polypeptides with a degradable sequence. And, in the study by Xu *et al.*, gelatin was used as a gatekeeper and as a degradable substrate for MMPs in gelatin-functionalized MSNs. These particles were validated in an MMP2-overexpressing colon cancer cell line and a xenograft mouse model. However, the pore sealing effectiveness was poor in this system. Contrary to that, we here show effective MMP2/9 sequence-specific release of cargo from the avidin-capped MSN system in two NSCLC cell lines and in mouse and human lungs. For these, we optimized a novel *ex vivo* tissue culturing system (3D-LTC) to validate our particles, as an extension of the previous study by Uhl *et al.* (Uhl *et al.*, 2015). The 3D-LTC technique offers high resolution and spatio-temporal imaging of our nanoparticles and their therapeutic efficacy in specific regions (*e.g.*, diseased *versus* healthy areas) within the complex 3D structure of tumorous lung tissue. Although there have been studies where 3D-LTCs were used to assess short-term toxicological profiling of nanoparticles (Nassimi *et al.*, 2009; Neuhaus *et al.*, 2013; Paranjpe *et al.*, 2013), here we studied the therapeutic efficiency of nanoparticles in relevant disease models. For murine lung tumors, we exploited the *Kras* mutant transgenic mice which develop primary lung adenocarcinoma soon after birth (Johnson *et al.*, 2001). This mouse model closely resembles human lung cancer pathophysiology and is thus more relevant than the commonly used xenograft models of mice. Moreover, targeting *Kras* mutant tumors is of additional importance, as *Kras* mutation has no approved therapy and is associated with poor prognosis of the disease and reduced responsiveness to common agents (Cappuzzo *et al.*, 2008; Eberhard *et al.*, 2005; Überall *et al.*, 2008). Furthermore, with the 3D-LTCs, we were able to prove our findings also in healthy *versus* tumorous human tissue, which represents an achievement in closing the gap between drug development and clinical application. By this method, we could clarify that local MMP9 concentrations are high enough to cleave our nanoparticles in *Kras* mutant mice tumors as well as in human lung tumors compared to their healthy counterparts. As MMP9 overexpression correlates with metastatic potency of the cancer cells (Itoh *et al.*, 1999; Roy *et al.*, 2009), it is highly probable that the targeted cells are pro-metastatic cell types. Indeed, the cells which were affected by our MSNs in *Kras* mutant mice slices were MMP9-overexpressing cells, as observed by spatio-temporal analysis, and the absence of cell death taking place in WT and tumor-free regions of the *Kras* mutant lungs. Contrary to that, slices that were exposed to free drugs had evenly distributed cell death patterns. Indeed, quantification analysis of the observed cell death between the tumorous *versus* tumor-free regions at the 3D-LTCs revealed that the effectiveness of the drugs had only around 2-fold increase when the drugs were given freely, whereas tumor

cell-specific targeting rose up to 10-25 fold when the drugs were released by our functionalized MSNs. Additionally, we also confirmed our 5-10 fold increase in cell death in the combinatorial therapy by 3D-LTCs as observed *in vitro*. Combining common therapeutics with proteasome inhibitors has been an interesting approach for several malignancies as well as lung cancers. Several clinical and preclinical trials have shown that, the FDA-approved proteasome inhibitor bortezomib can be synergistically combined with numerous chemotherapeutic agents as well as with radiotherapy, showing good tolerability and no significant enhanced toxicity (Cao et al., 2013; Davies et al., 2007a). Particularly, a phase II clinical trial study with bortezomib in combination with carboplatin has shown encouraging results with progression-free and improved overall survival rates in non-small cell lung cancer patients (Davies et al., 2004). To our knowledge, our report is the first where nanoparticle-based controlled release of a proteasome inhibitor in combination with cisplatin shows significantly superior antitumor activity. Last but not least, we have shown the feasibility of our nanoparticles in diseased versus healthy human lung tissue. We demonstrated that the cisplatin loaded MMP9-responsive MSNs resulted in notable cell death in human 3D-LTCs with lung adenocarcinoma and lung metastasis whereas no significant signs of apoptosis were observed in the healthy 3D-LTCs from the same patients. Moreover, this controlled release effect was MMP9 sequence-specific as we did not see MSN-induced apoptosis in non-cleavable linker bearing cisplatin-loaded nanoparticles. To our knowledge, this is the first study validating the effectiveness of MMP9-responsive controlled drug release to human tissue with cancer.

Synthesis and characterization of the particles was conducted by Christian Argyo.

Experiments for all other sections were conducted in collaboration with Sabine van Rijt.

6 Combination therapy of lung cancer by EGFR- and CCR2-targeted MSNs

Parts of this chapter have previously been submitted for publication as:

Böyükbas D.A., Datz S., Meyer-Schwickerath C., Vreka M., Yang L., Göbl D., Agalioti T., Argyo C., van Rijt S.H., Lindner M., Eickelberg O., Stöger T., Schmid O., Stathopoulos G.T., Bein T., and Meiners S. (2016). *Cellular resolution is essential for validation of active targeting of nanoparticles in vivo.*

6.1 Introduction

The use of nanoparticles as therapeutic agents for cancer therapy has attracted great attention in the past decades (Torchilin, 2014). In particular, nanoparticle-based active targeting of tumor cells has emerged as a potential therapeutic approach to increase drug doses within the tumor while reducing systemic toxicity (Min et al., 2015; Peer et al., 2007). Cell-specific targeting can be achieved by functionalization of nanoparticles with targeting ligands on their surface that bind to receptors that are specifically overexpressed on cancer cells. In this context, nanoparticles targeting the epidermal growth factor receptor (EGFR) have attracted notable attention (Master and Sen Gupta, 2012). This receptor is overexpressed in several types of cancers including breast carcinoma, colon carcinoma, and lung cancer (Ciriello et al., 2013; Normanno et al., 2006). Nanoparticles are often functionalized with EGFR targeting ligands and designed to deliver either silencing agents against defined oncogenes or chemotherapeutic drugs (Master and Sen Gupta, 2012). These nanoparticles are then preferentially recognized and bound by the tumor cells overexpressing EGFR; then they are rapidly taken up into the cells by receptor-mediated endocytosis where the drug is released into the cytoplasm to specifically kill the tumor cells (Mickler et al., 2012). Receptor-mediated targeting via nanoparticles also offers the promise of targeting different types of cells at the same time. In particular, inflammatory immune cells such as tumor-associated macrophages have been identified as a major culprit supporting malignant and metastatic tumor growth (McAllister and Weinberg, 2014; Quail and Joyce, 2013). Accordingly, complementary targeting of tumor and tumor-associated immune cells has

emerged as a novel approach for cancer therapy (Sharma and Allison, 2015; Wolchok and Chan, 2014), yet has hardly been exploited for nanoparticle-mediated cell targeting (Conde et al., 2015; Shao et al., 2014). Such complementary targeting strategies require comprehensive validation of cell-specific targeting *in vivo* with cellular resolution. While many *in vivo* studies demonstrate effective targeting of tumor tissue and therapeutic efficiency of receptor-targeting nanoparticles in mouse tumor models (Brinkman et al., 2016; Lu et al., 2016; Patil et al., 2015), most of these studies, however, lack proof of cell-specific targeting and nanoparticle-induced killing of tumor cells but rather show accumulation of nanoparticles in the target tissue (Bölükbas and Meiners, 2015; Nascimento et al., 2016; Sadhukha et al., 2013; Taratula et al., 2013). We here analyzed complementary targeting of tumor and tumor-associated immune cells by application of fluorescently labeled mesoporous silica nanoparticles (MSN) that had been coupled to EGFR- and C-C chemokine receptor type 2 (CCR2)-specific targeting ligands (Auvynet et al., 2016; Li et al., 2005) *in vitro* and *in vivo*. Cell-specific targeting efficiency of EGFR- and CCR2-ligand bound nanoparticles was validated using two distinct delivery strategies, *i.e.* systemic delivery via intravenous injection and local intratracheal delivery to the lung. This also allowed us to test targeting specificity of nanoparticles in two different biological environments which are known to form distinct protein coronas on nanoparticles that may influence receptor-mediated targeting (Hadjidemetriou et al., 2015; Mirshafiee et al., 2013; Pisani et al., 2017; Raesch et al., 2015; Salvati et al., 2013; Tenzer et al., 2013). Intriguingly, proven *in vitro* cellular targeting specificity of ligand-functionalized nanoparticles was severely hampered *in vivo* in two distinct tumor mouse models irrespective of particle delivery via the blood or the lung due to highly effective foreign body clearance mechanisms.

6.2 Results

6.2.1 Complementary expression of EGFR and CCR2 in lung cancer

The EGF receptor is commonly overexpressed in NSCLC and is correlated with poor prognosis of patients (de Mello et al., 2011; Sharma et al., 2007). CCR2 is a chemokine receptor that is specifically overexpressed in tumor-associated macrophages and promotes metastatic spread of tumor cells in preclinical cancer models including lung cancer (Fritz et al., 2015; Hiratsuka et al., 2013; Qian et al., 2011; Quatromoni and Eruslanov, 2012; Schmall et al., 2015). For our complementary targeting approach, we first validated cell-type specific

overexpression of EGFR and CCR2 in tumors of lung cancer patients. Pronounced overexpression of EGFR was observed in infiltrating nests of lung tumor cells (Figure 6.1A), while CCR2 was strongly overexpressed in the surrounding stroma as depicted by immunohistochemical staining of the same patient material (Figure 6.1B). These data validate the combined use of EGFR- and CCR2-specific targeting nanoparticles as a valid approach to obtain specific targeting of lung tumors and tumor-associated immune cells at the same time.

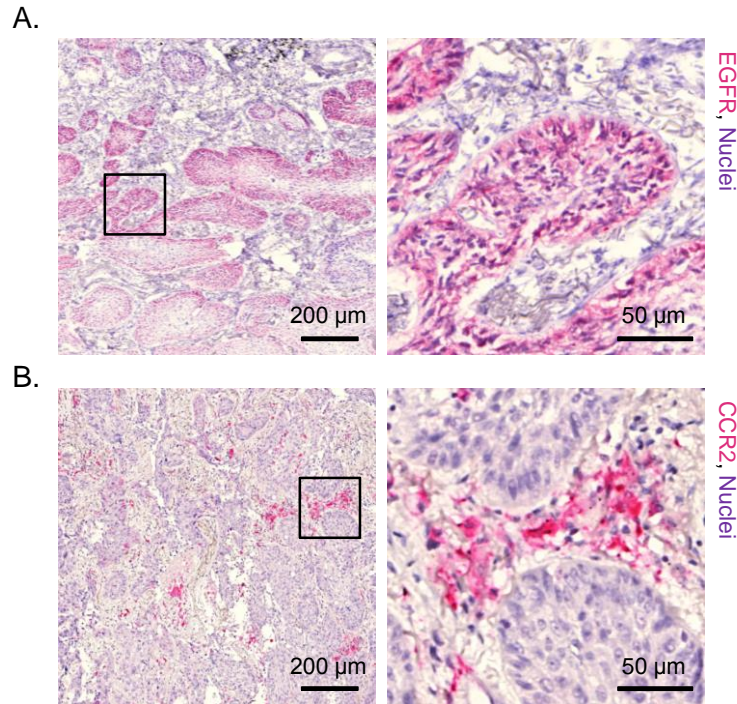


Figure 6.1 EGFR and CCR2 expression in non-small cell lung cancer (NSCLC). Immunohistochemical staining of (A) EGFR (pink) is observed in infiltrating tumor nests whereas (B) CCR2 (pink) mainly localizes to desmoplastic stroma of NSCLC tumors of the patient.

6.2.2 Synthesis and characterization of the receptor-targeted MSNs

Functionalized MSNs were synthesized according to previous reports, resulting in functionalization of the internal pore system with thiol groups and of the external particle surface with amino groups (Figure 6.2B) (Cauda et al., 2009). The additional core functionalization was used for covalent attachment of fluorescent dyes for particle tracking in our *in vitro* and *in vivo* studies. The external surface of the MSNs was functionalized with a pH-cleavable linker system containing a biotin functionality on the outer periphery (Figure 6.2A(i)). The glycoprotein avidin was attached to the outer surface of the particles via

noncovalent association with the biotin groups, thus acting as a bulky gatekeeper of the internal pore system (Figure 6.2(ii)). In our study, these MSN_{AVI} nanoparticles served as the non-targeting particle control. Different targeting ligands were attached to the outer surface of the avidin gatekeepers such as the natural ligand of the EGFR, *i.e.* EGF, an artificial ligand GE11, and the artificial CCR2 antagonist ECL1i referred to as particles MSN_{EGF} , MSN_{GE11} , and MSN_{ECL1i} , respectively (Figure 6.2A(iii)) (Auvynet et al., 2016; Cauda et al., 2009; Li et al., 2005). All MSN types showed colloidal stability in aqueous and mucosal solutions (Figures 6.2C&D) and pH-responsive release behavior for independently manufactured batches as analyzed by release of propidium iodide as a model cargo (Figure 6.2E). Additional comprehensive characterization of the MSN particle systems with thermogravimetric analysis, nitrogen sorption, zeta potential measurements, and IR spectroscopy confirmed successful synthesis of a pH-cleavable MSN system with different targeting ligands that was subsequently used for specific *in vitro* and *in vivo* cellular targeting experiments (data not shown; experiments were conducted by our collaboration partners at the Physical Chemistry Department in the Ludwig-Maximilians-University of Munich).

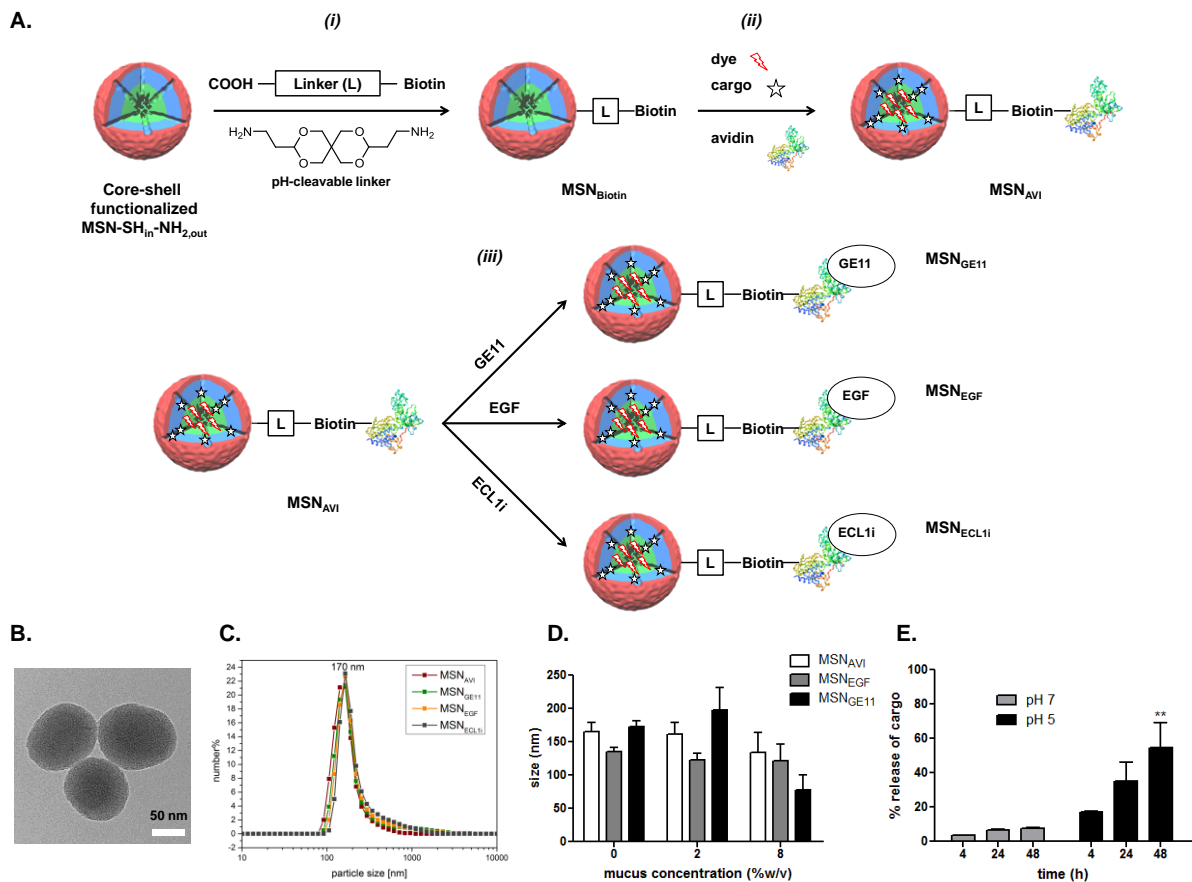


Figure 6.2 Synthesis scheme and characterization of pH-responsive mesoporous silica nanoparticles (MSNs) with different targeting ligands. (A) Delayed co-condensation process leads to different core

(green, thiol groups) and shell (red, amino groups) functionalization of MSN-SH_{in}-NH_{2,out}. (i) In a three step modulation approach, first the amino groups were transformed into carboxy groups. EDC amidation with the pH-cleavable linker and subsequent addition of biotin leads to covalent attachment and results in MSN_{Biotin}. (ii) After cargo loading and covalent attachment of the dyes at the thiol groups in the inner pore system, avidin efficiently seals the mesopores and results in MSN_{AVI}. (iii) On the outer surface different targeting ligands were added (MSN_{GE11}, MSN_{EGF}, MSN_{ECLi}). Characterization of MSNs. (B) Transmission electron micrograph (TEM) of MSN-SH_{in}-NH_{2,out}. Scale bar = 50 nm. (C) Dynamic light scattering (DLS) of MSN_{AVI} (red), MSN_{GE11} (light green), MSN_{EGF} (orange) and MSN_{ECLi} (grey) in water. (D) Variance in size distribution in healthy (2%) *versus* cancerous (8%) mucus conditions. (E) Time-dependent pH-responsive percent release statistics at pH 7 and pH 5. * means a significant increase in the release of the cargo at pH 5 compared to pH 7 (** $p < 0.01$). Values given are an average of three independent experiments \pm SEM.

6.2.3 Receptor-mediated targeting of MSNs *in vitro*

We analyzed *in vitro* receptor-specific targeting of EGFR-abundant cells with fluorescently labeled functionalized MSNs in two human NSCLC cell lines that differ in their basal EGFR expression. EGFR is strongly overexpressed in A549 cells compared to H520 cells as determined by Western blot analysis (Figure 6.3A & 6.4A). Of note, we always applied the nanoparticles in the presence of 10% FCS to allow for *in vitro* protein corona formation (Mirshafiee et al., 2013; Salvati et al., 2013). Confocal microscopy revealed pronounced uptake of the targeted MSNs in EGFR-abundant A549 cells. EGF receptor staining confirmed co-localization of the fluorescently labeled MSNs with EGFR, thus validating that the uptake was EGFR-mediated (Figure 6.3B). Importantly, the uptake was confirmed for different MSN particles presenting both the natural EGFR ligand, EGF, and the artificial ligand, GE11, using several independent batches of nanoparticle preparations. In contrast, EGFR-scarce H520 cells showed only a minor uptake of GE11-functionalized MSNs (Figure 6.3B right panel and Figure 6.4B). In flow cytometry analysis, we observed significant increase in the uptake when the particles were EGFR-targeted with EGF or GE11 compared to non-targeted MSN_{AVI} particles in A549 cells (Figure 6.3C). Specificity of our CCR2-targeted MSNs was tested in the presence of serum in the mouse alveolar macrophage cell line MH-S, which expresses increased levels of CCR2, as determined by Western blot analysis (Figure 6.5A). Treatment of MH-S cells with CCR2-ligand functionalized and fluorescently labeled MSNs showed strong uptake of particles that co-localized with CCR2 staining indicating receptor-mediated uptake of these MSNs. In contrast, non-targeted MSN_{AVI} particles were only

minimally taken up by MH-S cells (Figure 6.5A). In addition, the CCR2-scarce lung adenocarcinoma cell line A549 cells (Figure 6.6A) showed a much less pronounced uptake when compared to the MH-S cells, thus demonstrating CCR2-specific delivery of our CCR2-targeted MSNs (Figure 6.6B). Flow cytometry analysis confirmed the significant increase in uptake in MH-S cells upon CCR2-targeting with independent batches of particle preparations (Figure 6.5B).

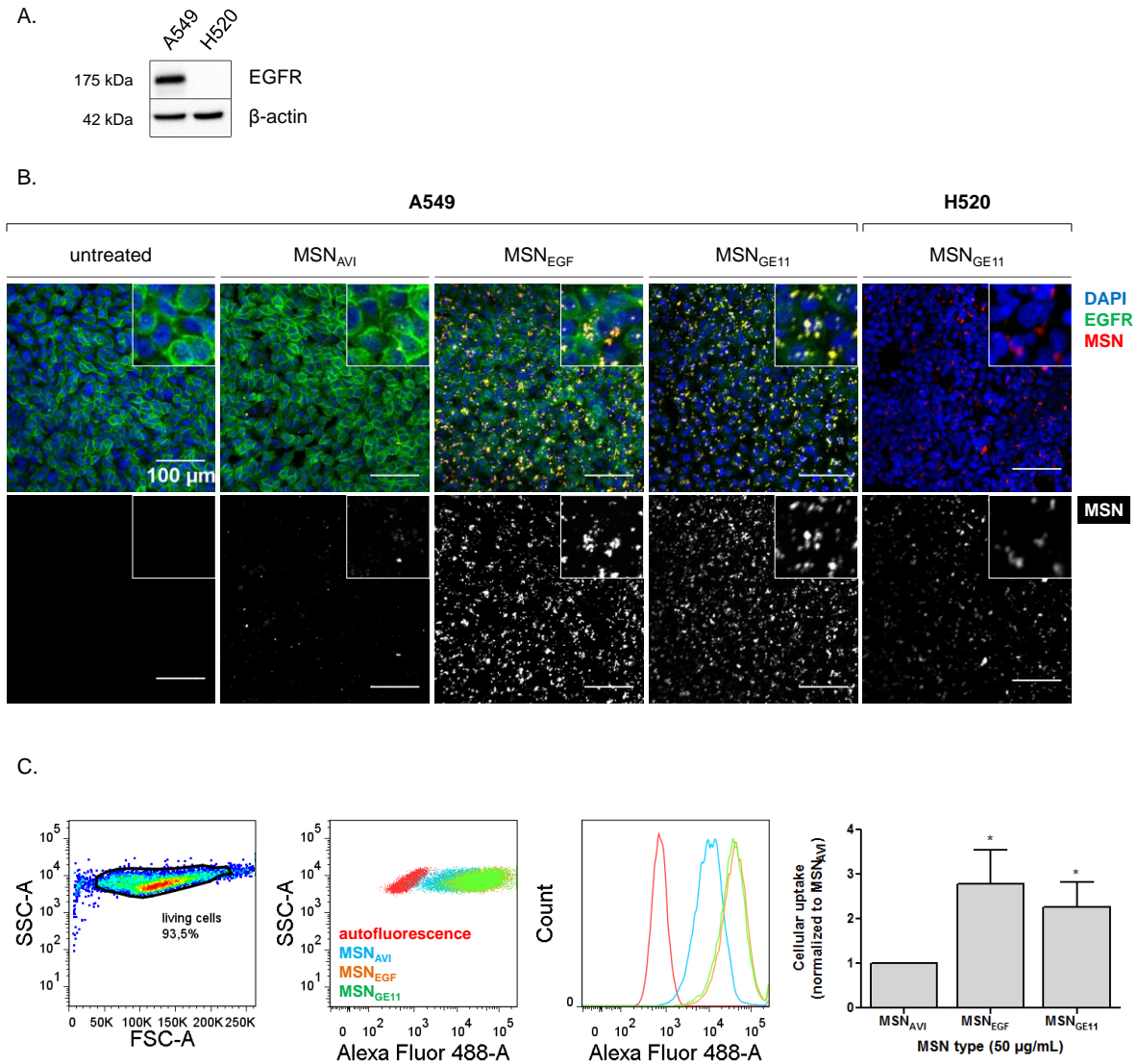


Figure 6.3 EGFR-specific uptake of MSNs *in vitro*. (A) Basal EGFR overexpression in A549 but not in H520 cells at the protein level, assessed by Western blot analysis. (B) EGFR-targeted *versus* non-targeted uptake of ATTO 633-labeled MSN_{AVI}, MSN_{EGF}, and MSN_{GE11} within 1 h by A549 cells compared to MSN_{GE11} uptake in H520 cells co-stained for EGFR by immunofluorescence, measured by confocal microscopy. Nuclear staining (DAPI) is shown in blue, EGFR staining in green and ATTO 633-labeled MSNs in red in the merged images, and in gray in the single channel for better

resolution. (C) Quantification of the ATTO 488-labeled MSN_{AVI} , MSN_{EGF} , and MSN_{GE11} uptake within 1 h by A549 cells by flow cytometry analysis. After gating for the viable cells, medians of the histogram curves were obtained. Autofluorescence signals of the untreated cells were blanked from the treated cells. * indicates a significant increase in the uptake of MSN_{EGF} and MSN_{GE11} compared to MSN_{AVI} ($p < 0.05$). Values given are an average of six independent experiments using different particle preparations \pm SEM.

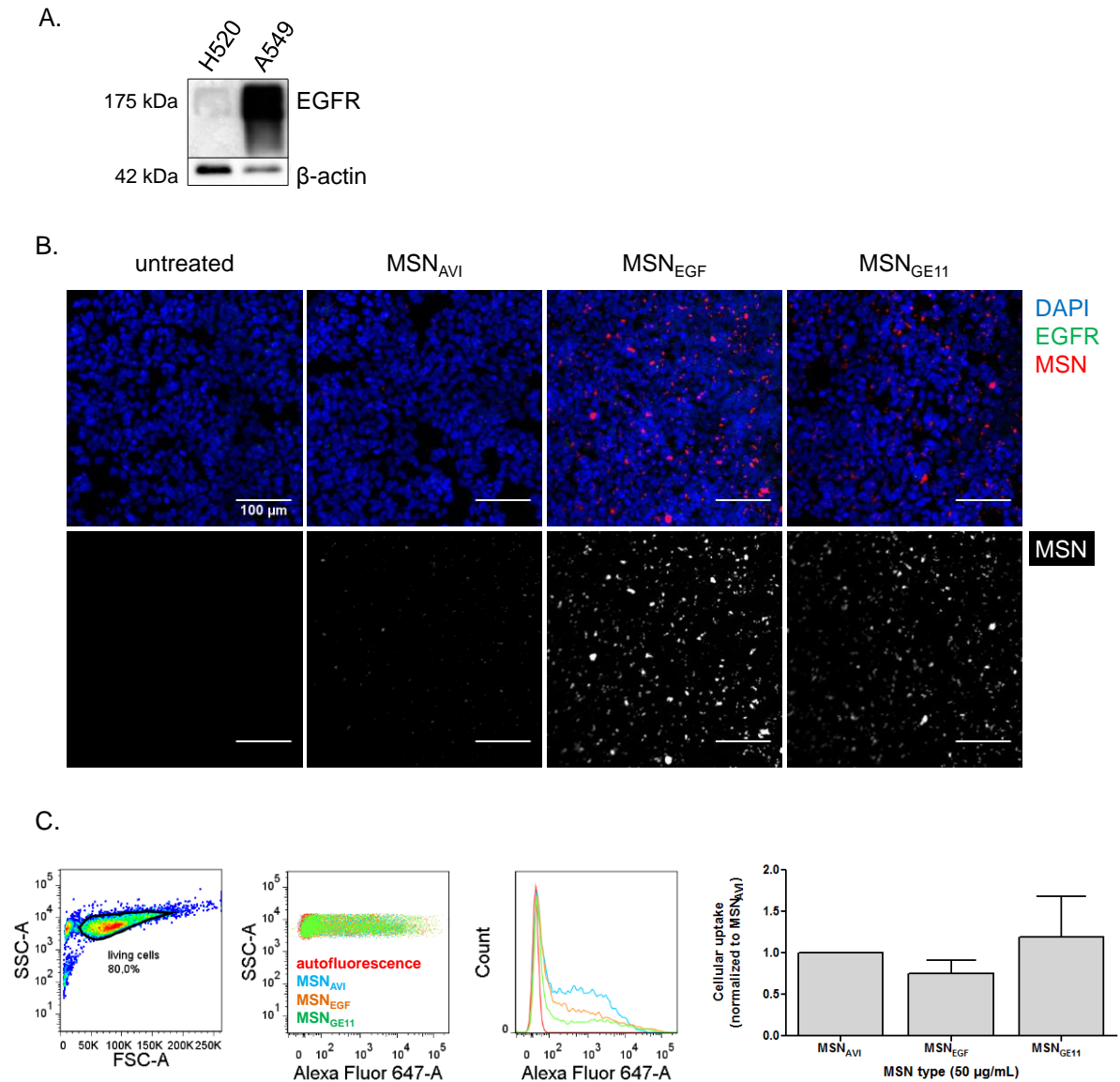
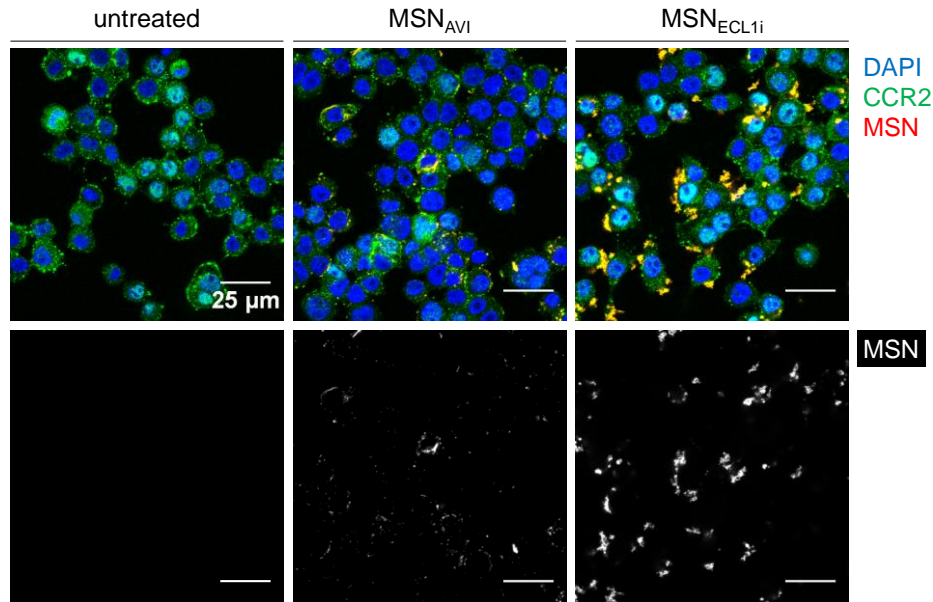


Figure 6.4 EGFR-targeted MSN uptake in H520 cells *in vitro*. (A) Basal EGFR overexpression in A549 cells in comparison to only limited EGFR expression in H520 cells at the protein level, assessed by Western blot analysis. (B) EGFR-targeted *versus* non-targeted uptake of ATTO 633-labeled MSN_{AVI} , MSN_{EGF} , and MSN_{GE11} in 1 h in EGFR-scarce H520 cells co-stained for EGFR by immunofluorescence, measured by confocal microscopy. Nuclear staining (DAPI) is shown in blue, EGFR staining in green, and ATTO 633-labeled MSNs in red in the merged image, and in gray in the single channel for improved resolution. Scale bar = 100 μ m. (C) Quantification of the

ATTO 633-labeled MSN_{AVI} , MSN_{EGF} , and MSN_{GE11} uptake in 1 h in H520 cells by flow cytometry analysis. After gating for the viable cells, median fluorescence intensities from the histogram curves were obtained. Autofluorescence signals of the untreated cells were blanked from the treated cells. Values given are an average of six independent experiments \pm SEM.

A.



B.

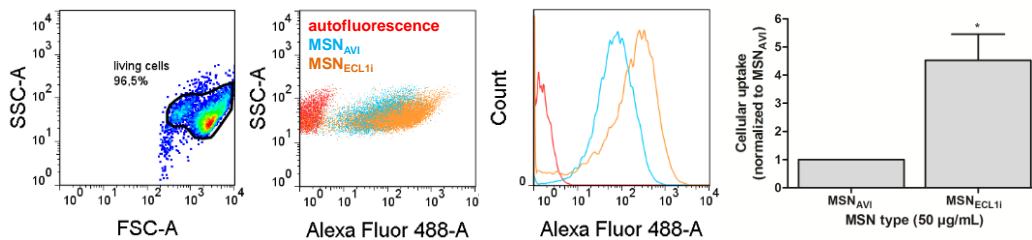


Figure 6.5 CCR2-specific uptake of MSNs *in vitro*. (A) CCR2-targeted *versus* non-targeted uptake of ATTO 633-labeled MSN_{AVI} and MSN_{ECL1i} in one hour in MH-S cells immunofluorescently co-stained for CCR2, measured by confocal microscopy (B) Quantification of ATTO 488-labeled MSN_{AVI} and MSN_{ECL1i} uptake within 1 h in MH-S cells by flow cytometry analysis. After gating for the viable cells, medians of the histogram curves were obtained. Autofluorescence signals of the untreated cells were blanked from the treated cells. * means a significant increase in the uptake of MSN_{ECL1i} compared to MSN_{AVI} ($p < 0.05$). Values given are an average of four independent experiments using different particle preparations \pm SEM.

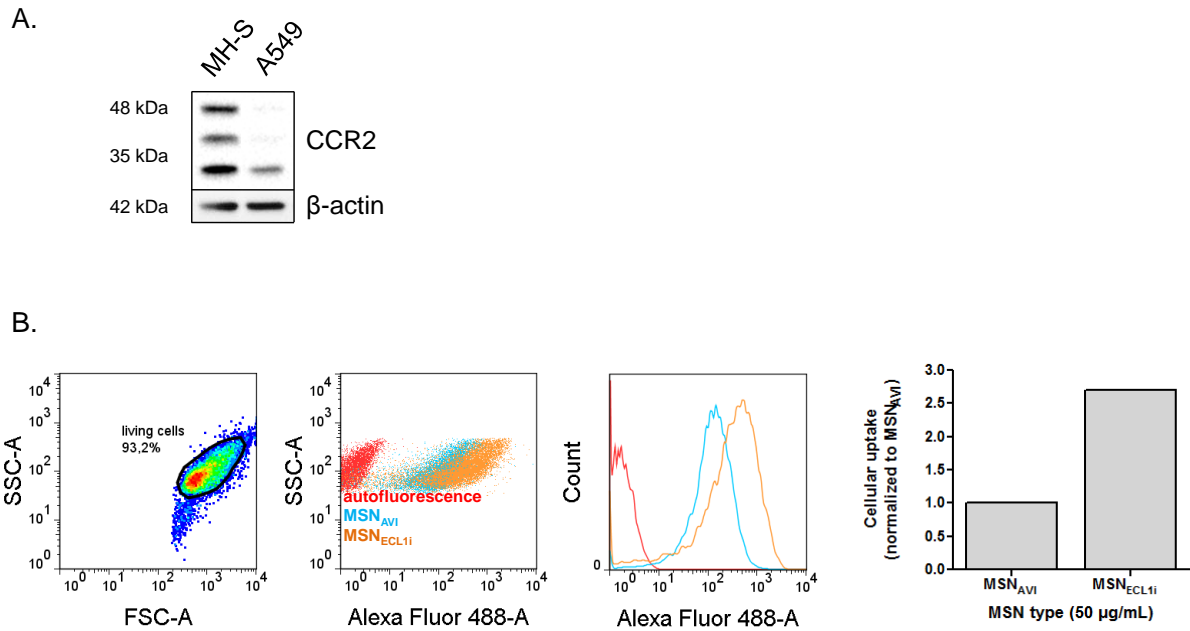


Figure 6.6 CCR2-targeted MSNs uptake in A549 cells *in vitro*. (A) Basal CCR2 overexpression in MH-S cells *versus* A549 cells at the protein level, assessed by Western blot analysis. (B) Quantification of the ATTO 488- labeled MSN_{AVI} and MSN_{ECLIi} uptake in 1 h in CCR2-scarce A549 cells by flow cytometry analysis. After gating for the viable cells, median fluorescence intensities from the histogram curves were obtained. Autofluorescence signals of the untreated cells were blanked from the treated cells. Values given are of a single experiment.

6.2.4 Systemic delivery of MSN_{GE11} versus MSN_{AVI} in mouse flank tumor models

In vivo, we first analyzed receptor-mediated targeting of the EGFR-functionalized nanoparticles in flank tumor bearing mouse models by systemic delivery via the bloodstream. In the blood, nanoparticles are reported to be immediately coated with a distinct protein corona (Hadjidemetriou et al., 2015). EGFR-targeting specificity was assessed by using genetically engineered murine melanoma cells (B16F10), that express only low levels of EGFR (B16F10^{EGFR-}) and a derivative of these cells stably transfected to overexpress EGFR (B16F10^{EGFR+}) (Figure 6.7A). These cell lines were injected subcutaneously into the left and right flanks of a syngeneic and immunologically fully competent mouse strain (C57BL/6) for flank tumor formation. In a complementary approach, genetically engineered murine Lewis lung carcinoma cells (LLC), which endogenously overexpresses EGFR (LLC^{EGFR+}) and a derivative of these cells in which EGFR had been knocked down via stable

short-hairpin-mediated RNA silencing (LLC^{EGFR^-}) were used (Figure 6.8A). With this approach, we are able to control for EGFR-specific targeting of our functionalized nanoparticles to tumor cells within the same mouse, as receptor-negative tumor cells serve as an internal control for receptor-specific targeting. This animal model thus allows for an unprecedented control of receptor-mediated targeting specificity. In both settings, cells grew to form tumors of similar size of 1-2 cm³ within two weeks with similar histology. ATTO 633-labeled EGFR-targeted nanoparticles were then systemically applied via retro-orbital intravenous injection and biodistribution of the particles was compared to labeled but non-targeted MSN_{AVI} particles by *in vivo* fluorescence imaging. Fluorescence signals were low and close to the detection limit of our near-infrared bioimaging system but indicated accumulation of nanoparticles in the liver (data not shown). We investigated the biodistribution of the systemically applied MSNs on the cellular level by comparative immunofluorescence analysis of the right and left flank tumors and of several internal organs. Both the targeted and non-targeted fluorescently-labeled MSNs were mainly localized in the liver and spleen with only little uptake into the flank tumors, lungs, and kidneys (Figure 6.7B). Quantification of the immunofluorescence signal per cell nucleus confirmed that the delivery of the MSNs to the liver was much more effective than to other organs or tumors (Figure 6.7C). Importantly, we did not observe any difference in the uptake between EGFR overexpressing and EGFR-scarce B16F10 tumor cells. Very similar data were obtained with the second set of EGFR-abundant and -scarce LLC tumor cells (Figure 6.8&9). Likewise, quantification of nanoparticle-derived fluorescence in tissue homogenates of flank tumors and the liver revealed pronounced accumulation of fluorescence signals in liver homogenates regardless of MSN functionalization in the LLC flank tumor model (Figure 6.8D).

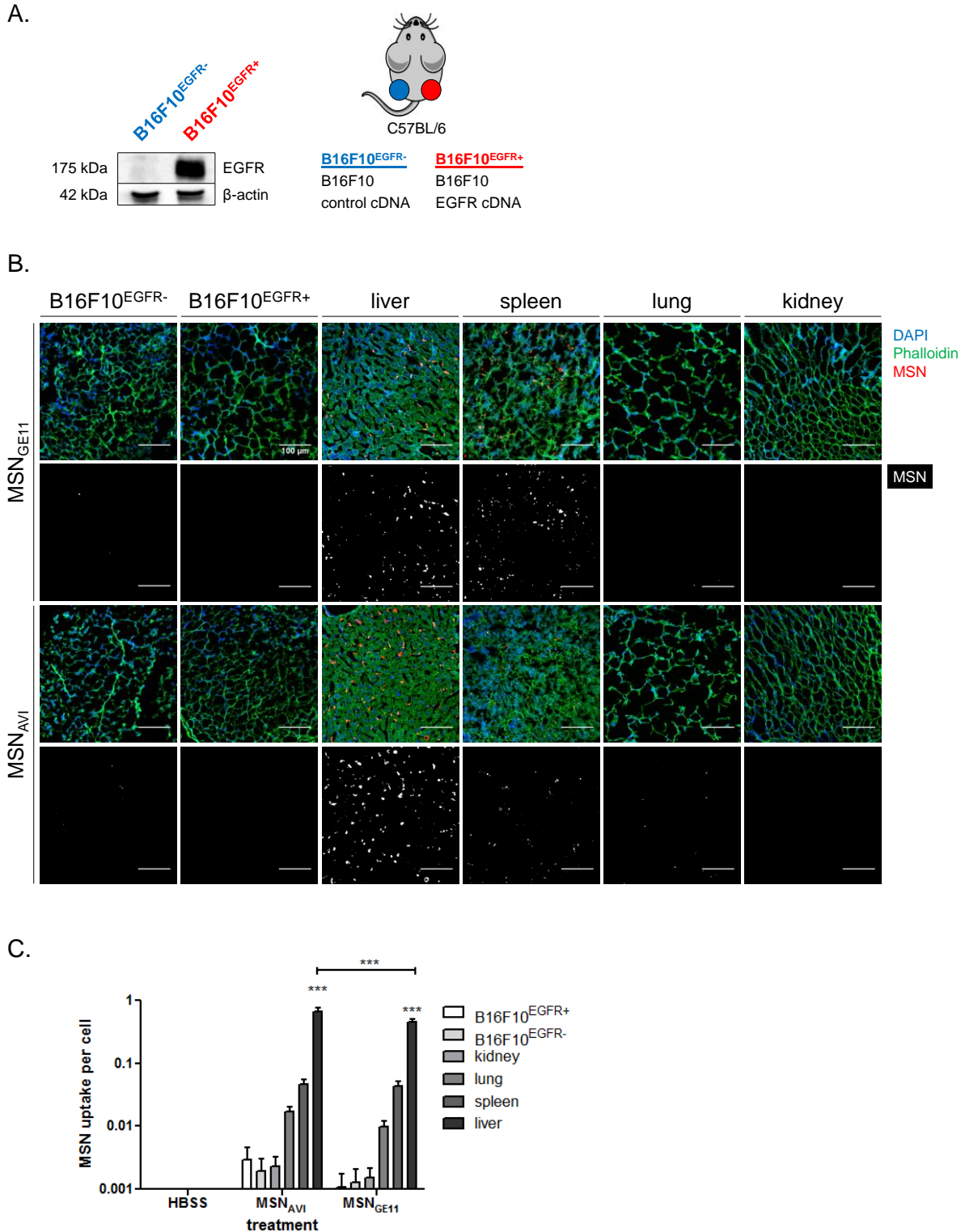


Figure 6.6 Biodistribution of EGFR- targeted versus non-targeted nanoparticles in mice with B16F10^{EGFR-} and B16F10^{EGFR+} syngeneic tumors. (A) Overexpression of EGFR protein in cDNA transfected B16F10 cells in comparison to control vector transfected cells *in vitro* by Western blot analysis. (B) Histological analysis of the intravenously administered MSN_{AVI} and MSN_{GE11} biodistribution in the EGFR-abundant B16F10^{EGFR+} tumors, EGFR-scarce B16F10^{EGFR-} tumors, livers,

spleens, lungs, and kidneys of the mice three days after treatment by means of confocal microscopy. Nuclear staining (DAPI) is shown in blue, actin staining (phalloidin) in green and ATTO 633-labeled MSNs in red in the merged image, and in gray in the single channel for improved resolution. To obtain reliable qualitative data on the distribution of the particles in these tissues, we analyzed 5 mice per group with 5 random sections and 3 images per section taken in a blinded manner. (C) Quantification of the MSN_{AVI} and MSN_{GE11} uptake per nuclei observed in histological analyses in B16F10^{EGFR-} and B16F10^{EGFR+} tumors, kidneys, lungs, spleens, and livers, respectively. In the HBSS control, animals only received HBSS buffer and no particles. *** indicates a significant increase in MSN uptake in the livers compared to the tumors ($p < 0.001$). Values given are averages \pm SEM of three different images/tissue sections per mouse in each group (n = 5 per MSN type).

shown are representative for three different regions from each mice ($n = 5$ mice treated). Scale bar = 100 μm . (C) Quantification of the MSN_{AVI} and MSN_{GE11} uptake per nuclei observed in histological analyses in $\text{LLC}^{\text{EGFR}^+}$ and $\text{LLC}^{\text{EGFR}^-}$ tumors, kidneys, lungs, spleens, and livers, respectively. (D) Quantitative dosimetric analyses of the MSN_{AVI} and MSN_{GE11} fluorescence achieved from the homogenates of $\text{LLC}^{\text{EGFR}^+}$ and $\text{LLC}^{\text{EGFR}^-}$ tumors *versus* livers of the treated mice. In the HBSS control, animals only received HBSS buffer and no particles. *** means a significant increase in MSN uptake in the livers compared to the tumors ($p < 0.001$). Values given are average of three different images per each treated mice \pm SEM ($n = 5$ per MSN type).

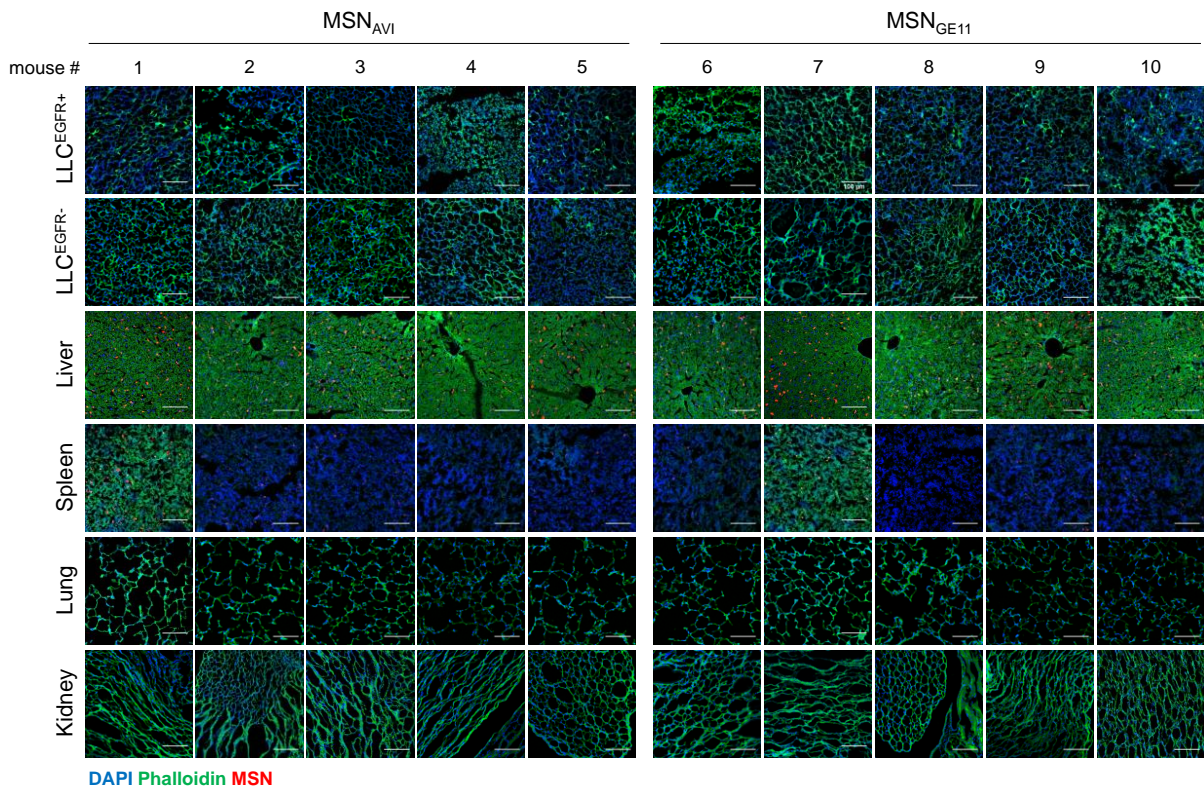


Figure 6.8 Organ-specific biodistribution of EGFR- targeted versus non-targeted MSNs in mice bearing $\text{LLC}^{\text{EGFR}^+}$ versus $\text{LLC}^{\text{EGFR}^-}$ syngeneic flank tumors. Histological analysis of the biodistribution of retro-orbitally administered MSN_{AVI} and MSN_{GE11} in the EGFR-abundant $\text{LLC}^{\text{EGFR}^+}$ tumors, EGFR-scarce $\text{LLC}^{\text{EGFR}^-}$ tumors, livers, spleens, lungs, and kidneys of each of the treated mice by confocal microscopy. Nuclear staining (DAPI) is shown in blue, actin staining (phalloidin) in green, and ATTO 633-labeled MSNs in red. Images shown are representative for three different regions from each mice ($n = 5$ mice per MSN type). Scale bar = 100 μm .

6.2.5 Local intratracheal delivery of MSN_{GE11} and MSN_{ECL1i} in *Kras* mutant transgenic mouse model

In order to assess the targeting specificity of our functionalized nanoparticles by a different delivery route and in the presence of a different biological environment, *i.e.* the lung lining fluid, we evaluated local delivery of targeted MSNs into the lungs via instillation using the *Kras*^{LA2} mouse model for lung cancer. In this mouse model, transgenic mice spontaneously develop lung tumors upon random activation of oncogenic *Kras* signaling, resulting in a more realistic tumor model than the inducible cancer models (Johnson et al., 2001; Zitvogel et al., 2016). As such, this mouse model closely resembles the onset of NSCLC in patients where activation of *Kras* has been shown to be the most prominent oncogenic driver mutation (Ciriello et al., 2013; Martin et al., 2013). Immunohistochemical staining for EGFR and CCR2 confirmed that the receptors are overexpressed in these lung tumors, thus validating the *Kras*^{LA2} lung tumor model as a suitable model for investigating EGFR- and CCR2-specific targeting via functionalized nanoparticles (Figure 6.9). For *in vivo* evaluation of receptor-specific uptake of EGFR- and CCR2-targeted MSNs by tumor and tumor-associated immune cells, fluorescently labeled targeted (MSN_{GE11}, MSN_{ECL1i}) and non-targeted MSNs (MSN_{AVI}) were intratracheally instilled directly into the lungs of tumor-bearing *Kras*^{LA2} mice. The biodistribution of the fluorescently-labeled MSNs was evaluated three days after administration on the cellular level using confocal microscopy of the lung, liver, and spleen sections as described before. Translocation of MSNs to secondary organs was not detected (Srinivasarao et al., 2015) (Figure 6.10), instead MSNs were retained in the lungs of the *Kras*^{LA2} mice (Figure 6.11). In the tumorous lungs, particle uptake was detected in smaller hyperplastic lesions of the lung but not in large and solid tumors, except for the edges of these tumors (Figure 6.11). Nanoparticles also localized to tumor-free lung tissue regardless of their functionalization (Figure 6.11). Importantly, we did not observe any difference in cellular uptake of EGFR-, CCR2-targeted nanoparticles, and non-targeted MSN_{AVI} particles on the cellular resolution level. Remarkably, the nanoparticles did accumulate in specific cells both in the tumor-free and in tumorous regions. Immunofluorescence staining with the macrophage marker CD68 identified these cells as alveolar macrophages (Figure 6.12). These cells are specialized tissue-resident macrophages of the lung that colonize the alveolar surface and play an essential role in the pulmonary defense against particles and pathogens (Lambrecht, 2006). Of note, these cells stained also strongly positive for both EGFR and CCR2, in both the tumor-free and the tumorous lesions

of *Kras*^{LA2} tumor mice (Figure 6.13). Uptake of nanoparticles, however, was independent of the receptor expression as also the non-targeted MSN_{AVI} nanoparticles were efficiently taken up by EGFR- and CCR2-positive alveolar macrophages (Figure 6.13). Moreover, lung carcinoma cells that overexpressed both EGFR and CCR2 did not preferentially take up EGFR- and CCR2-targeted MSNs, respectively (Figures 6.9 and 6.13C&D). These data reveal disturbance of targeting specificity of functionalized nanoparticles in the lung.

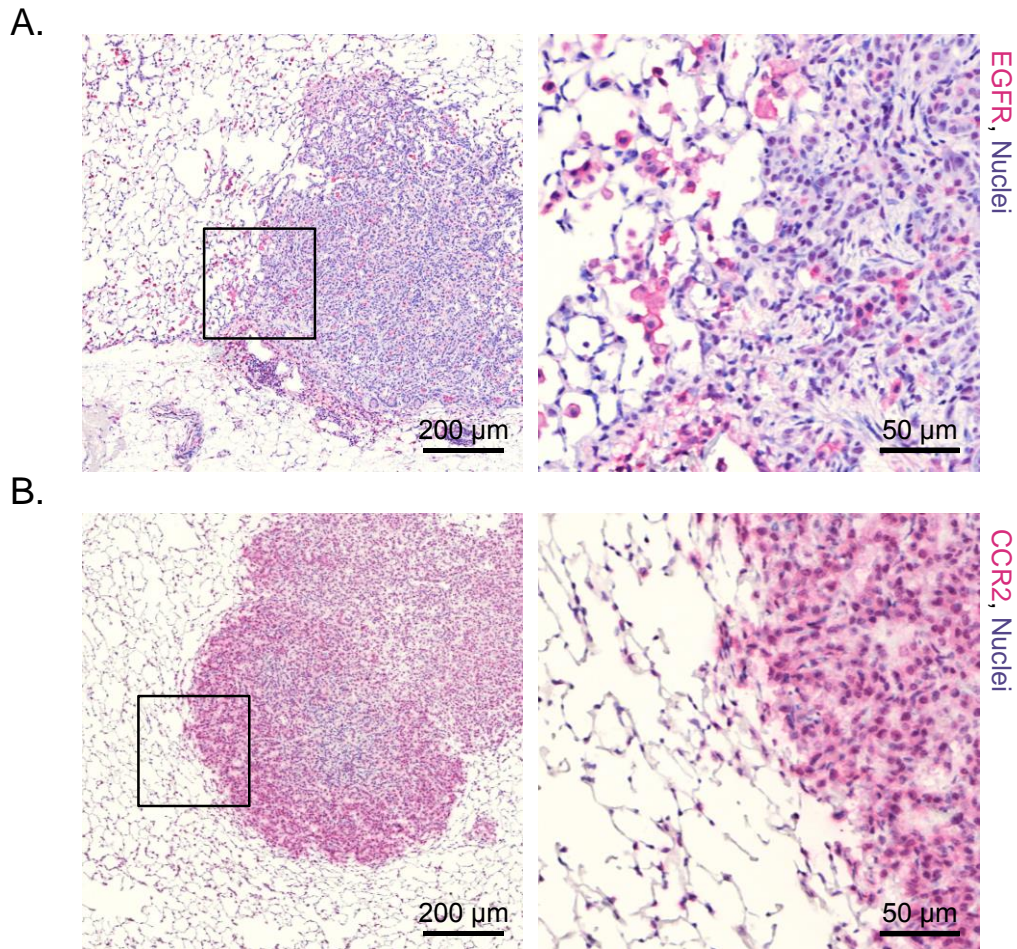


Figure 6.9 EGFR and CCR2 expression in the lungs of *Kras*^{LA2} transgenic mice with lung cancer. Immunohistochemical staining of (A) EGFR (pink) is overexpressed heterogeneously in tumor cells and immune cells whereas (B) CCR2 (pink) is overexpressed rather homogeneously in tumor cells and immune cells of the *Kras*^{LA2} mutant mouse with lung cancer, respectively.

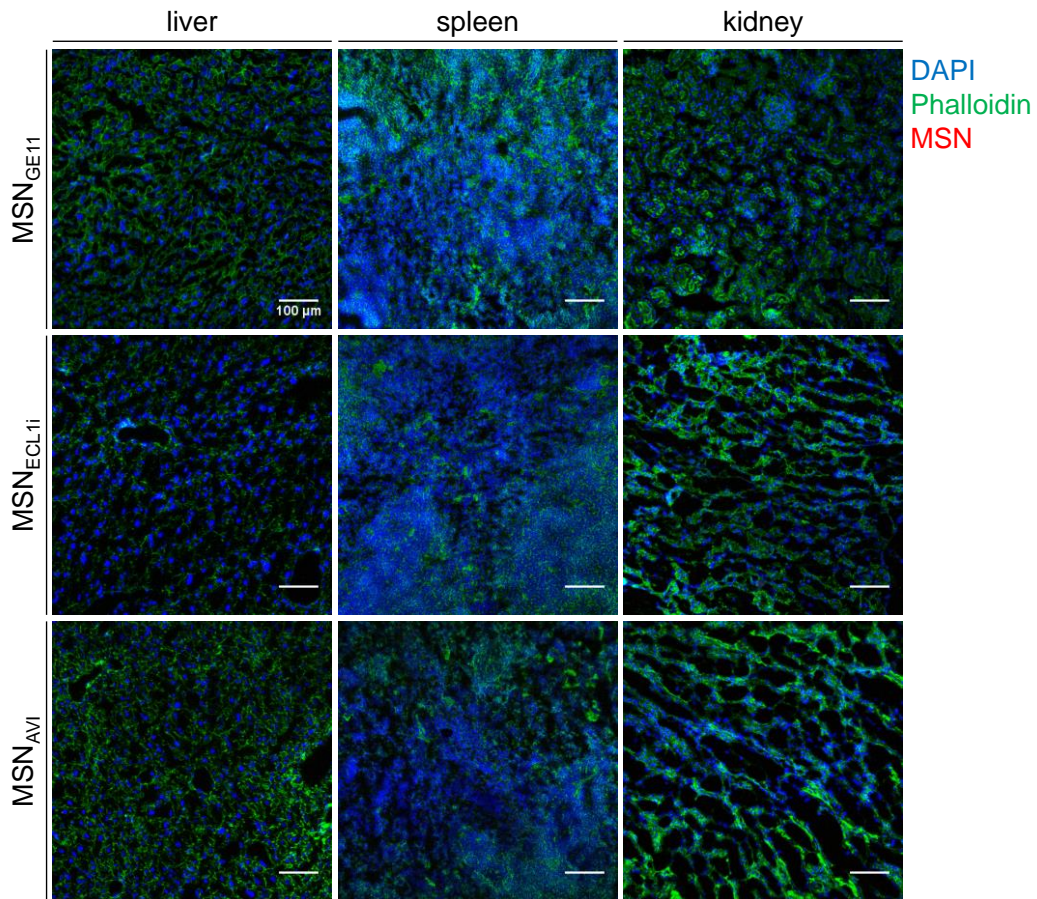


Figure 6.10 Biodistribution of MSNs after local delivery to the lungs in major organs of *Kras^{LA2}* mutant mice. Histological analysis of the biodistribution of ATTO 633-labeled MSN_{AVI}, MSN_{GE11}, and MSN_{ECLIi} in livers, spleens, and kidneys of the *Kras^{LA2}* mutant mice three days after instillation. Nuclear staining (DAPI) is shown in blue, actin staining (phalloidin) in green, and ATTO 633-labeled MSNs in red. Images shown are representative for three different regions from each mice (n = 5 per MSN type). Scale bar = 100 μm.

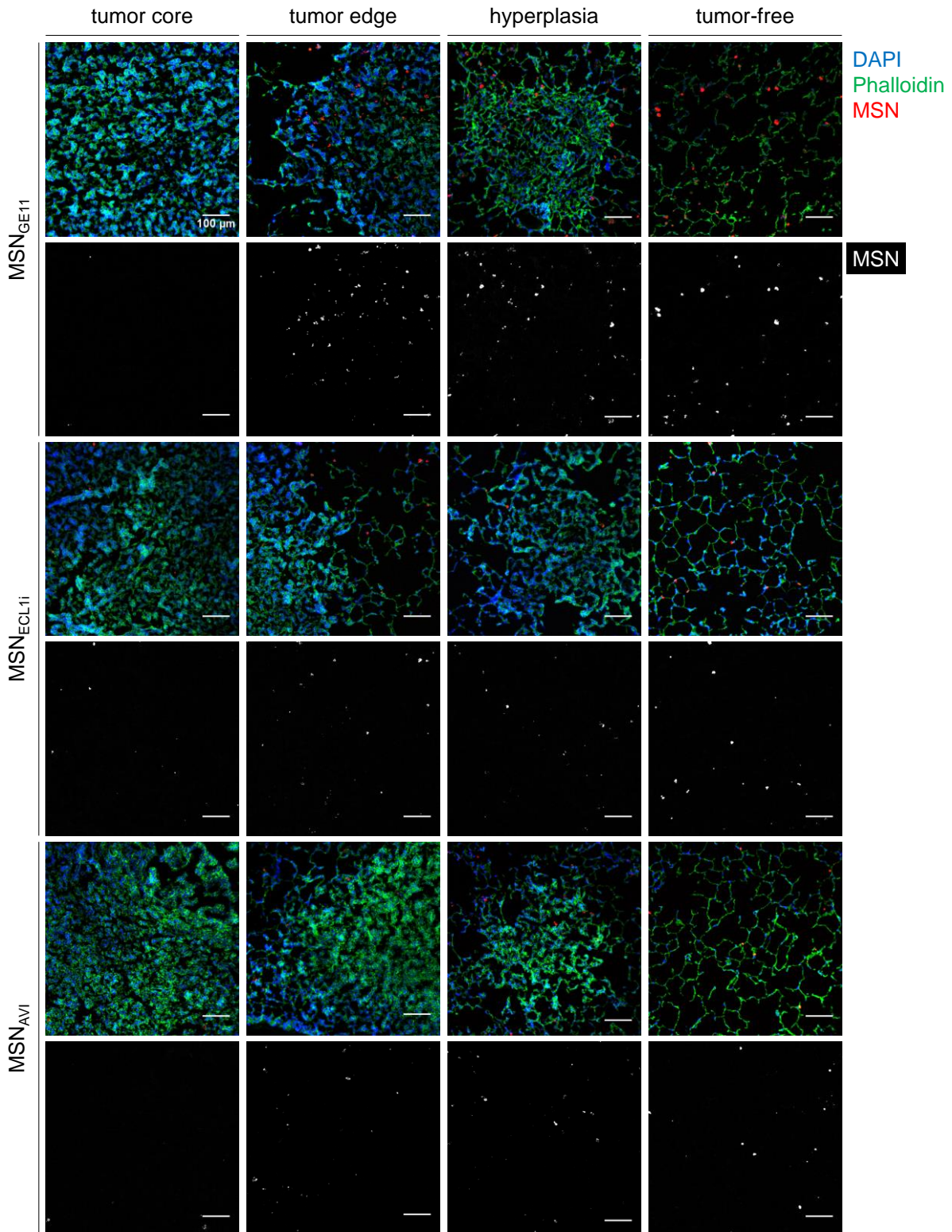


Figure 6.11 Cellular distribution of instilled nanoparticles in the lungs of *Kras*^{LA2} mutant mice. Histological analysis of ATTO 633-labeled MSN_{AVI}, MSN_{GE11}, and MSN_{ECL11} uptake in solid tumor cores *versus* their edges, and in hyperplastic or in tumor-free regions of the tumorous lungs. Nuclear staining (DAPI) is shown in blue, actin staining (phalloidin) in green, and ATTO 633-labeled MSNs in red in the merged images, and in gray in the single channels for more clear observation. To obtain

reliable qualitative data on the distribution of the particles in these tissues, we analyzed five mice per group with five random sections and three images per section taken in a blinded manner. Images shown are representative for three different regions from each group of mice (n = 5 per MSN type).

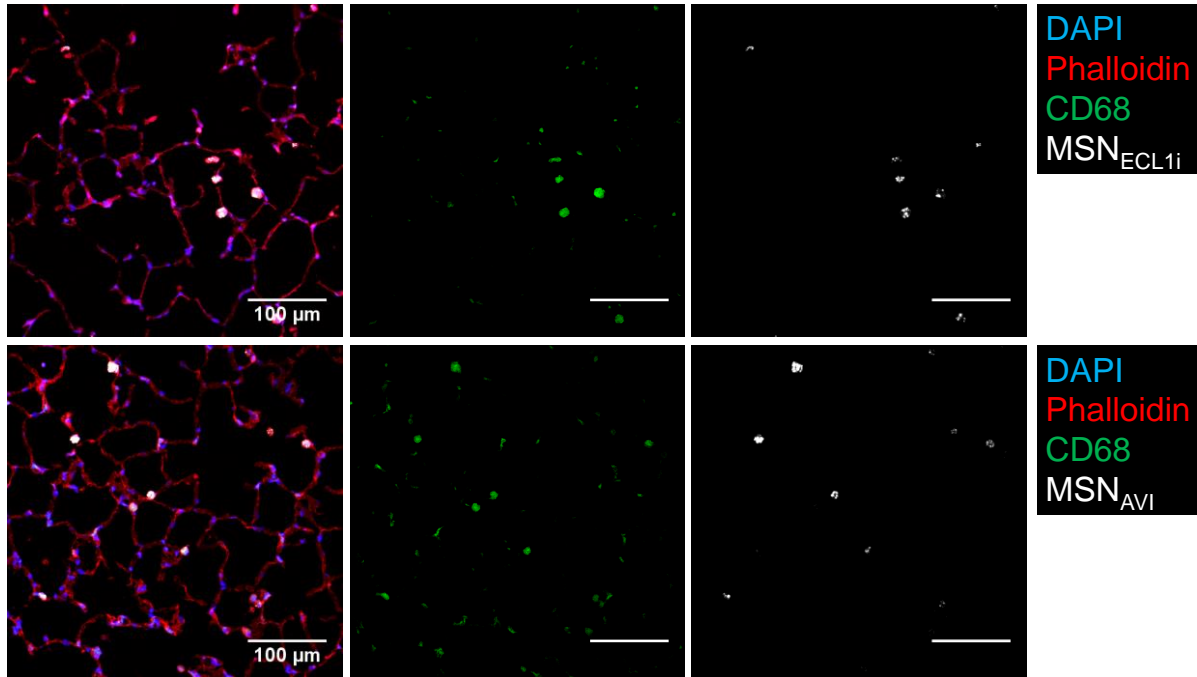


Figure 6.12 CCR2-targeted and non-targeted MSNs accumulate in CD68 positive macrophages in *Kras^{LA2}* mutant lungs. Immunofluorescence co-staining for the macrophage marker CD68 in tumor-free regions of the lungs of *Kras^{LA2}* mice with ATTO 633-labeled MSNs. Nuclear staining (DAPI) is shown in blue, actin staining (phalloidin) in red, CD68 staining in green, and ATTO 633-labeled MSNs in gray. Images shown are representative for three different regions from each mice (n = 5 per MSN type). Scale bar = 100 μ m.

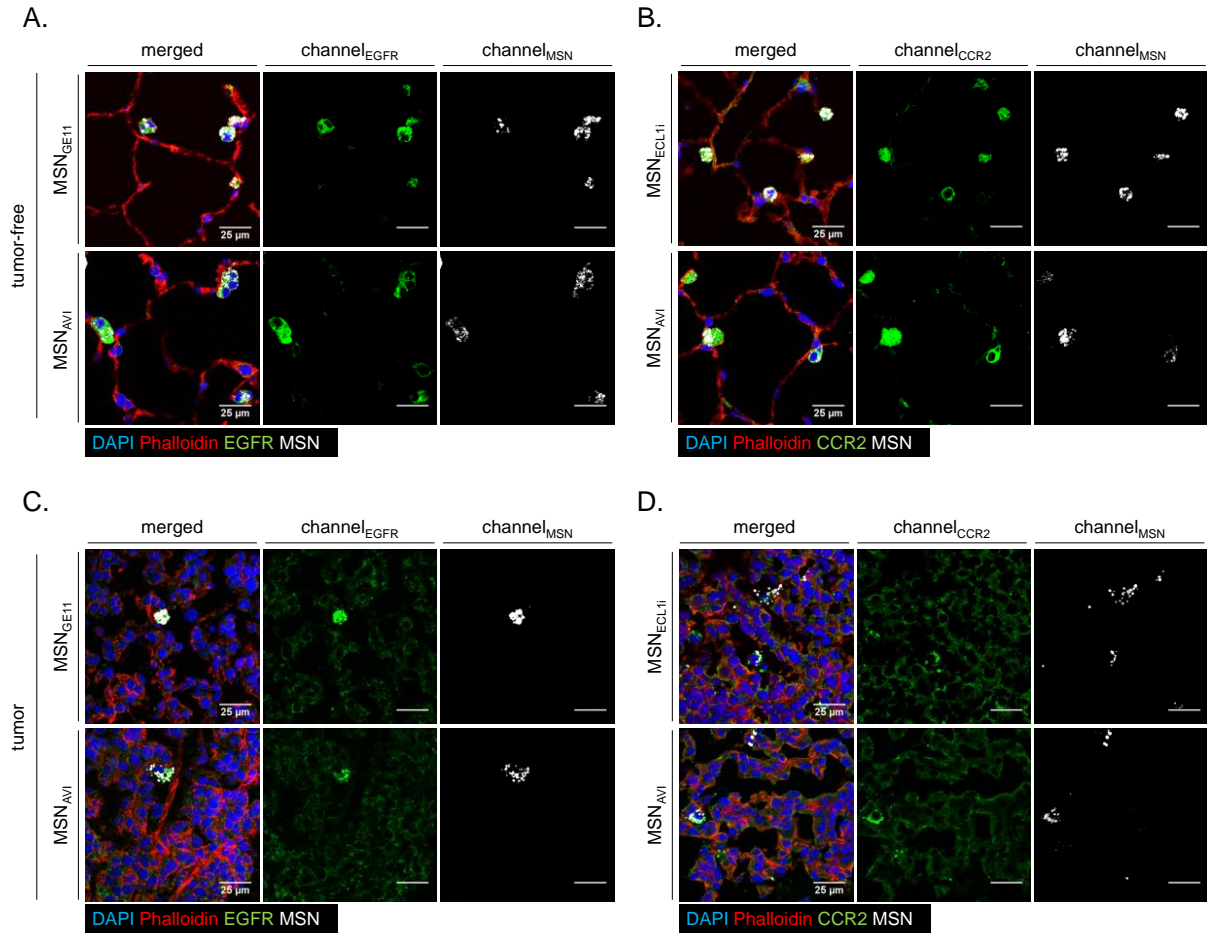


Figure 6.13 Nanoparticles localize to alveolar macrophages in *Kras*^{LA2} mutant lungs. Immunofluorescence co-staining for (A) EGFR and (B) CCR2 in tumor-free regions compared to (C) EGFR and (D) CCR2 co-staining in tumor regions of the mutant lungs with lung cancer that had been treated with ATTO 633-labeled MSN^{AVI} versus MSN^{GE11} or MSN^{ECL11}. Nuclear staining (DAPI) is shown in blue, actin staining (phalloidin) in red, receptor staining (EGFR for A & C, CCR2 for B & D) in green, and ATTO 633-labeled MSNs in gray. Images shown are representative for three different regions from each group of mice (n = 5 per MSN type).

6.2.6 Protein corona formation on MSNs in distinct biological environments

We next evaluated protein corona formation on non-targeted MSN_{AVI} versus targeted MSN_{GE11} in three different biological environments, *i.e.* cell culture medium in the presence of cell culture media containing 10% FCS, human serum, and murine lung lining fluid. Silver staining of the proteins adsorbed on the nanoparticles revealed a noteworthy presence of protein corona in all three conditions for both targeted and non-targeted MSNs (Figure 6.14). These data suggest that protein corona formation on functionalized MSNs per se does not affect active targeting of receptors but might facilitate out-competition of particle uptake by phagocytosing mononuclear cells.

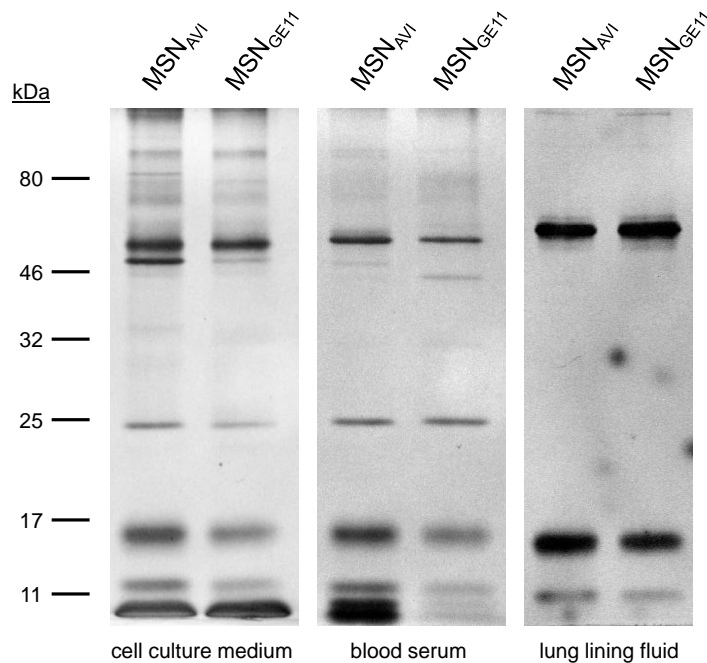


Figure 6.14 Protein corona formation on the surface of the nanoparticles in distinct biological environments. Silver staining of the protein corona formed on the surface of MSN_{AVI} and MSN_{GE11} in cell culture medium with 10% FCS, human blood serum, and murine lung lining fluid, overnight.

6.3 Discussion

In conclusion, *in vitro* validated nanoparticle-mediated targeting of receptors on tumor and tumor-associated immune cells is strongly deprived *in vivo*. This failure in cellular targeting specificity is particularly obvious for the lung-delivered nanoparticles as the alveolar macrophages of the *Kras*-mutant mice strongly overexpressed both EGFR and CCR2, but efficiently entrapped targeted as well as non-targeted nanoparticles to a similar extent. Enhanced cell-specific uptake by macrophages of the lung compared to tumor cells would have escaped analysis if only particle uptake within the tissue would have been monitored as done previously (Bölükbas and Meiners, 2015; Nascimento et al., 2016; Sadhukha et al., 2013; Taratula et al., 2013). Similarly, analysis of cell-specific particle uptake in the flank tumor models also unambiguously revealed loss of cellular targeting specificity. Our data thus emphasize the need for analyzing cellular targeting specificities with cellular resolution also in the major target organs. This is particularly relevant when aiming for combination targeting of different cell populations with distinct ligand-functionalized nanoparticles.

These findings do not rule out that targeted nanoparticles have therapeutic effects in mouse tumor models as indicated by numerous studies using MSNs and other nanomaterials (Davis et al., 2010; Liu et al., 2016; Meng et al., 2011; Wagner, 2007). Our findings, however, indicate that these therapeutic effects may not always be due to a direct nanoparticle-mediated tumor killing but may also involve bystander effects such as cytotoxicity of tissue-resident phagocytic cells, immune-modulatory effects, and unspecific drug release from nanoparticles in the liver into the circulation. Some of these effects may have even been mitigated in previous studies due to the use of immunocompromised mice. As recently outlined by Wilhelm and Torrice (Torrice, 2016; Wilhelm et al., 2016), numbers of contradictory reports on *in vivo* tumor targeting efficiency of nanomedicines are on the rise and may explain the ineffective translation of nanomedicines into clinical practice. Our data also suggest that targeting specificity *in vivo* is probably not solely related to the shielding of ligand-receptor interactions on target cells by formation of a protein corona on the nanoparticles (Salvati et al., 2013; Tenzer et al., 2013) as cell-specific targeting was hampered in two distinct biological environments, *i.e.* the blood and the lung. Our own and other published data indicate that blood-derived serum and the lung lining fluid form distinct protein coronas on nanoparticles *in vitro* (Figure 6.14) (Tenzer et al., 2013). Moreover, protein corona also forms rapidly in cell culture medium containing serum where receptor-mediated targeting was effective (Figure 6.14). Taken together, our study argues in favor of a

stringent validation of cell-specific targeting with cellular-resolution when using nanoparticle-based targeting strategies. Moreover, closing the translational gap in nanomedicine calls first for physiologically relevant animal models, such as the *Kras*^{LA2} mice as used here which develop spontaneous lung tumors closely resembling the human situation, and second for rigorous biological testing of nanoparticles using state of the art molecular manipulation of cells and animals critically.

Synthesis and characterization of the particles was conducted by Stefan Datz.

Experiments for CCR2-targeted MSN_{ECLi} particles were conducted in collaboration with Charlotte Meyer-Schwickerath.

7 Concluding remarks

The aim of this study was to investigate whether novel mesoporous silica nanoparticles (MSNs) are appropriate nanoformulations to use for a more targeted lung cancer therapy. For this, we tried to provide insights on the effects of different functionalizations on the particles *in vitro* and *in vivo*. Additionally, we examined protease-stimulated release of drugs from these nanoparticles in several *in vitro* and *ex vivo* models. Moreover, we inspected cell-specific targeting ability of such particles in *in vitro* and *in vivo* settings.

In the first part of this study, we compared the biodistribution and preferential uptake of avidin protein functionalized *versus* non-functionalized MSNs in healthy mice lungs. To achieve that, wild-type adult BALB/c mice were exposed to fluorescently-labeled MSNs for 1, 3, or 7 days by intratracheal delivery. Both MSN types were detected in the alveolar architecture of the lungs, yet the non-functionalized nanoparticles were mostly associated with alveolar macrophages at all time points. In contrast, avidin-functionalized MSNs were first distributed homogeneously in the alveolar epithelial cells of the lungs, which was then followed by alveolar macrophage clearance of the particles between 3-7 days. The biokinetics of avidin-functionalized MSNs are encouraging, since drug-encapsulated MSNs would have sufficient time to release the drugs into the epithelial cells of the lung which would then be followed by the clearance of the already emptied MSNs by the alveolar macrophages. Moreover, non-functionalized nanoparticles showed more toxic effects on the alveolar macrophages in comparison to avidin-functionalized ones *in vitro*. Thus, this study clearly confirms that the use of avidin-functionalization on the mesoporous silica nanoparticles is of advantage for enhanced biodistribution and biocompatibility of the instilled nanoparticles.

Having validated the feasibility of the avidin-functionalization for local application of the MSNs into the lungs, in the second part, we set out our goal to investigate stimuli-responsive release of chemotherapeutic agents from these nanoparticles in lung cancer environment. For this, we utilized MMP9-specific peptide linkers to attach the avidin capping on the openings of the MSN pores. Our *in vitro* data revealed enhanced therapeutic efficacy of the particles which was confirmed by significant cell death as a result of MMP9 sequence-specific release of the drugs in human lung cancer cell lines. To extend our *in vitro* findings, we exploited the novel 3D-lung tissue cultures (3D-LTC) system and exposed tumorous *versus* tumor-free lung slices from the mice and human to drug loaded nanoparticles. In accordance with our *in vitro* results, our detailed confocal microscopy analyses proved MMP9-specific drug release

in both human and mouse slices that had high levels of the MMP9 enzyme. Most interestingly, the highest efficacy was achieved in nanoparticles encapsulated with both cisplatin and bortezomib at their single non-toxic doses, demonstrating synergistic therapeutic effect on 3D-LTCs. Consequently, via *in vitro* and *ex vivo* models, this study validates enhanced therapeutic efficacy of avidin-functionalized MMP9-cleavable linker bearing mesoporous silica nanoparticles for use in lung cancer treatment.

At this point, it is important to note that nanoparticle exposure on 3D-LTCs faces limitations regarding nanoparticle penetration through the tissue slices. While drugs that were released from functionalized MSNs upon MMP9-induced cleavage of the linkers were able to penetrate through the tissue and cause tumor cell-specific death, we were unable to observe efficient penetration of ligand-functionalized MSNs and effective tumor cell-specific targeting. Our unpublished data are in accordance with data published by Hirn *et al.* (Hirn *et al.*, 2014), where nanoparticles applied on 3D-LTCs are observed to mainly remain at the surficial regions of the tissue with no diffusion into the underlying parts.

To translate our *in vitro* and *ex vivo* findings in tumorous lungs *in vivo*, we explored cell-targeting ability of lung cancer cell and tumor-associated macrophage targeted mesoporous silica nanoparticles for combination therapy in mouse models, respectively. We confirmed complementary overexpression of EGFR in lung cancer tumors and CCR2 in tumor-associated macrophages from human and mice by immunohistochemistry, and therefore decided to target these receptors with the particles. Before animal experiments, we confirmed superior uptake of EGFR- and CCR2-targeted nanoparticles in cell culture experiments. To compare our *in vitro* findings in *in vivo* setting, we exploited two different strategies, *i.e.* intravenous (IV) and intratracheal (IT) application of the targeted MSNs. IV administration of the particles was conducted in two different syngeneic flank tumor models of C57BL/6 mice with double tumors with alternating EGFR expressions, *i.e.*, LLC^{EGFR+} / LLC^{EGFR-} and B16F10^{EGFR+} / B16F10^{EGFR-}. 3 days after IV application, the nanoparticles were found to be significantly more accumulated in the livers of the mice as observed by confocal microscopy. Furthermore, this liver accumulation effect was independent of the functionalization of the particles and EGFR expression levels in the flank tumors in both flank tumor models. For local IT instillation of the MSNs, we treated adult *Kras* mutant mice with lung tumors. 3 days after IT instillation, fluorescently-labeled particles were detected in the alveolar space, mostly taken up by hyperplastic cells at

preneoplastic sites and solid tumor edges, and alveolar macrophages again independent of their functionalization. In order to relate this loss of cell-targeting specificity *in vivo*, we evaluated protein corona formation on the surface of our nanoparticles in different biological environments. Our preliminary data confirmed comparable protein corona formation on both targeted and non-targeted MSNs by silver staining which could be attributed as one of the players *in vivo* contributing to this unspecific uptake of the targeted MSNs.

Taken together, IT applied avidin functionalized-mesoporous silica nanoparticles can reach the alveolar space and be taken up by epithelial cells with no cytotoxic behavior at early time points. The controlled release function from these nanoparticles enables achieving enhanced local therapeutic efficiency with significantly less adverse effects. However, *in vitro* feasibility of cell-specific delivery of these particles with receptor-specific ligands showed significant loss of targeting specificity in lung cancer cells and tumor-associated macrophages after IV and IT applications in mouse models. After all, this study demonstrates the necessity to analyze biodistribution and targeting specificity of functionalized nanoparticles with cellular resolution *in vivo* and hence stresses the urgent need for stringent analysis for detection and elimination of these factors before reaching clinical translation.

References

- Adelstein, D.J., and Rodriguez, C.P. (2008). Current and emerging standards of concomitant chemoradiotherapy. Paper presented at: Seminars in oncology (Elsevier).
- Ageitos, J.M., Chuah, J.-A., and Numata, K. (2016). Chapter 1 Design Considerations for Properties of Nanocarriers on Disposition and Efficiency of Drug and Gene Delivery. In *Nanomedicines: Design, Delivery and Detection* (The Royal Society of Chemistry), pp. 1-22.
- Ahn, H.K., Jung, M., Sym, S.J., Shin, D.B., Kang, S.M., Kyung, S.Y., Park, J.-W., Jeong, S.H., and Cho, E.K. (2014). A phase II trial of Cremorphor EL-free paclitaxel (Genexol-PM) and gemcitabine in patients with advanced non-small cell lung cancer. *Cancer chemotherapy and pharmacology* *74*, 277-282.
- Alberti, D., Protti, N., Toppino, A., Deagostino, A., Lanzardo, S., Bortolussi, S., Altieri, S., Voena, C., Chiarle, R., and Crich, S.G. (2015). A theranostic approach based on the use of a dual boron/Gd agent to improve the efficacy of Boron Neutron Capture Therapy in the lung cancer treatment. *Nanomedicine: Nanotechnology, Biology and Medicine*.
- Argyo, C., Weiss, V., Bräuchle, C., and Bein, T. (2013). Multifunctional mesoporous silica nanoparticles as a universal platform for drug delivery. *Chemistry of Materials* *26*, 435-451.
- Auvynet, C., de Chanville, C.B., Hermand, P., Dorgham, K., Piesse, C., Pouchy, C., Carlier, L., Poupel, L., Barthélémy, S., and Felouzis, V. (2016). ECL1i, d (LGTFLKC), a novel, small peptide that specifically inhibits CCL2-dependent migration. *The FASEB Journal* *30*, 2370-2381.
- Aznar, E., Mondragón, L., Ros-Lis, J.V., Sancenón, F., Marcos, M.D., Martínez-Máñez, R., Soto, J., Pérez-Payá, E., and Amorós, P. (2011). Finely tuned temperature-controlled cargo release using paraffin-capped mesoporous silica nanoparticles. *Angewandte Chemie* *123*, 11368-11371.
- Babu, A., Templeton, A.K., Munshi, A., and Ramesh, R. (2013). Nanoparticle-based drug delivery for therapy of lung cancer: progress and challenges. *Journal of Nanomaterials* *2013*, 14.
- Badrzadeh, F., Rahmati-Yamchi, M., Badrzadeh, K., Valizadeh, A., Zarghami, N., Farkhani, S.M., and Akbarzadeh, A. (2014). Drug delivery and nanodetection in lung cancer. *Artificial cells, nanomedicine, and biotechnology*, 1-17.
- Balkwill, F.R., Capasso, M., and Hagemann, T. (2012). The tumor microenvironment at a glance. *J Cell Sci* *125*, 5591-5596.
- Bandyopadhyay, A., Das, T., and Yeasmin, S. (2015). *Nanoparticles in Lung Cancer Therapy: Recent Trends* (Springer).
- Barenholz, Y.C. (2012). Doxil®—the first FDA-approved nano-drug: lessons learned. *Journal of controlled release* *160*, 117-134.

- Beyerle, A., Braun, A., Banerjee, A., Ercal, N., Eickelberg, O., Kissel, T.H., and Stoeger, T. (2011). Inflammatory responses to pulmonary application of PEI-based siRNA nanocarriers in mice. *Biomaterials* 32, 8694-8701.
- Böyükbas, D.A., and Meiners, S. (2015). Lung cancer nanomedicine: potentials and pitfalls. *Nanomedicine* 10, 3203-3212.
- Brahmer, J.R., Tykodi, S.S., Chow, L.Q., Hwu, W.-J., Topalian, S.L., Hwu, P., Drake, C.G., Camacho, L.H., Kauh, J., and Odunsi, K. (2012). Safety and activity of anti-PD-L1 antibody in patients with advanced cancer. *New England Journal of Medicine* 366, 2455-2465.
- Brinkman, A.M., Chen, G., Wang, Y., Hedman, C.J., Sherer, N.M., Havighurst, T.C., Gong, S., and Xu, W. (2016). Aminoflavone-loaded EGFR-targeted unimolecular micelle nanoparticles exhibit anti-cancer effects in triple negative breast cancer. *Biomaterials* 101, 20-31.
- Cao, B., Li, J., and Mao, X. (2013). Dissecting bortezomib: development, application, adverse effects and future direction. *Current pharmaceutical design* 19, 3190-3200.
- Cappuzzo, F., Varella-Garcia, M., Finocchiaro, G., Skokan, M., Gajapathy, S., Carnaghi, C., Rimassa, L., Rossi, E., Ligorio, C., and Di Tommaso, L. (2008). Primary resistance to cetuximab therapy in EGFR FISH-positive colorectal cancer patients. *British Journal of cancer* 99, 83-89.
- Cariboni, U., and Stella, G.M. (2015). Surgical options to early-stage lung cancer: can "the less" mean "the safe"? *Minerva medica* 106, 17-21.
- Casaluce, F., Sgambato, A., Sacco, P.C., Palazzolo, G., Maione, P., Rossi, A., Ciardiello, F., and Gridelli, C. (2014). Emerging drugs targeting PD-1 and PD-L1: reality or hope? *Expert opinion on emerging drugs* 19, 557-569.
- Cauda, V., Schlossbauer, A., Kecht, J., Zürner, A., and Bein, T. (2009). Multiple core-shell functionalized colloidal mesoporous silica nanoparticles. *Journal of the American Chemical Society* 131, 11361-11370.
- Cerami, E., Gao, J., Dogrusoz, U., Gross, B.E., Sumer, S.O., Aksoy, B.A., Jacobsen, A., Byrne, C.J., Heuer, M.L., and Larsson, E. (2012). The cBio cancer genomics portal: an open platform for exploring multidimensional cancer genomics data. *Cancer discovery* 2, 401-404.
- Chen, F., Ehlerding, E.B., and Cai, W. (2014). Theranostic nanoparticles. *Journal of Nuclear Medicine* 55, 1919-1922.
- Chen, X., and Liu, Z. (2016). Dual responsive mesoporous silica nanoparticles for targeted co-delivery of hydrophobic and hydrophilic anticancer drugs to tumor cells. *Journal of Materials Chemistry B*.
- Chen, Y., Chen, H., and Shi, J. (2013). In Vivo Bio-Safety Evaluations and Diagnostic/Therapeutic Applications of Chemically Designed Mesoporous Silica Nanoparticles. *Advanced Materials* 25, 3144-3176.

- Chen, Y., Zhu, X., Zhang, X., Liu, B., and Huang, L. (2010). Nanoparticles modified with tumor-targeting scFv deliver siRNA and miRNA for cancer therapy. *Molecular Therapy* *18*, 1650-1656.
- Cheng, L., Huang, F.-Z., Cheng, L.-F., Zhu, Y.-Q., Hu, Q., Li, L., Wei, L., and Chen, D.-W. (2014). GE11-modified liposomes for non-small cell lung cancer targeting: preparation, ex vitro and in vivo evaluation. *International journal of nanomedicine* *9*, 921.
- Chien, M.-P., Carlini, A.S., Hu, D., Barback, C.V., Rush, A.M., Hall, D.J., Orr, G., and Gianneschi, N.C. (2013a). Enzyme-directed assembly of nanoparticles in tumors monitored by in vivo whole animal imaging and ex vivo super-resolution fluorescence imaging. *Journal of the American Chemical Society* *135*, 18710-18713.
- Chien, M.P., Thompson, M.P., Barback, C.V., Ku, T.H., Hall, D.J., and Gianneschi, N.C. (2013b). Enzyme-Directed Assembly of a Nanoparticle Probe in Tumor Tissue. *Advanced Materials* *25*, 3599-3604.
- Chiou, G.-Y., Cherng, J.-Y., Hsu, H.-S., Wang, M.-L., Tsai, C.-M., Lu, K.-H., Chien, Y., Hung, S.-C., Chen, Y.-W., and Wong, C.-I. (2012). Cationic polyurethanes-short branch PEI-mediated delivery of Mir145 inhibited epithelial–mesenchymal transdifferentiation and cancer stem-like properties and in lung adenocarcinoma. *Journal of Controlled Release* *159*, 240-250.
- Choi, H.S., Ashitate, Y., Lee, J.H., Kim, S.H., Matsui, A., Insin, N., Bawendi, M.G., Semmler-Behnke, M., Frangioni, J.V., and Tsuda, A. (2010). Rapid translocation of nanoparticles from the lung airspaces to the body. *Nat Biotech* *28*, 1300-1303.
- Choi, S.H., Byeon, H.J., Choi, J.S., Thao, L., Kim, I., Lee, E.S., Shin, B.S., Lee, K.C., and Youn, Y.S. (2015). Inhalable self-assembled albumin nanoparticles for treating drug-resistant lung cancer. *Journal of Controlled Release* *197*, 199-207.
- Chong, C.R., and Jänne, P.A. (2013). The quest to overcome resistance to EGFR-targeted therapies in cancer. *Nature medicine* *19*, 1389-1400.
- Chono, S., Tanino, T., Seki, T., and Morimoto, K. (2007). Uptake characteristics of liposomes by rat alveolar macrophages: influence of particle size and surface mannose modification. *Journal of pharmacy and pharmacology* *59*, 75-80.
- Chono, S., Tanino, T., Seki, T., and Morimoto, K. (2008). Efficient drug targeting to rat alveolar macrophages by pulmonary administration of ciprofloxacin incorporated into mannosylated liposomes for treatment of respiratory intracellular parasitic infections. *Journal of Controlled Release* *127*, 50-58.
- Chow, E.K.-H., and Ho, D. (2013). Cancer nanomedicine: from drug delivery to imaging. *Science translational medicine* *5*, 216rv214-216rv214.
- Chuang, J.C., Liang, Y., and Wakelee, H.A. (2017). Neoadjuvant and Adjuvant Therapy for Non–Small Cell Lung Cancer. *Hematology/Oncology Clinics of North America* *31*, 31-44.
- Chung, T.-H., Wu, S.-H., Yao, M., Lu, C.-W., Lin, Y.-S., Hung, Y., Mou, C.-Y., Chen, Y.-C., and Huang, D.-M. (2007). The effect of surface charge on the uptake and biological

function of mesoporous silica nanoparticles in 3T3-L1 cells and human mesenchymal stem cells. *Biomaterials* 28, 2959-2966.

Ciriello, G., Miller, M.L., Aksoy, B.A., Senbabaoglu, Y., Schultz, N., and Sander, C. (2013). Emerging landscape of oncogenic signatures across human cancers. *Nature genetics* 45, 1127-1133.

Collins, L.G., Haines, C., Perkel, R., and Enck, R.E. (2007). Lung cancer: diagnosis and management. *Am Fam Physician* 75, 56-63.

Conde, J., Bao, C., Tan, Y., Cui, D., Edelman, E.R., Azevedo, H.S., Byrne, H.J., Artzi, N., and Tian, F. (2015). Dual Targeted Immunotherapy via In Vivo Delivery of Biohybrid RNAi-Peptide Nanoparticles to Tumor-Associated Macrophages and Cancer Cells. *Advanced Functional Materials* 25, 4183-4194.

Conde, J., Tian, F., Hernández, Y., Bao, C., Cui, D., Janssen, K.-P., Ibarra, M.R., Baptista, P.V., Stoeger, T., and Jesús, M. (2013). In vivo tumor targeting via nanoparticle-mediated therapeutic siRNA coupled to inflammatory response in lung cancer mouse models. *Biomaterials* 34, 7744-7753.

Coussens, L.M., and Werb, Z. (2002). Inflammation and cancer. *Nature* 420, 860-867.

Cox, G., Jones, J.L., and O'Byrne, K.J. (2000). Matrix metalloproteinase 9 and the epidermal growth factor signal pathway in operable non-small cell lung cancer. *Clinical Cancer Research* 6, 2349-2355.

Crisp, J.L., Savariar, E.N., Glasgow, H.L., Ellies, L.G., Whitney, M.A., and Tsien, R.Y. (2014). Dual Targeting of Integrin $\alpha\beta 3$ and Matrix Metalloproteinase-2 for Optical Imaging of Tumors and Chemotherapeutic Delivery. *Molecular cancer therapeutics* 13, 1514-1525.

Dasari, S., and Tchounwou, P.B. (2014). Cisplatin in cancer therapy: molecular mechanisms of action. *European journal of pharmacology* 740, 364-378.

Davies, A., Lara, P., Lau, D., Mack, P., Gumerlock, P., Gandara, D., Schenkein, D., and Doroshov, J. (2004). The proteasome inhibitor, bortezomib, in combination with gemcitabine (Gem) and carboplatin (Carbo) in advanced non-small cell lung cancer (NSCLC): final results of a phase I California Cancer Consortium study. Paper presented at: ASCO Annual Meeting Proceedings.

Davies, A.M., Ho, C., Metzger, A.S., Beckett, L.A., Christensen, S., Tanaka, M., Lara, P.N., Lau, D.H., and Gandara, D.R. (2007a). Phase I study of two different schedules of bortezomib and pemetrexed in advanced solid tumors with emphasis on non-small cell lung cancer. *Journal of Thoracic Oncology* 2, 1112-1116.

Davies, A.M., Lara, P.N., Mack, P.C., and Gandara, D.R. (2007b). Incorporating bortezomib into the treatment of lung cancer. *Clinical Cancer Research* 13, 4647s-4651s.

Davis, M.E., Zuckerman, J.E., Choi, C.H.J., Seligson, D., Tolcher, A., Alabi, C.A., Yen, Y., Heidel, J.D., and Ribas, A. (2010). Evidence of RNAi in humans from systemically administered siRNA via targeted nanoparticles. *Nature* 464, 1067-1070.

- Dawidczyk, C.M., Kim, C., Park, J.H., Russell, L.M., Lee, K.H., Pomper, M.G., and Searson, P.C. (2014). State-of-the-art in design rules for drug delivery platforms: lessons learned from FDA-approved nanomedicines. *Journal of Controlled Release* 187, 133-144.
- De La Zerda, A., Zavaleta, C., Keren, S., Vaithilingam, S., Bodapati, S., Liu, Z., Levi, J., Smith, B.R., Ma, T.-J., Oralkan, O., *et al.* (2008). Carbon nanotubes as photoacoustic molecular imaging agents in living mice. *Nat Nano* 3, 557-562.
- de Mello, R.A., Marques, D.S., de Mello, R.A., Medeiros, R., Medeiros, R., and Araújo, A.M. (2011). Epidermal growth factor receptor and K-Ras in non-small cell lung cancer-molecular pathways involved and targeted therapies. *World J Clin Oncol* 2, 367-376.
- Doane, T.L., and Burda, C. (2012). The unique role of nanoparticles in nanomedicine: imaging, drug delivery and therapy. *Chemical Society Reviews* 41, 2885-2911.
- Dubey, S., and Powell, C.A. (2008). Update in lung cancer 2007. *American journal of respiratory and critical care medicine* 177, 941-946.
- Duffy, M. (2013). The war on cancer: are we winning? *Tumor Biology* 34, 1275-1284.
- Duncan, R., and Gaspar, R. (2011). Nanomedicine(s) under the microscope. *Molecular pharmaceutics* 8, 2101-2141.
- Eberhard, D.A., Johnson, B.E., Amler, L.C., Goddard, A.D., Heldens, S.L., Herbst, R.S., Ince, W.L., Jänne, P.A., Januario, T., and Johnson, D.H. (2005). Mutations in the epidermal growth factor receptor and in KRAS are predictive and prognostic indicators in patients with non-small-cell lung cancer treated with chemotherapy alone and in combination with erlotinib. *Journal of Clinical Oncology* 23, 5900-5909.
- Egeblad, M., and Werb, Z. (2002). New functions for the matrix metalloproteinases in cancer progression. *Nature Reviews Cancer* 2, 161-174.
- El-Badrawy, M.K., Yousef, A.M., Shaalan, D., and Elsamanoudy, A.Z. (2014). Matrix metalloproteinase-9 expression in lung cancer patients and its relation to serum mmp-9 activity, pathologic type, and prognosis. *Journal of bronchology & interventional pulmonology* 21, 327-334.
- Ene, C.I., and Fine, H.A. (2011). Many tumors in one: a daunting therapeutic prospect. *Cancer cell* 20, 695-697.
- Fantini, M., Gianni, L., Santelmo, C., Drudi, F., Castellani, C., Affatato, A., Nicolini, M., and Ravaioli, A. (2010). Lipoplatin treatment in lung and breast cancer. *Chemotherapy research and practice* 2011.
- Ferlay, J., Soerjomataram, I., Ervik, M., Dikshit, R., Eser, S., Mathers, C., Rebelo, M., Parkin, D., Forman, D., and Bray, F. (2013). GLOBOCAN 2012 v1. 0. Cancer incidence and mortality worldwide: IARC CancerBase.
- Ferreira, A., Cemlyn-Jones, J., and Cordeiro, C.R. (2013). Nanoparticles, nanotechnology and pulmonary nanotoxicology. *Revista Portuguesa de Pneumologia (English Edition)* 19, 28-37.

- Field, R.W., and Withers, B.L. (2012). Occupational and environmental causes of lung cancer. *Clinics in chest medicine* 33, 681-703.
- Fife, B.T., and Bluestone, J.A. (2008). Control of peripheral T-cell tolerance and autoimmunity via the CTLA-4 and PD-1 pathways. *Immunological reviews* 224, 166-182.
- Fritz, J.M., Tennis, M.A., Orlicky, D.J., Lin, H., Ju, C., Redente, E.F., Choo, K.S., Staab, T.A., Bouchard, R.J., and Merrick, D.T. (2015). Depletion of tumor-associated macrophages slows the growth of chemically induced mouse lung adenocarcinomas. *M1/M2 Macrophages: The Arginine Fork in the Road to Health and Disease*, 117.
- Fujita, Y., Kuwano, K., and Ochiya, T. (2015). Development of small RNA delivery systems for lung cancer therapy. *International journal of molecular sciences* 16, 5254-5270.
- Ganesh, S., Iyer, A.K., Morrissey, D.V., and Amiji, M.M. (2013a). Hyaluronic acid based self-assembling nanosystems for CD44 target mediated siRNA delivery to solid tumors. *Biomaterials* 34, 3489-3502.
- Ganesh, S., Iyer, A.K., Weiler, J., Morrissey, D.V., and Amiji, M.M. (2013b). Combination of siRNA-directed gene silencing with cisplatin reverses drug resistance in human non-small cell lung cancer. *Molecular Therapy—Nucleic Acids* 2, e110.
- Gialeli, C., Theocharis, A.D., and Karamanos, N.K. (2011). Roles of matrix metalloproteinases in cancer progression and their pharmacological targeting. *FEBS journal* 278, 16-27.
- Giri, S., Trewyn, B.G., Stellmaker, M.P., and Lin, V.S.Y. (2005). Stimuli-responsive controlled-release delivery system based on mesoporous silica nanorods capped with magnetic nanoparticles. *Angewandte Chemie International Edition* 44, 5038-5044.
- Glass, J.J., Yuen, D., Rae, J., Johnston, A.P., Parton, R.G., Kent, S.J., and De Rose, R. (2016). Human immune cell targeting of protein nanoparticles—caveospheres. *Nanoscale* 8, 8255-8265.
- Gray, B.P., McGuire, M.J., and Brown, K.C. (2013). A liposomal drug platform overrides peptide ligand targeting to a cancer biomarker, irrespective of ligand affinity or density. *PloS one* 8, e72938.
- Gridelli, C., Rossi, A., Carbone, D.P., Guarize, J., Karachaliou, N., Mok, T., Petrella, F., Spaggiari, L., and Rosell, R. (2015). Non-small-cell lung cancer. *Nature Reviews Disease Primers* 1, 15009.
- Grilley-Olson, J.E., Keedy, V.L., Sandler, A., Moore, D.T., Socinski, M.A., and Stinchcombe, T.E. (2015). A Randomized Phase II Study of Carboplatin With Weekly or Every-3-Week Nanoparticle Albumin-Bound Paclitaxel (Abraxane) in Patients With Extensive-Stage Small Cell Lung Cancer. *The Oncologist*, theoncologist. 2014-0327.
- Gu, F.X., Karnik, R., Wang, A.Z., Alexis, F., Levy-Nissenbaum, E., Hong, S., Langer, R.S., and Farokhzad, O.C. (2007). Targeted nanoparticles for cancer therapy. *Nano today* 2, 14-21.

- Gu, G., Xia, H., Hu, Q., Liu, Z., Jiang, M., Kang, T., Miao, D., Tu, Y., Pang, Z., and Song, Q. (2013). PEG-co-PCL nanoparticles modified with MMP-2/9 activatable low molecular weight protamine for enhanced targeted glioblastoma therapy. *Biomaterials* 34, 196-208.
- Guo, L., Fan, L., Ren, J., Pang, Z., Ren, Y., Li, J., Wen, Z., Qian, Y., Zhang, L., and Ma, H. (2012). Combination of TRAIL and actinomycin D liposomes enhances antitumor effect in non-small cell lung cancer. *International journal of nanomedicine* 7, 1449.
- Guo, Y., Wang, L., Lv, P., and Zhang, P. (2015). Transferrin-conjugated doxorubicin-loaded lipid-coated nanoparticles for the targeting and therapy of lung cancer. *Oncology Letters* 9, 1065-1072.
- Haber, Daniel A., Gray, Nathanael S., and Baselga, J. (2011). The Evolving War on Cancer. *Cell* 145, 19-24.
- Hadjidemetriou, M., Al-Ahmady, Z., Mazza, M., Collins, R.F., Dawson, K., and Kostarelos, K. (2015). In vivo biomolecule corona around blood-circulating, clinically used and antibody-targeted lipid bilayer nanoscale vesicles. *ACS nano* 9, 8142-8156.
- Han, Y., Li, Y., Zhang, P., Sun, J., Li, X., Sun, X., and Kong, F. (2014). Nanostructured lipid carriers as novel drug delivery system for lung cancer gene therapy. *Pharmaceutical development and technology*, 1-5.
- Hanahan, D., and Coussens, L.M. (2012). Accessories to the crime: functions of cells recruited to the tumor microenvironment. *Cancer cell* 21, 309-322.
- Hanahan, D., and Weinberg, R.A. (2000). The hallmarks of cancer. *cell* 100, 57-70.
- Hatakeyama, H., Akita, H., Ito, E., Hayashi, Y., Oishi, M., Nagasaki, Y., Danev, R., Nagayama, K., Kaji, N., and Kikuchi, H. (2011). Systemic delivery of siRNA to tumors using a lipid nanoparticle containing a tumor-specific cleavable PEG-lipid. *Biomaterials* 32, 4306-4316.
- He, Q., Zhang, Z., Gao, F., Li, Y., and Shi, J. (2011). In vivo biodistribution and urinary excretion of mesoporous silica nanoparticles: effects of particle size and PEGylation. *small* 7, 271-280.
- Herbst, R.S., Heymach, J.V., and Lippman, S.M. (2008). Lung Cancer. *New England Journal of Medicine* 359, 1367-1380.
- Herbst, R.S., Soria, J.-C., Kowanetz, M., Fine, G.D., Hamid, O., Gordon, M.S., Sosman, J.A., McDermott, D.F., Powderly, J.D., and Gettinger, S.N. (2014). Predictive correlates of response to the anti-PD-L1 antibody MPDL3280A in cancer patients. *Nature* 515, 563-567.
- Hiratsuka, S., Ishibashi, S., Tomita, T., Watanabe, A., Akashi-Takamura, S., Murakami, M., Kijima, H., Miyake, K., Aburatani, H., and Maru, Y. (2013). Primary tumours modulate innate immune signalling to create pre-metastatic vascular hyperpermeability foci. *Nature communications* 4, 1853.
- Hirn, S., Haberl, N., Loza, K., Epple, M., Kreyling, W.G., Rothen-Rutishauser, B., Rehberg, M., and Krombach, F. (2014). Proinflammatory and cytotoxic response to nanoparticles in precision-cut lung slices. *Beilstein journal of nanotechnology* 5, 2440-2449.

- Howell, M., Wang, C., Mahmoud, A., Hellermann, G., Mohapatra, S., and Mohapatra, S. (2013). Dual-function theranostic nanoparticles for drug delivery and medical imaging contrast: perspectives and challenges for use in lung diseases. *Drug delivery and translational research* 3, 352-363.
- Hrkach, J., Von Hoff, D., Ali, M.M., Andrianova, E., Auer, J., Campbell, T., De Witt, D., Figa, M., Figueiredo, M., and Horhota, A. (2012). Preclinical development and clinical translation of a PSMA-targeted docetaxel nanoparticle with a differentiated pharmacological profile. *Science translational medicine* 4, 128ra139-128ra139.
- Huang, R., Wei, Y., Hung, R.J., Liu, G., Su, L., Zhang, R., Zong, X., Zhang, Z.-F., Morgenstern, H., and Brüske, I. (2015). Associated links among smoking, chronic obstructive pulmonary disease, and small cell lung cancer: a pooled analysis in the International Lung Cancer Consortium. *EBioMedicine* 2, 1677-1685.
- Huang, X., Li, L., Liu, T., Hao, N., Liu, H., Chen, D., and Tang, F. (2011). The shape effect of mesoporous silica nanoparticles on biodistribution, clearance, and biocompatibility in vivo. *ACS nano* 5, 5390-5399.
- Hudson, S.P., Padera, R.F., Langer, R., and Kohane, D.S. (2008). The biocompatibility of mesoporous silicates. *Biomaterials* 29, 4045-4055.
- Iniesta, P., Morán, A., De Juan, C., Gómez, A., Hernando, F., García-Aranda, C., Frías, C., Díaz-López, A., Rodríguez-Jimenez, F., and Balibrea, J. (2007). Biological and clinical significance of MMP-2, MMP-9, TIMP-1 and TIMP-2 in non-small cell lung cancer. *Oncology reports* 17, 217-224.
- Irvine, D.J., Hanson, M.C., Rakhra, K., and Tokatlian, T. (2015). Synthetic nanoparticles for vaccines and immunotherapy. *Chemical reviews* 115, 11109-11146.
- Itoh, T., Tanioka, M., Matsuda, H., Nishimoto, H., Yoshioka, T., Suzuki, R., and Uehira, M. (1999). Experimental metastasis is suppressed in MMP-9-deficient mice. *Clinical & experimental metastasis* 17, 177-181.
- Jain, N.K., Mishra, V., and Mehra, N.K. (2013). Targeted drug delivery to macrophages. *Expert opinion on drug delivery* 10, 353-367.
- Jain, R.K., and Stylianopoulos, T. (2010). Delivering nanomedicine to solid tumors. *Nature reviews Clinical oncology* 7, 653-664.
- Janib, S.M., Moses, A.S., and MacKay, J.A. (2010). Imaging and drug delivery using theranostic nanoparticles. *Advanced drug delivery reviews* 62, 1052-1063.
- Jett, J.R., and Carr, L.L. (2013). Targeted Therapy for Non-Small Cell Lung Cancer. *American journal of respiratory and critical care medicine* 188, 907-912.
- Johnson, L., Mercer, K., Greenbaum, D., Bronson, R.T., Crowley, D., Tuveson, D.A., and Jacks, T. (2001). Somatic activation of the K-ras oncogene causes early onset lung cancer in mice. *Nature* 410, 1111-1116.
- Jokerst, J.V., and Gambhir, S.S. (2011). Molecular imaging with theranostic nanoparticles. *Accounts of chemical research* 44, 1050-1060.

- Karra, N., Nassar, T., Ripin, A.N., Schwob, O., Borlak, J., and Benita, S. (2013). Antibody conjugated PLGA nanoparticles for targeted delivery of paclitaxel palmitate: efficacy and biofate in a lung cancer mouse model. *Small* 9, 4221-4236.
- Kessenbrock, K., Plaks, V., and Werb, Z. (2010). Matrix metalloproteinases: regulators of the tumor microenvironment. *Cell* 141, 52-67.
- Key, J., Kim, Y.-S., Tatulli, F., Palange, A., O'Neill, B., Aryal, S., Ramirez, M., Liu, X., Ferrari, M., and Munden, R. (2014). Opportunities for nanotheranosis in lung cancer and pulmonary metastasis. *Clinical and translational imaging* 2, 427-437.
- Kim, D.-W., Kim, S.-Y., Kim, H.-K., Kim, S.-W., Shin, S., Kim, J., Park, K., Lee, M., and Heo, D. (2007). Multicenter phase II trial of Genexol-PM, a novel Cremophor-free, polymeric micelle formulation of paclitaxel, with cisplatin in patients with advanced non-small-cell lung cancer. *Annals of oncology* 18, 2009-2014.
- Kim, H.J., Kim, K.H., Yun, J., Kim, S.H., Kim, H.J., Lee, S.-C., Bae, S.B., Kim, C.K., Lee, N.S., and Lee, K.T. (2011). Phase II clinical trial of Genexol®(Paclitaxel) and Carboplatin for patients with advanced non-small cell lung cancer. *Cancer Research and Treatment* 43, 19-23.
- Kim, I., Byeon, H.J., Kim, T.H., Lee, E.S., Oh, K.T., Shin, B.S., Lee, K.C., and Youn, Y.S. (2013). Doxorubicin-loaded porous PLGA microparticles with surface attached TRAIL for the inhalation treatment of metastatic lung cancer. *Biomaterials* 34, 6444-6453.
- Kim, Y.-D., Park, T.-E., Singh, B., Maharjan, S., Choi, Y.-J., Choung, P.-H., Arote, R.B., and Cho, C.-S. (2015). Nanoparticle-mediated delivery of siRNA for effective lung cancer therapy. *Nanomedicine* 10, 1165-1188.
- Koukourakis, M., Romanidis, K., Froudarakis, M., Kyrgias, G., Koukourakis, G., Retalis, G., and Bahlitzanakis, N. (2002). Concurrent administration of Docetaxel and Stealth® liposomal doxorubicin with radiotherapy in non-small cell lung cancer: excellent tolerance using subcutaneous amifostine for cytoprotection. *British journal of cancer* 87, 385-392.
- Kreyling, W.G., Semmler-Behnke, M., Takenaka, S., and Möller, W. (2013). Differences in the Biokinetics of Inhaled Nano- versus Micrometer-Sized Particles. *Accounts of Chemical Research* 46, 714-722.
- Kulkarni, P.S., Haldar, M.K., Nahire, R.R., Katti, P., Ambre, A.H., Muhonen, W.W., Shabb, J.B., Padi, S.K., Singh, R.K., and Borowicz, P.P. (2014). MMP-9 Responsive PEG cleavable nanovesicles for efficient delivery of chemotherapeutics to pancreatic cancer. *Molecular pharmaceutics* 11, 2390-2399.
- Kupferschmidt, N., Xia, X., Labrador, R.H., Atluri, R., Ballell, L., and Garcia-Bennett, A.E. (2013). In vivo oral toxicological evaluation of mesoporous silica particles. *Nanomedicine* 8, 57-64.
- Labiris, N., and Dolovich, M. (2003). Pulmonary drug delivery. Part I: physiological factors affecting therapeutic effectiveness of aerosolized medications. *British journal of clinical pharmacology* 56, 588-599.
- Lambrecht, B.N. (2006). Alveolar macrophage in the driver's seat. *Immunity* 24, 366-368.

- Lammers, P.E., Lu, B., Horn, L., Shyr, Y., and Keedy, V. (2015). nab-Paclitaxel in Combination With Weekly Carboplatin With Concurrent Radiotherapy in Stage III Non-Small Cell Lung Cancer. *The Oncologist*, theoncologist. 2015-0030.
- Langer, C.J., Hirsh, V., Ko, A., Renschler, M.F., and Socinski, M.A. (2014). Weekly nab-Paclitaxel in Combination With Carboplatin as First-Line Therapy in Patients With Advanced Non-Small-Cell Lung Cancer: Analysis of Safety and Efficacy in Patients With Renal Impairment. *Clinical lung cancer*.
- Lee, J.-H., Jang, J.-t., Choi, J.-s., Moon, S.H., Noh, S.-h., Kim, J.-w., Kim, J.-G., Kim, I.-S., Park, K.I., and Cheon, J. (2011). Exchange-coupled magnetic nanoparticles for efficient heat induction. *Nat Nano* 6, 418-422.
- Li, H., Yu, S.S., Miteva, M., Nelson, C.E., Werfel, T., Giorgio, T.D., and Duvall, C.L. (2013). Matrix Metalloproteinase Responsive, Proximity-Activated Polymeric Nanoparticles for siRNA Delivery. *Advanced functional materials* 23, 3040-3052.
- Li, J., Chen, Y.-C., Tseng, Y.-C., Mozumdar, S., and Huang, L. (2010). Biodegradable calcium phosphate nanoparticle with lipid coating for systemic siRNA delivery. *Journal of Controlled Release* 142, 416-421.
- Li, J., Yang, Y., and Huang, L. (2012a). Calcium phosphate nanoparticles with an asymmetric lipid bilayer coating for siRNA delivery to the tumor. *Journal of Controlled Release* 158, 108-114.
- Li, Z., Barnes, J.C., Bosoy, A., Stoddart, J.F., and Zink, J.I. (2012b). Mesoporous silica nanoparticles in biomedical applications. *Chemical Society Reviews* 41, 2590-2605.
- Li, Z., Zhao, R., Wu, X., Sun, Y., Yao, M., Li, J., Xu, Y., and Gu, J. (2005). Identification and characterization of a novel peptide ligand of epidermal growth factor receptor for targeted delivery of therapeutics. *The FASEB journal* 19, 1978-1985.
- Lim, E.K., Kim, T., Paik, S., Haam, S., Huh, Y.M., and Lee, K. (2015). Nanomaterials for theranostics: recent advances and future challenges. *Chem Rev* 115, 327-394.
- Lin, Y.-S., and Haynes, C.L. (2010). Impacts of mesoporous silica nanoparticle size, pore ordering, and pore integrity on hemolytic activity. *Journal of the American Chemical Society* 132, 4834-4842.
- Liu, H., Liu, T., Wu, X., Li, L., Tan, L., Chen, D., and Tang, F. (2012a). Targeting gold nanoshells on silica nanorattles: a drug cocktail to fight breast tumors via a single irradiation with near-infrared laser light. *Advanced Materials* 24, 755-761.
- Liu, J., Chu, L., Wang, Y., Duan, Y., Feng, L., Yang, C., Wang, L., and Kong, D. (2011). Novel peptide-dendrimer conjugates as drug carriers for targeting nonsmall cell lung cancer. *Int J Nanomedicine* 6, 59-69.
- Liu, L., Liu, X., Xu, Q., Wu, P., Zuo, X., Zhang, J., Deng, H., Wu, Z., and Ji, A. (2014). Self-assembled nanoparticles based on the c (RGDfk) peptide for the delivery of siRNA targeting the VEGFR2 gene for tumor therapy. *International journal of nanomedicine* 9, 3509.

- Liu, Q., Li, R.-T., Qian, H.-Q., Yang, M., Zhu, Z.-S., Wu, W., Qian, X.-P., Yu, L.-X., Jiang, X.-Q., and Liu, B.-R. (2012b). Gelatinase-stimuli strategy enhances the tumor delivery and therapeutic efficacy of docetaxel-loaded poly (ethylene glycol)-poly (varepsilon-caprolactone) nanoparticles. *Int J Nanomedicine* 7, 281-295.
- Liu, X., Situ, A., Kang, Y., Villabroza, K.R., Liao, Y., Chang, C.H., Donahue, T., Nel, A.E., and Meng, H. (2016). Irinotecan delivery by lipid-coated mesoporous silica nanoparticles shows improved efficacy and safety over liposomes for pancreatic cancer. *ACS nano* 10, 2702-2715.
- Lu, J., Li, Z., Zink, J.I., and Tamanoi, F. (2012). In vivo tumor suppression efficacy of mesoporous silica nanoparticles-based drug-delivery system: enhanced efficacy by folate modification. *Nanomedicine: Nanotechnology, Biology and Medicine* 8, 212-220.
- Lu, J., Liong, M., Li, Z., Zink, J.I., and Tamanoi, F. (2010). Biocompatibility, biodistribution, and drug-delivery efficiency of mesoporous silica nanoparticles for cancer therapy in animals. *Small* 6, 1794-1805.
- Lu, X., Zhu, T., Chen, C., and Liu, Y. (2014). Right or Left: The Role of Nanoparticles in Pulmonary Diseases. *International journal of molecular sciences* 15, 17577-17600.
- Lu, Y., Liu, L., Wang, Y., Li, F., Zhang, J., Ye, M., Zhao, H., Zhang, X., Zhang, M., and Zhao, J. (2016). siRNA delivered by EGFR-specific scFv sensitizes EGFR-TKI-resistant human lung cancer cells. *Biomaterials* 76, 196-207.
- Lynch, T.J., Bondarenko, I., Luft, A., Serwatowski, P., Barlesi, F., Chacko, R., Sebastian, M., Neal, J., Lu, H., and Cuillerot, J.-M. (2012). Ipilimumab in combination with paclitaxel and carboplatin as first-line treatment in stage IIIB/IV non-small-cell lung cancer: results from a randomized, double-blind, multicenter phase II study. *Journal of Clinical Oncology* 30, 2046-2054.
- Mackowiak, S.A., Schmidt, A., Weiss, V., Argyo, C., von Schirnding, C., Bein, T., and Bräuchle, C. (2013). Targeted Drug Delivery in Cancer Cells with Red-Light Photoactivated Mesoporous Silica Nanoparticles. *Nano Letters* 13, 2576-2583.
- Mantovani, A., and Sica, A. (2010). Macrophages, innate immunity and cancer: balance, tolerance, and diversity. *Current opinion in immunology* 22, 231-237.
- Martin, P., Leighl, N.B., Tsao, M.-S., and Shepherd, F.A. (2013). KRAS mutations as prognostic and predictive markers in non-small cell lung cancer. *Journal of Thoracic Oncology* 8, 530-542.
- Martins, S.J., Takagaki, T.Y., Silva, A.G., Gallo, C.P., Silva, F.B., and Capelozzi, V.L. (2009). Prognostic relevance of TTF-1 and MMP-9 expression in advanced lung adenocarcinoma. *Lung Cancer* 64, 105-109.
- Master, A.M., and Sen Gupta, A. (2012). EGF receptor-targeted nanocarriers for enhanced cancer treatment. *Nanomedicine* 7, 1895-1906.
- Matsumura, Y., and Maeda, H. (1986). A new concept for macromolecular therapeutics in cancer chemotherapy: mechanism of tumorotropic accumulation of proteins and the antitumor agent smancs. *Cancer research* 46, 6387-6392.

- McAllister, S.S., and Weinberg, R.A. (2014). The tumour-induced systemic environment as a critical regulator of cancer progression and metastasis. *Nature cell biology* *16*, 717-727.
- Meng, H., Xue, M., Xia, T., Ji, Z., Tarn, D.Y., Zink, J.I., and Nel, A.E. (2011). Use of size and a copolymer design feature to improve the biodistribution and the enhanced permeability and retention effect of doxorubicin-loaded mesoporous silica nanoparticles in a murine xenograft tumor model. *ACS nano* *5*, 4131-4144.
- Mertens, M.E., Frese, J., Bolukbas, D.A., Hrdlicka, L., Golombek, S., Koch, S., Mela, P., Jockenhovel, S., Kiessling, F., and Lammers, T. (2014). FMN-coated fluorescent USPIO for cell labeling and non-invasive MR imaging in tissue engineering. *Theranostics* *4*, 1002-1013.
- Mickler, F.M., Möckl, L., Ruthardt, N., Ogris, M., Wagner, E., and Bräuchle, C. (2012). Tuning nanoparticle uptake: live-cell imaging reveals two distinct endocytosis mechanisms mediated by natural and artificial EGFR targeting ligand. *Nano letters* *12*, 3417-3423.
- Min, Y., Caster, J.M., Eblan, M.J., and Wang, A.Z. (2015). Clinical translation of nanomedicine. *Chemical reviews* *115*, 11147-11190.
- Minna, J.D., Roth, J.A., and Gazdar, A.F. (2002). Focus on lung cancer. *Cancer cell* *1*, 49-52.
- Mirshafiee, V., Mahmoudi, M., Lou, K., Cheng, J., and Kraft, M.L. (2013). Protein corona significantly reduces active targeting yield. *Chemical communications* *49*, 2557-2559.
- Mitchell, M.J., Wayne, E., Rana, K., Schaffer, C.B., and King, M.R. (2014). TRAIL-coated leukocytes that kill cancer cells in the circulation. *Proceedings of the National Academy of Sciences* *111*, 930-935.
- Morton, S.W., Lee, M.J., Deng, Z.J., Dreaden, E.C., Siouve, E., Shopsowitz, K.E., Shah, N.J., Yaffe, M.B., and Hammond, P.T. (2014). A nanoparticle-based combination chemotherapy delivery system for enhanced tumor killing by dynamic rewiring of signaling pathways. *Science signaling* *7*, ra44.
- Mosser, D.M., and Edwards, J.P. (2008). Exploring the full spectrum of macrophage activation. *Nature reviews immunology* *8*, 958-969.
- Moyer, T.J., Zmolek, A.C., and Irvine, D.J. (2016). Beyond antigens and adjuvants: formulating future vaccines. *Journal of Clinical Investigation* *126*, 799.
- Muraoka, D., Harada, N., Hayashi, T., Tahara, Y., Momose, F., Sawada, S.-i., Mukai, S.-a., Akiyoshi, K., and Shiku, H. (2014). Nanogel-based immunologically stealth vaccine targets macrophages in the medulla of lymph node and induces potent antitumor immunity. *ACS nano* *8*, 9209-9218.
- Murray, P.J., and Wynn, T.A. (2011). Protective and pathogenic functions of macrophage subsets. *Nature reviews immunology* *11*, 723-737.
- Na, H.K., Kim, M.H., Park, K., Ryoo, S.R., Lee, K.E., Jeon, H., Ryoo, R., Hyeon, C., and Min, D.H. (2012). Efficient functional delivery of siRNA using mesoporous silica nanoparticles with ultralarge pores. *Small* *8*, 1752-1761.

- Nascimento, A.V., Gattacceca, F., Singh, A., Bousbaa, H., Ferreira, D., Sarmiento, B., and Amiji, M.M. (2016). Biodistribution and pharmacokinetics of Mad2 siRNA-loaded EGFR-targeted chitosan nanoparticles in cisplatin sensitive and resistant lung cancer models. *Nanomedicine* *11*, 767-781.
- Nassimi, M., Schleh, C., Lauenstein, H.-D., Hussein, R., Lübbers, K., Pohlmann, G., Switalla, S., Sewald, K., Müller, M., and Krug, N. (2009). Low cytotoxicity of solid lipid nanoparticles in in vitro and ex vivo lung models. *Inhalation toxicology* *21*, 104-109.
- Network, C.G.A.R. (2012). Comprehensive genomic characterization of squamous cell lung cancers. *Nature* *489*, 519-525.
- Network, C.G.A.R. (2014). Comprehensive molecular profiling of lung adenocarcinoma. *Nature* *511*, 543-550.
- Neuhaus, V., Schwarz, K., Klee, A., Seehase, S., Förster, C., Pfennig, O., Jonigk, D., Fieguth, H.-G., Koch, W., and Warnecke, G. (2013). Functional testing of an inhalable nanoparticle based influenza vaccine using a human precision cut lung slice technique. *PLoS One* *8*, e71728.
- Normanno, N., De Luca, A., Bianco, C., Strizzi, L., Mancino, M., Maiello, M.R., Carotenuto, A., De Feo, G., Caponigro, F., and Salomon, D.S. (2006). Epidermal growth factor receptor (EGFR) signaling in cancer. *Gene* *366*, 2-16.
- Numico, G., Castiglione, F., Granetto, C., Garrone, O., Mariani, G., Di Costanzo, G., La Ciura, P., Gasco, M., Ostellino, O., and Porcile, G. (2002). Single-agent pegylated liposomal doxorubicin (Caelix®) in chemotherapy pretreated non-small cell lung cancer patients: a pilot trial. *Lung cancer* *35*, 59-64.
- Ozeki, T., and Tagami, T. (2014). Drug/polymer nanoparticles prepared using unique spray nozzles and recent progress of inhaled formulation. *asian journal of pharmaceutical sciences* *9*, 236-243.
- Paez, J.G., Jänne, P.A., Lee, J.C., Tracy, S., Greulich, H., Gabriel, S., Herman, P., Kaye, F.J., Lindeman, N., and Boggon, T.J. (2004). EGFR mutations in lung cancer: correlation with clinical response to gefitinib therapy. *Science* *304*, 1497-1500.
- Paranjpe, M., Neuhaus, V., Finke, J., Richter, C., Gothsch, T., Kwade, A., Büttgenbach, S., Braun, A., and Müller-Goymann, C. (2013). In vitro and ex vivo toxicological testing of sildenafil-loaded solid lipid nanoparticles. *Inhalation toxicology* *25*, 536-543.
- Patel, A.R., Chougule, M., and Singh, M. (2014a). EphA2 targeting pegylated nanocarrier drug delivery system for treatment of lung cancer. *Pharmaceutical research* *31*, 2796-2809.
- Patel, A.R., Chougule, M.B., Lim, E., Francis, K.P., Safe, S., and Singh, M. (2014b). Theranostic tumor homing nanocarriers for the treatment of lung cancer. *Nanomedicine: Nanotechnology, Biology and Medicine* *10*, 1053-1063.
- Patil, R., Ljubimov, A.V., Gangalum, P.R., Ding, H., Portilla-Arias, J., Wagner, S., Inoue, S., Konda, B., Rekechenetskiy, A., and Chesnokova, A. (2015). MRI virtual biopsy and treatment of brain metastatic tumors with targeted nanobioconjugates: nanoclinic in the brain. *ACS nano* *9*, 5594-5608.

- Patlakas, G., Bouros, D., Tsantekidou-Pozova, S., and Koukourakis, M.I. (2005). Triplet chemotherapy with docetaxel, gemcitabine and liposomal doxorubicin, supported with subcutaneous amifostine and hemopoietic growth factors, in advanced non-small cell lung cancer. *Anticancer research* 25, 1427-1431.
- Peer, D., Karp, J.M., Hong, S., Farokhzad, O.C., Margalit, R., and Langer, R. (2007). Nanocarriers as an emerging platform for cancer therapy. *Nature nanotechnology* 2, 751-760.
- Pei, Y., and Yeo, Y. (2016). Drug delivery to macrophages: Challenges and opportunities. *Journal of controlled release : official journal of the Controlled Release Society* 240, 202-211.
- Peng, X.-H., Wang, Y., Huang, D., Wang, Y., Shin, H.J., Chen, Z., Spewak, M.B., Mao, H., Wang, X., and Wang, Y. (2011). Targeted delivery of cisplatin to lung cancer using ScFvEGFR-heparin-cisplatin nanoparticles. *ACS Nano* 5, 9480-9493.
- Pisani, C., Gaillard, J.-C., Odorico, M., Nyalosaso, J.L., Charnay, C., Guari, Y., Chopineau, J., Devoisselle, J.-M., Armengaud, J., and Prat, O. (2017). The timeline of corona formation around silica nanocarriers highlights the role of the protein interactome. *Nanoscale*.
- Pollard, J.W. (2008). Macrophages define the invasive microenvironment in breast cancer. *Journal of leukocyte biology* 84, 623-630.
- Pollard, J.W. (2009). Trophic macrophages in development and disease. *Nature reviews immunology* 9, 259-270.
- Popat, A., Liu, J., Lu, G.Q.M., and Qiao, S.Z. (2012). A pH-responsive drug delivery system based on chitosan coated mesoporous silica nanoparticles. *Journal of Materials Chemistry* 22, 11173-11178.
- Project, T.C.L.C.G., and NGM, N.G.M. (2013). A genomics-based classification of human lung tumors. *Science translational medicine* 5, 209ra153.
- Qian, B.-Z., Li, J., Zhang, H., Kitamura, T., Zhang, J., Campion, L.R., Kaiser, E.A., Snyder, L.A., and Pollard, J.W. (2011). CCL2 recruits inflammatory monocytes to facilitate breast-tumour metastasis. *Nature* 475, 222-225.
- Qian, B.-Z., and Pollard, J.W. (2010). Macrophage diversity enhances tumor progression and metastasis. *Cell* 141, 39-51.
- Quail, D.F., and Joyce, J.A. (2013). Microenvironmental regulation of tumor progression and metastasis. *Nature medicine* 19, 1423-1437.
- Quatromoni, J.G., and Eruslanov, E. (2012). Tumor-associated macrophages: function, phenotype, and link to prognosis in human lung cancer. *American journal of translational research* 4, 376.
- Raesch, S.S., Tenzer, S., Storck, W., Rurainski, A., Selzer, D., Ruge, C.A., Perez-Gil, J., Schaefer, U.F., and Lehr, C.-M. (2015). Proteomic and lipidomic analysis of nanoparticle corona upon contact with lung surfactant reveals differences in protein, but not lipid composition. *ACS nano* 9, 11872-11885.

- Rau, J.L. (2005). The inhalation of drugs: advantages and problems. *Respiratory care* 50, 367-382.
- Rink, J.S., Plebanek, M.P., Tripathy, S., and Thaxton, C.S. (2013). Update on current and potential nanoparticle cancer therapies. *Current opinion in oncology* 25, 646.
- Rizvi, N.A., Hellmann, M.D., Snyder, A., Kvistborg, P., Makarov, V., Havel, J.J., Lee, W., Yuan, J., Wong, P., and Ho, T.S. (2015). Mutational landscape determines sensitivity to PD-1 blockade in non-small cell lung cancer. *Science* 348, 124-128.
- Roeb, E., Schleinkofer, K., Kernebeck, T., Pötsch, S., Jansen, B., Behrmann, I., Matern, S., and Grötzinger, J. (2002). The matrix metalloproteinase 9 (mmp-9) hemopexin domain is a novel gelatin binding domain and acts as an antagonist. *Journal of Biological Chemistry* 277, 50326-50332.
- Roy, R., Yang, J., and Moses, M.A. (2009). Matrix metalloproteinases as novel biomarkers and potential therapeutic targets in human cancer. *Journal of Clinical Oncology* 27, 5287-5297.
- Ruano-Ravina, A., Pereyra, M.F., Castro, M.T., Pérez-Ríos, M., Abal-Arca, J., and Barros-Dios, J.M. (2014). Genetic susceptibility, residential radon, and lung cancer in a radon prone area. *Journal of Thoracic Oncology* 9, 1073-1080.
- Ruge, C.A., Kirch, J., and Lehr, C.-M. (2013). Pulmonary drug delivery: from generating aerosols to overcoming biological barriers—therapeutic possibilities and technological challenges. *The Lancet Respiratory Medicine* 1, 402-413.
- Sadhukha, T., Wiedmann, T.S., and Panyam, J. (2013). Inhalable magnetic nanoparticles for targeted hyperthermia in lung cancer therapy. *Biomaterials* 34, 5163-5171.
- Salvati, A., Pitek, A.S., Monopoli, M.P., Prapainop, K., Bombelli, F.B., Hristov, D.R., Kelly, P.M., Åberg, C., Mahon, E., and Dawson, K.A. (2013). Transferrin-functionalized nanoparticles lose their targeting capabilities when a biomolecule corona adsorbs on the surface. *Nature nanotechnology* 8, 137-143.
- Samantas, E., Kalofonos, H., Linardou, H., Nicolaidis, C., Mylonakis, N., Fountzilas, G., Kosmidis, P., and Skarlos, D. (2000). Phase II study of pegylated liposomal doxorubicin: Inactive in recurrent small-cell lung cancer A Hellenic Cooperative Oncology Group Study. *Annals of oncology* 11, 1395-1397.
- Sarfati, G., Dvir, T., Elkabets, M., Apte, R.N., and Cohen, S. (2011). Targeting of polymeric nanoparticles to lung metastases by surface-attachment of YIGSR peptide from laminin. *Biomaterials* 32, 152-161.
- Sauer, A.M., Schlossbauer, A., Ruthardt, N., Cauda, V., Bein, T., and Bräuchle, C. (2010). Role of endosomal escape for disulfide-based drug delivery from colloidal mesoporous silica evaluated by live-cell imaging. *Nano letters* 10, 3684-3691.
- Sawyers, C. (2004). Targeted cancer therapy. *Nature* 432, 294-297.

- Schlossbauer, A., Kecht, J., and Bein, T. (2009). Biotin–Avidin as a Protease-Responsive Cap System for Controlled Guest Release from Colloidal Mesoporous Silica. *Angewandte Chemie* *121*, 3138-3141.
- Schmall, A., Al-Tamari, H.M., Herold, S., Kampschulte, M., Weigert, A., Wietelmann, A., Vipotnik, N., Grimminger, F., Seeger, W., and Pullamsetti, S.S. (2015). Macrophage and cancer cell cross-talk via CCR2 and CX3CR1 is a fundamental mechanism driving lung cancer. *American journal of respiratory and critical care medicine* *191*, 437-447.
- Schmitt, F., Lagopoulos, L., Käuper, P., Rossi, N., Busso, N., Barge, J., Wagnières, G., Laue, C., Wandrey, C., and Juillerat-Jeanneret, L. (2010). Chitosan-based nanogels for selective delivery of photosensitizers to macrophages and improved retention in and therapy of articular joints. *Journal of Controlled Release* *144*, 242-250.
- Schulze, K., Imbeaud, S., Letouzé, E., Alexandrov, L.B., Calderaro, J., Rebouissou, S., Couchy, G., Meiller, C., Shinde, J., and Soysouvanh, F. (2015). Exome sequencing of hepatocellular carcinomas identifies new mutational signatures and potential therapeutic targets. *Nature genetics*.
- Schütz, C.A., Juillerat-Jeanneret, L., Mueller, H., Lynch, I., and Riediker, M. (2013). Therapeutic nanoparticles in clinics and under clinical evaluation. *Nanomedicine* *8*, 449-467.
- Shao, K., Singha, S., Clemente-Casares, X., Tsai, S., Yang, Y., and Santamaria, P. (2014). Nanoparticle-based immunotherapy for cancer. *ACS nano* *9*, 16-30.
- Sharma, P., and Allison, J.P. (2015). The future of immune checkpoint therapy. *Science* *348*, 56-61.
- Sharma, S.V., Bell, D.W., Settleman, J., and Haber, D.A. (2007). Epidermal growth factor receptor mutations in lung cancer. *Nature Reviews Cancer* *7*, 169-181.
- Shaw, A.T., and Engelman, J.A. (2013). ALK in lung cancer: past, present, and future. *Journal of Clinical Oncology* *31*, 1105-1111.
- Shen, J., Meng, Q., Sui, H., Yin, Q., Zhang, Z., Yu, H., and Li, Y. (2013). iRGD Conjugated TPGS mediates codelivery of paclitaxel and survivin shRNA for the reversal of lung cancer resistance. *Molecular pharmaceutics* *11*, 2579-2591.
- Shi, H., Ye, X., He, X., Wang, K., Cui, W., He, D., Li, D., and Jia, X. (2014). Au@ Ag/Au nanoparticles assembled with activatable aptamer probes as smart “nano-doctors” for image-guided cancer thermotherapy. *Nanoscale* *6*, 8754-8761.
- Shigematsu, H., Lin, L., Takahashi, T., Nomura, M., Suzuki, M., Wistuba, I.I., Fong, K.M., Lee, H., Toyooka, S., and Shimizu, N. (2005). Clinical and biological features associated with epidermal growth factor receptor gene mutations in lung cancers. *Journal of the National Cancer Institute* *97*, 339-346.
- Shou, Y., Hirano, T., Gong, Y., Kato, Y., Yoshida, K., Ohira, T., Ikeda, N., Konaka, C., Ebihara, Y., and Zhao, F. (2001). Influence of angiogenic factors and matrix metalloproteinases upon tumour progression in non-small-cell lung cancer. *British journal of cancer* *85*, 1706.

- Siegel, R.L., Miller, K.D., and Jemal, A. (2016). Cancer statistics, 2016. *CA: a cancer journal for clinicians* 66, 7-30.
- Singh, N., Karambelkar, A., Gu, L., Lin, K., Miller, J.S., Chen, C.S., Sailor, M.J., and Bhatia, S.N. (2011). Bioresponsive mesoporous silica nanoparticles for triggered drug release. *Journal of the American Chemical Society* 133, 19582-19585.
- Skubitz, K.M. (2002). Phase II Trial of Pegylated-Liposomal Doxorubicin (Doxil™) in Mesothelioma 1. *Cancer investigation* 20, 693-699.
- Soda, M., Choi, Y.L., Enomoto, M., Takada, S., Yamashita, Y., Ishikawa, S., Fujiwara, S., Watanabe, H., Kurashina, K., Hatanaka, H., *et al.* (2007). Identification of the transforming EML4-ALK fusion gene in non-small-cell lung cancer. *Nature* 448, 561-566.
- Spira, A., and Ettinger, D.S. (2004). Multidisciplinary management of lung cancer. *New England Journal of Medicine* 350, 379-392.
- Srinivasarao, M., Galliford, C.V., and Low, P.S. (2015). Principles in the design of ligand-targeted cancer therapeutics and imaging agents. *Nature Reviews Drug Discovery* 14, 203-219.
- Stathopoulos, G., Antoniou, D., Dimitroulis, J., Stathopoulos, J., Marosis, K., and Michalopoulou, P. (2011). Comparison of liposomal cisplatin versus cisplatin in non-squamous cell non-small-cell lung cancer. *Cancer chemotherapy and pharmacology* 68, 945-950.
- Stathopoulos, G., and Boulikas, T. (2011). Lipoplatin formulation review article. *Journal of drug delivery* 2012.
- Stephens, P., Hunter, C., Bignell, G., Edkins, S., Davies, H., Teague, J., Stevens, C., O'meara, S., Smith, R., and Parker, A. (2004). Lung cancer: intragenic ERBB2 kinase mutations in tumours. *Nature* 431, 525-526.
- Stoeger, T., Reinhard, C., Takenaka, S., Schroepel, A., Karg, E., Ritter, B., Heyder, J., and Schulz, H. (2006). Instillation of six different ultrafine carbon particles indicates a surface area threshold dose for acute lung inflammation in mice. *Environmental health perspectives*, 328-333.
- Subramanian, J., and Govindan, R. (2007). Lung cancer in never smokers: a review. *Journal of Clinical Oncology* 25, 561-570.
- Sukumar, U.K., Bhushan, B., Dubey, P., Matai, I., Sachdev, A., and Packirisamy, G. (2013). Emerging applications of nanoparticles for lung cancer diagnosis and therapy. *International Nano Letters* 3, 1-17.
- Sun, S., Schiller, J.H., and Gazdar, A.F. (2007). Lung cancer in never smokers—a different disease. *Nature Reviews Cancer* 7, 778-790.
- Sundarraj, S., Thangam, R., Sujitha, M.V., Vimala, K., and Kannan, S. (2014). Ligand-conjugated mesoporous silica nanorattles based on enzyme targeted prodrug delivery system for effective lung cancer therapy. *Toxicology and applied pharmacology* 275, 232-243.

- Sung, J.C., Pulliam, B.L., and Edwards, D.A. (2007). Nanoparticles for drug delivery to the lungs. *Trends in biotechnology* 25, 563-570.
- Suzuki, H., Aoki, K., Chiba, K., Sato, Y., Shiozawa, Y., Shiraishi, Y., Shimamura, T., Niida, A., Motomura, K., and Ohka, F. (2015). Mutational landscape and clonal architecture in grade II and III gliomas. *Nature genetics*.
- Tang, F., Li, L., and Chen, D. (2012). Mesoporous silica nanoparticles: synthesis, biocompatibility and drug delivery. *Advanced Materials* 24, 1504-1534.
- Tao, Z., Toms, B.B., Goodisman, J., and Asefa, T. (2009). Mesoporosity and functional group dependent endocytosis and cytotoxicity of silica nanomaterials. *Chemical research in toxicology* 22, 1869-1880.
- Taratula, O., Garbuzenko, O., Savla, R., Andrew Wang, Y., He, H., and Minko, T. (2011a). Multifunctional nanomedicine platform for cancer specific delivery of siRNA by superparamagnetic iron oxide nanoparticles-dendrimer complexes. *Current drug delivery* 8, 59-69.
- Taratula, O., Garbuzenko, O.B., Chen, A.M., and Minko, T. (2011b). Innovative strategy for treatment of lung cancer: targeted nanotechnology-based inhalation co-delivery of anticancer drugs and siRNA. *Journal of drug targeting* 19, 900-914.
- Taratula, O., Kuzmov, A., Shah, M., Garbuzenko, O.B., and Minko, T. (2013). Nanostructured lipid carriers as multifunctional nanomedicine platform for pulmonary co-delivery of anticancer drugs and siRNA. *Journal of Controlled Release* 171, 349-357.
- Tenzer, S., Docter, D., Kuharev, J., Musyanovych, A., Fetz, V., Hecht, R., Schlenk, F., Fischer, D., Kiouptsi, K., and Reinhardt, C. (2013). Rapid formation of plasma protein corona critically affects nanoparticle pathophysiology. *Nature nanotechnology* 8, 772-781.
- Thorley, A.J., and Tetley, T.D. (2013). New perspectives in nanomedicine. *Pharmacology & therapeutics* 140, 176-185.
- Topalian, S.L., Hodi, F.S., Brahmer, J.R., Gettinger, S.N., Smith, D.C., McDermott, D.F., Powderly, J.D., Carvajal, R.D., Sosman, J.A., and Atkins, M.B. (2012). Safety, activity, and immune correlates of anti-PD-1 antibody in cancer. *New England Journal of Medicine* 366, 2443-2454.
- Torchilin, V.P. (2014). Multifunctional, stimuli-sensitive nanoparticulate systems for drug delivery. *Nature reviews Drug discovery* 13, 813-827.
- Torricc, M. (2016). Does nanomedicine have a delivery problem? (ACS Publications).
- Tsoutsou, P.G., Froudarakis, M.E., Bouros, D., and Koukourakis, M.I. (2008). Hypofractionated/accelerated radiotherapy with cytoprotection (HypoARC) combined with vinorelbine and liposomal doxorubicin for locally advanced non-small cell lung cancer (NSCLC). *Anticancer research* 28, 1349-1354.
- Turk, B.E., Huang, L.L., Piro, E.T., and Cantley, L.C. (2001). Determination of protease cleavage site motifs using mixture-based oriented peptide libraries. *Nature biotechnology* 19, 661-667.

- Überall, I., Kolář, Z., Trojanec, R., Berkovcova, J., and Hajduch, M. (2008). The status and role of ErbB receptors in human cancer. *Experimental and molecular pathology* 84, 79-89.
- Uhl, F.E., Vierkotten, S., Wagner, D.E., Burgstaller, G., Costa, R., Koch, I., Lindner, M., Meiners, S., Eickelberg, O., and Königshoff, M. (2015). Preclinical validation and imaging of Wnt-induced repair in human 3D lung tissue cultures. *European Respiratory Journal*, ERJ-01832-02014.
- Vallhov, H., Kupferschmidt, N., Gabrielsson, S., Paulie, S., Strømme, M., Garcia-Bennett, A.E., and Scheynius, A. (2012). Adjuvant properties of mesoporous silica particles tune the development of effector T cells. *Small* 8, 2116-2124.
- van Rijt, S., Bölükbas, D., Argyo, C., Wipplinger, K., Naureen, M., Datz, S., Eickelberg, O., Meiners, S., Bein, T., and Schmid, O. (2016). Applicability of avidin protein coated mesoporous silica nanoparticles as drug carriers in the lung. *Nanoscale* 8, 8058-8069.
- van Rijt, S.H., Bein, T., and Meiners, S. (2014). Medical nanoparticles for next generation drug delivery to the lungs. *European Respiratory Journal* 44, 765-774.
- van Rijt, S.H., Bölükbas, D.A., Argyo, C., Datz, S., Lindner, M., Eickelberg, O., Königshoff, M., Bein, T., and Meiners, S. (2015). Protease-mediated release of chemotherapeutics from mesoporous silica nanoparticles to ex vivo human and mouse lung tumors. *ACS nano* 9, 2377-2389.
- Vanneman, M., and Dranoff, G. (2012). Combining immunotherapy and targeted therapies in cancer treatment. *Nature Reviews Cancer* 12, 237-251.
- Vecchione, L., Jacobs, B., Normanno, N., Ciardiello, F., and Tejpar, S. (2011). EGFR-targeted therapy. *Experimental cell research* 317, 2765-2771.
- Vivero-Escoto, J.L., Slowing, I.I., Trewyn, B.G., and Lin, V.S.Y. (2010). Mesoporous silica nanoparticles for intracellular controlled drug delivery. *Small* 6, 1952-1967.
- Wagner, E. (2007). Programmed drug delivery: nanosystems for tumor targeting. *Expert Opinion on Biological Therapy* 7, 587-593.
- Wagner, V., Dullaart, A., Bock, A.-K., and Zweck, A. (2006). The emerging nanomedicine landscape. *Nature biotechnology* 24, 1211-1217.
- Wang, A.Z., Langer, R., and Farokhzad, O.C. (2012). Nanoparticle delivery of cancer drugs. *Annual review of medicine* 63, 185-198.
- Wang, C., Ding, C., Kong, M., Dong, A., Qian, J., Jiang, D., and Shen, Z. (2011). Tumor-targeting magnetic lipoplex delivery of short hairpin RNA suppresses IGF-1R overexpression of lung adenocarcinoma A549 cells in vitro and in vivo. *Biochemical and biophysical research communications* 410, 537-542.
- Wang, Y., Xu, Z., Guo, S., Zhang, L., Sharma, A., Robertson, G.P., and Huang, L. (2013). Intravenous delivery of siRNA targeting CD47 effectively inhibits melanoma tumor growth and lung metastasis. *Molecular Therapy* 21, 1919-1929.

- Weissleder, R., Nahrendorf, M., and Pittet, M.J. (2014). Imaging macrophages with nanoparticles. *Nature materials* *13*, 125-138.
- Westra, W.H. (2000). Early glandular neoplasia of the lung. *Respiratory research* *1*, 1.
- Wijagkanalan, W., Kawakami, S., Higuchi, Y., Yamashita, F., and Hashida, M. (2011). Intratracheally instilled mannosylated cationic liposome/NF κ B decoy complexes for effective prevention of LPS-induced lung inflammation. *Journal of controlled release* *149*, 42-50.
- Wilhelm, S., Tavares, A.J., Dai, Q., Ohta, S., Audet, J., Dvorak, H.F., and Chan, W.C. (2016). Analysis of nanoparticle delivery to tumours. *Nature Reviews Materials* *1*, 16014.
- Wistuba, I.I., and Gazdar, A.F. (2006). Lung cancer preneoplasia. *Annu Rev Pathol Mech Dis* *1*, 331-348.
- Wistuba, I.I., Mao, L., and Gazdar, A.F. (2002). Smoking molecular damage in bronchial epithelium. *Oncogene* *21*, 7298-7306.
- Wolchok, J.D., and Chan, T.A. (2014). Cancer: Antitumour immunity gets a boost. *Nature* *515*, 496-498.
- Xu, J.-H., Gao, F.-P., Li, L.-L., Ma, H.L., Fan, Y.-S., Liu, W., Guo, S.-S., Zhao, X.-Z., and Wang, H. (2013). Gelatin-mesoporous silica nanoparticles as matrix metalloproteinases-degradable drug delivery systems in vivo. *Microporous and Mesoporous Materials* *182*, 165-172.
- Yamada, R., Kostova, M.B., Anchoori, R.K., Xu, S., Neamati, N., and Khan, S. (2010). Biological evaluation of paclitaxel-peptide conjugates as a model for MMP2-targeted drug delivery. *Cancer biology & therapy* *9*, 192-203.
- Yang, J., Choi, J., Bang, D., Kim, E., Lim, E.K., Park, H., Suh, J.S., Lee, K., Yoo, K.H., Kim, E.K., *et al.* (2011). Convertible organic nanoparticles for near-infrared photothermal ablation of cancer cells. *Angewandte Chemie (International ed in English)* *50*, 441-444.
- Yang, S.-G., Chang, J.-E., Shin, B., Park, S., Na, K., and Shim, C.-K. (2010). ^{99m}Tc-hematoporphyrin linked albumin nanoparticles for lung cancer targeted photodynamic therapy and imaging. *Journal of Materials Chemistry* *20*, 9042-9046.
- Yang, Y., Hu, Y., Wang, Y., Li, J., Liu, F., and Huang, L. (2012a). Nanoparticle delivery of pooled siRNA for effective treatment of non-small cell lung cancer. *Molecular pharmaceutics* *9*, 2280-2289.
- Yang, Y., Li, J., Liu, F., and Huang, L. (2012b). Systemic delivery of siRNA via LCP nanoparticle efficiently inhibits lung metastasis. *Molecular Therapy* *20*, 609-615.
- Yonenaga, N., Kenjo, E., Asai, T., Tsuruta, A., Shimizu, K., Dewa, T., Nango, M., and Oku, N. (2012). RGD-based active targeting of novel polycation liposomes bearing siRNA for cancer treatment. *Journal of Controlled Release* *160*, 177-181.
- Yu, T., Greish, K., McGill, L.D., Ray, A., and Ghandehari, H. (2012). Influence of geometry, porosity, and surface characteristics of silica nanoparticles on acute toxicity: their vasculature effect and tolerance threshold. *ACS nano* *6*, 2289-2301.

- Zhang, J., Patel, L., and Pienta, K.J. (2010). CC chemokine ligand 2 (CCL2) promotes prostate cancer tumorigenesis and metastasis. *Cytokine & growth factor reviews* *21*, 41-48.
- Zhang, J., Yuan, Z.-F., Wang, Y., Chen, W.-H., Luo, G.-F., Cheng, S.-X., Zhuo, R.-X., and Zhang, X.-Z. (2013a). Multifunctional envelope-type mesoporous silica nanoparticles for tumor-triggered targeting drug delivery. *Journal of the American Chemical Society* *135*, 5068-5073.
- Zhang, Y., Kim, W.Y., and Huang, L. (2013b). Systemic delivery of gemcitabine triphosphate via LCP nanoparticles for NSCLC and pancreatic cancer therapy. *Biomaterials* *34*, 3447-3458.
- Zhang, Y., Schwerbrock, N.M., Rogers, A.B., Kim, W.Y., and Huang, L. (2013c). Codelivery of VEGF siRNA and gemcitabine monophosphate in a single nanoparticle formulation for effective treatment of NSCLC. *Molecular Therapy* *21*, 1559-1569.
- Zhao, S., Chu, Z., Blanco, V.M., Nie, Y., Hou, Y., and Qi, X. (2015). SapC-DOPS Nanovesicles as Targeted Therapy for Lung Cancer. *Molecular cancer therapeutics* *14*, 491-498.
- Zhao, Y.-L., Li, Z., Kabehie, S., Botros, Y.Y., Stoddart, J.F., and Zink, J.I. (2010). pH-operated nanopistons on the surfaces of mesoporous silica nanoparticles. *Journal of the American Chemical Society* *132*, 13016-13025.
- Zhao, Y., Sun, X., Zhang, G., Trewyn, B.G., Slowing, I.I., and Lin, V.S.-Y. (2011). Interaction of mesoporous silica nanoparticles with human red blood cell membranes: size and surface effects. *ACS nano* *5*, 1366-1375.
- Zhu, L., Wang, T., Perche, F., Taigind, A., and Torchilin, V.P. (2013). Enhanced anticancer activity of nanopreparation containing an MMP2-sensitive PEG-drug conjugate and cell-penetrating moiety. *Proceedings of the National Academy of Sciences* *110*, 17047-17052.
- Zijlmans, H.J., Fleuren, G.J., Baelde, H.J., Eilers, P.H., Kenter, G.G., and Gorter, A. (2006). The absence of CCL2 expression in cervical carcinoma is associated with increased survival and loss of heterozygosity at 17q11. 2. *The Journal of pathology* *208*, 507-517.
- Zitvogel, L., Pitt, J.M., Daillère, R., Smyth, M.J., and Kroemer, G. (2016). Mouse models in oncoimmunology. *Nature Reviews Cancer*.
- Zöchbauer-Müller, S., and Minna, J.D. (2000). The biology of lung cancer including potential clinical applications. *Chest surgery clinics of North America* *10*, 691-708.

Abbreviations

$\alpha_v\beta_3$	Alpha-v beta-3 integrin
$\alpha_v\beta_6$	Alpha-v beta-6 integrin
Ab	Antibody
ALK	Anaplastic lymphoma kinase
BCA	Bicinchoninic acid assay
BCL2	B-cell lymphoma 2
BRAF	V-Raf murine sarcoma viral oncogene homolog B
Calcein-AM	Calcein acetoxymethyl ester
CB	Cisplatin + bortezomib treatment
CCL2	C-C motif chemokine ligand 2
CCR2	C-C chemokine receptor type 2
CD44	Cluster of differentiation 44
CD47	Cluster of differentiation 47
CD80	Cluster of differentiation
CGARN	Cancer Genome Atlas Research Network
Cisplatin	cis-Diamineplatinum(II) dichloride
CLCGP	Clinical Lung Cancer Genome Project
Cl-AM	Calcein-AM
c-MET	Hepatocyte growth factor receptor
cMSN	MMP9-cleavable mesoporous silica nanoparticle
CMYC	V-myc avian myelocytomatosis viral oncogene homolog
CO ₂	Carbon dioxide
COPD	Chronic obstructive lung disease
CT	Computer tomography
CTLA4	Cytotoxic T-lymphocyte-associated protein 4
Da	Dalton
DAPI	4',6-Diamidin-2-phenylindol
DMEM	Dulbecco's modified eagle medium
DMSO	Dimethyl sulfoxide

DR 4/5	Death receptor 4/5
DTT	Dithiothreitol
ECM	Extracellular matrix
EDTA	Ethylenediaminetetraacetate
EGFR	Epidermal growth factor receptor
EGFR-TKI	EGFR-TK inhibitor
EMA	European Medicines Agency
EML4	Echinoderm microtubule-associated protein like 4
EphA2	Ephrin type-A receptor 2
EPR	Enhanced permeability and retention
ES	E-selectin
EV	Empty vector
F12	Nutrient mixture F-12
FBS	Fetal bovine serum
FDA	U.S. Food and Drug Administration
FTIC	Fluorescein isothiocyanate
FVB	Friend virus B
Gt	Goat
HBSS	Hank's balanced salt solution
HER2	Receptor tyrosine-protein kinase erbB-2
HRP	Horseradish peroxidase
ICF	Immunocytofluorescence
IGF-1R	Insulin-like growth factor 1 receptor
IgG	Immunoglobulin G
IHC	Immunohistochemistry
IHF	Immunofluorescence in cryo-sections
IPF	Idiopathic pulmonary fibrosis
IT	Intratracheal
IV	Intravenous
kDa	Kilodaltons
KIT	KIT proto-oncogene receptor tyrosine kinase

KRAS	Kirsten rat sarcoma viral oncogene homolog
LA2	Latent allele type 2
LDLR	Low density lipoprotein receptor
LHRHR	Luteinizing hormone releasing hormone receptor
LLC	Lewis lung carcinoma cells
LTC	Lung tissue cultures
MMP	Matrix metalloproteinase
MMP2	Matrix metalloproteinase-2
MMP9	Matrix metalloproteinase-9
MRI	Magnetic resonance imaging
Ms	Mouse
MSN	Mesoporous silica nanoparticle
MSN _{AVI}	Avidin-functionalized MSNs
MSN _{ECLi}	ECLi-functionalized MSNs
MSN _{EGF}	EGF-functionalized MSNs
MSN _{GE11}	GE11-functionalized MSNs
MSN _{NH2}	Non-functionalized MSNs
MTT	2,5-diphenyltetrazolium bromide
NaCl	Sodium chloride
ncMSN	MMP9 non-cleavable mesoporous silica nanoparticle
NGM	Network Genomic Medicine
NSCLC	Non-small cell lung cancer
p53	Tumor suppressor p53
PAGE	Polyacrylamide gel electrophoresis
PBS	Phosphate buffered saline
PD1	Programmed cell death protein 1
PDL1	Programmed death-ligand 1
PDL2	Programmed death-ligand 2
PEG	Polyethylene glycol
PET	Positron emission tomography
PFA	Paraformaldehyde

PI	Propidium iodide
PSMA	Prostate-specific membrane antigen
PVDF	Polyvinylidenedifluoride
Rb	Rabbit
RB	Retinoblastoma protein
RIPA	Radioimmunoprecipitation assay
RPM	Revolutions per minute
RPMI	Roswell Park Memorial Institute medium
RT	Room temperature
SC	Subcutaneous
SCLC	Small cell lung cancer
SDS	Sodiumdodecylsulfate
shRNA	Small hairpin RNA
SPIONs	Superparamagnetic iron oxide nanoparticles
TAM	Tumor-associated macrophage
TK	Tyrosine kinase
TME	Tumor microenvironment
TP53	Tumor protein 53
Tris	Tris(hydroxymethyl)-aminomethane
WB	Western blot
WST-1	Water soluble tetrazolium-1
WT	Wild type
Yr	Year/s

Acknowledgements

First and foremost, I would like to express my sincere gratitude to my supervisor, Silke Meiners, for her constant guidance and support during my PhD study. This work could have not been done without her help indeed. I am mostly grateful for all that I have learnt from her which helped me shape my way as a young scientist.

I would also like to thank Oliver Eickelberg for giving me the opportunity to conduct my PhD work at the CPC as well as Manfred Ogris for his input in my thesis committee meetings. I cannot forget to thank the CPC Research School team, Melanie Königshoff, Camille Beunèche, and Doreen Franke for their great help and inspiration. I am further thankful for the support I received from our collaborators not only at the CPC, Tobias Stöger, Otmar Schmid, Malamati Vreka, Georgios Stathopoulos, and Ali Önder Yildirim on behalf of the CPC Small Animal Platform, but also at the Asklepios Clinic Gauting, namely Michael Lindner, for the supply of human tissue for our experiments.

Moreover, I would like to address my special thanks to our external collaborators at the Physical Chemistry Department of Ludwig-Maximilians-University, Thomas Bein, Stefan Datz, Christian Argyo, and Dorothée Gößl for their contributions and expertise regarding nanoparticle synthesis and characterization.

My deepest appreciation extends to my labmates, Alessandra Mossina, Amal Houssaini, Angela Dann, Anne Caniard, Charlotte Meyer-Schwickerath, Christina Lukas, Ilona Kammerl, Korbinian Berschneider, Nora Semren, Sabine van Rijt, Thomas Meul, and Vanessa Welk with whom we share endless memories.

Above all, I am indebted to my family for their everlasting care and support at all times.

Last but not least, I acknowledge the Excellence Cluster NanoSystems Initiative Munich for providing funding during my PhD studies and everyone who helped me on the way to accomplish this work including the proofreaders and the reviewers of this thesis, for their time and interest.

Eidesstattliche Versicherung

Hiermit erkläre ich, Deniz Ali Bölükbaş, an Eides statt, dass ich die vorliegende Dissertation mit dem Thema

„Development of novel nanoparticle-based therapeutics for treatment of lung cancer“

selbstständig verfasst, mich außer der angegebenen keiner weiteren Hilfsmittel bedient und alle Erkenntnisse, die aus dem Schrifttum ganz oder annähernd übernommen sind, als solche kenntlich gemacht und nach ihrer Herkunft unter Bezeichnung der Fundstelle einzeln nachgewiesen habe.

Ich erkläre des Weiteren, dass die hier vorgelegte Dissertation nicht in gleicher oder in ähnlicher Form bei einer anderen Stelle zur Erlangung eines akademischen Grades eingereicht wurde.

Ort/Datum

Unterschrift